

DTIC FILE COPY

WRDC-TR-89-2099



THERMAL ANALYSIS STUDY OF ANTIMONY SULFIDES

Lt Charles K. Kelley  
Lubrication Branch  
Fuels and Lubrication Division

July 1989

Final Technical Report for Period August 1987 - February 1989

APPROVED FOR PUBLIC RELEASE; DISTRIBUTION UNLIMITED

AERO PROPULSION AND POWER LABORATORY  
WRIGHT RESEARCH AND DEVELOPMENT CENTER  
AIR FORCE SYSTEMS COMMAND  
WRIGHT-PATTERSON AIR FORCE BASE, OHIO 45433-6563

DTIC  
FILED  
OCT 02 1989  
E D

89 10 2 064

AD-A212 993

## NOTICE

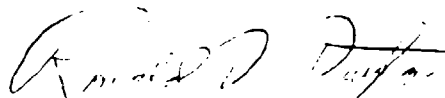
When Government drawings, specifications, or other data are used for any purpose other than in connection with a definitely Government-related procurement, the United States Government incurs no responsibility or any obligation whatsoever. The fact that the government may have formulated or in any way supplied the said drawings, specifications, or other data, is not to be regarded by implication, or otherwise in any manner construed, as licensing the holder, or any other person or corporation; or as conveying any rights or permission to manufacture, use, or sell any patented invention that may in any way be related thereto.

This report has been reviewed by the Office of Public Affairs (ASD/PA) and is releasable to the National Technical Information Service (NTIS). At NTIS, it will be available to the general public, including foreign nations.

This technical report has been reviewed and is approved for publication.

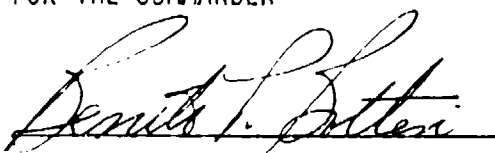


CHARLES K. KELLEY, 1Lt, USAF  
Lubrication Branch  
Fuels and Lubrication Division  
Aero Propulsion and Power Laboratory



RONALD D. DAYTON, Act' Chief  
Fuels and Lubrication Branch  
Aero Propulsion and Power Laboratory

FOR THE COMMANDER



BENITO P. POTTER, Chief  
Fuels and Lubrication Division  
Aero Propulsion and Power Laboratory

If your address has changed, if you wish to be removed from our mailing list, or if the addressee is no longer employed by your organization, please notify WRDC/POSL, Wright-Patterson AFB OH 45433-6563 to help us maintain a current mailing list.

Copies of this report should not be returned unless return is required by security considerations, contractual obligations, or notice on a specific document.

UNCLASSIFIED

SECURITY CLASSIFICATION OF THIS PAGE

REPORT DOCUMENTATION PAGE				Form Approved OMB No. 0704-0188		
1a. REPORT SECURITY CLASSIFICATION UNCLASSIFIED			1b. RESTRICTIVE MARKINGS NONE			
2a. SECURITY CLASSIFICATION AUTHORITY			3. DISTRIBUTION / AVAILABILITY OF REPORT Approved for Public Release; Distribution Unlimited			
2b. DECLASSIFICATION / DOWNGRADING SCHEDULE						
4. PERFORMING ORGANIZATION REPORT NUMBER(S) WRDC-TR-89-2099			5. MONITORING ORGANIZATION REPORT NUMBER(S)			
6a. NAME OF PERFORMING ORGANIZATION Aero Propulsion and Power Lab (AFSC, ASD, WRDC)		6b. OFFICE SYMBOL (if applicable) WRDC/POSL	7a. NAME OF MONITORING ORGANIZATION			
6c. ADDRESS (City, State, and ZIP Code) Wright-Patterson AFB OH 45433-6563			7b. ADDRESS (City, State, and ZIP Code)			
8a. NAME OF FUNDING / SPONSORING ORGANIZATION Aero Propulsion and Power Lab		8b. OFFICE SYMBOL (if applicable) WRDC/POSL	9. PROCUREMENT INSTRUMENT IDENTIFICATION NUMBER			
8c. ADDRESS (City, State, and ZIP Code) Wright-Patterson AFB OH 45433-6563			10. SOURCE OF FUNDING NUMBERS			
			PROGRAM ELEMENT NO. 62203F	PROJECT NO. 3048	TASK NO. 06	WORK UNIT ACCESSION NO. 26
11. TITLE (Include Security Classification) Thermal Analysis Study of Antimony Sulfides						
12. PERSONAL AUTHOR(S) Kelley, Charles K.						
13a. TYPE OF REPORT Final		13b. TIME COVERED FROM 87/8/1 TO 89/2/1		14. DATE OF REPORT (Year, Month, Day) July 1989		15. PAGE COUNT 84
16. SUPPLEMENTARY NOTATION						
17. COSATI CODES			18. SUBJECT TERMS (Continue on reverse if necessary and identify by block number)			
FIELD	GROUP	SUB-GROUP	Thermal Analysis			
11	08		Differential Scanning Calorimetry			
14	02		Antimony Sulfide			
			Thermogravimetric Analysis			
			Differential Thermal Analysis			
19. ABSTRACT (Continue on reverse if necessary and identify by block number)						
<p>An investigation of the thermal and oxidative behavior of a series of antimony sulfides was conducted using thermogravimetric analysis, differential scanning calorimetry, high temperature differential thermal analysis, and Fourier transform infrared spectroscopy. Antimony trisulfide was found thermally stable to 575 °C and oxidatively to 300 °C; above which it forms cubic Sb<sub>2</sub>O<sub>3</sub>. At temperatures above 600 °C, Sb<sub>2</sub>O<sub>4</sub> is formed. Antimony trisulfide undergoes a thermal reaction to produce Sb<sub>2</sub>S<sub>3</sub> between 195 and 230 °C. Antimony pentasulfide (containing 15 percent excess sulfur) undergoes a thermal transformation to yield Sb<sub>2</sub>S<sub>3</sub> between 193 and 239 °C. Removal of excess sulfur by extraction has little effect on the thermal or oxidative properties.</p>						
20. DISTRIBUTION / AVAILABILITY OF ABSTRACT <input type="checkbox"/> UNCLASSIFIED/UNLIMITED <input checked="" type="checkbox"/> SAME AS RPT <input type="checkbox"/> DTIC USERS			21. ABSTRACT SECURITY CLASSIFICATION UNCLASSIFIED			
22a. NAME OF RESPONSIBLE INDIVIDUAL Charles K. Kelley			22b. TELEPHONE (Include Area Code) (513) 255-7230		22c. OFFICE SYMBOL WRDC/POSL	

DD Form 1473, JUN 86

Previous editions are obsolete.

SECURITY CLASSIFICATION OF THIS PAGE

UNCLASSIFIED

## PREFACE

This technical report was prepared by the Lubrication Branch, Fuels and Lubrication Division, Aero Propulsion and Power Laboratory (APPL), Wright Research and Development Center (WRDC), Air Force Systems Command, Wright-Patterson Air Force Base, Ohio 45433-6563. The work herein was accomplished under Project 3048, Task 304806, Work Unit 30480626, "Turbine Engine Lubricant Research," during the period of August 1987 to February 1989 with Lt Charles K. Kelley as Project Engineer. Special acknowledgment is given to Dr Dennis Flentge of Cedarville College for performing the extractions, and to Messrs Edward Pitzer and Richard Homer of WRDC/POXX for providing expert technical support in the areas of FTIR spectroscopy and thermal analysis.

Accession For	
NTIS GRA&I	<input checked="" type="checkbox"/>
DTIC TAB	<input type="checkbox"/>
Unannounced	<input type="checkbox"/>
Justification	
By _____	
Distribution/ _____	
Availability Codes	
(Avail and/or	
Dist	Special
A-1	

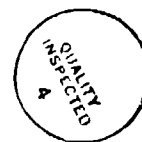


## TABLE OF CONTENTS

SECTION		PAGE
I	INTRODUCTION	1
II	EXPERIMENTAL	3
III	RESULTS AND DISCUSSION	5
IV	CONCLUSION	81
	REFERENCES	83

# LIST OF FIGURES

FIGURE		PAGE
1	TGA of Antimony Trisulfide	6
2	DTA and TGA of Antimony Trisulfide	7
3	DSC of Antimony Trisulfide	9
4	DSC of Antimony Trisulfide	10
5	Far IR of Antimony Trisulfide	11
6	Far IR of Oxidized Antimony Trisulfide	13
7	Far IR of Oxidized Antimony Trisulfide	14
8	Far IR of Antimony Oxides	15
9	Far IR of Antimony Oxides	16
10	Mid IR of Antimony Trisulfide	17
11	Mid IR of Antimony Trisulfide	18
12	Mid IR of Antimony Trisulfide	19
13	Mid IR of Antimony Oxides	20
14	Mid IR of Antimony Oxides	21
15	DSC of Antimony Trisulfide	22
16	DSC of Antimony Trisulfide	24
17	DSC of Amorphous Antimony Trisulfide	25
18	DSC of Amorphous Antimony Trisulfide	26
19	DSC Comparison of Amorphous Antimony Trisulfide in Air Versus N <sub>2</sub>	27
20	DSC of Crystalline Antimony Trisulfide	28
21	DSC of Antimony Trisulfide and Sulfur	30

# LIST OF FIGURES (CONTINUED)

FIGURE		PAGE
22	DSC of Antimony Trisulfide and Sulfur	31
23	DSC of Sulfur	32
24	TGA of Antimony Tetrasulfide	34
25	Far IR of Antimony Tetrasulfide	35
26	DSC of Antimony Tetrasulfide	36
27	Comparison of DSC and TGA for Antimony Tetrasulfide	38
28	DSC of Released Sulfur	39
29	DSC of Antimony Tetrasulfide	40
30	Far IR of Antimony Tetrasulfide	42
31	Far IR of Antimony Tetrasulfide	43
32	Mid IR of Antimony Tetrasulfide	44
33	Mid IR of Antimony Tetrasulfide	45
34	Mid IR of Antimony Tetrasulfide	46
35	DSC of Generated Antimony Trisulfide	47
36	DSC of Generated Antimony Trisulfide	49
37	DSC of Antimony Sulfide and Sulfur	50
38	DSC of Antimony Sulfide and Sulfur	51
39	Far IR of Antimony Pentasulfide	53
40	TGA of Antimony Pentasulfide	54
41	DSC of Antimony Pentasulfide	56
42	DSC--TGA Comparison of Antimony Pentasulfide	57
43	Far IR of Antimony Pentasulfide	58

# LIST OF FIGURES (CONCLUDED)

FIGURE		PAGE
44	TGA of Antimony Pentasulfide	60
45	DTA of Antimony Pentasulfide	61
46	DSC of Antimony Pentasulfide	62
47	Far IR of Antimony Pentasulfide	63
48	Mid IR of Antimony Pentasulfide	64
49	Mid IR of Antimony Pentasulfide	65
50	DSC of Generated Amorphous Antimony Trisulfide	67
51	DSC of Generated Crystalline Antimony Trisulfide	68
52	TGA of Extracted Antimony Pentasulfide	69
53	TGA of Extracted Versus Unextracted Antimony Pentasulfide	70
54	DSC of Generated Amorphous Antimony Trisulfide	71
55	DSC of Extracted Versus Unextracted Antimony Pentasulfide	73
56	Far IR of Extracted Antimony Pentasulfide	75
57	Mid IR of Extracted Antimony Pentasulfide	76
58	Mid IR of Extracted Antimony Pentasulfide	77
59	Far IR of Extracted Antimony Pentasulfide	78
60	DSC of Generated Amorphous Antimony Trisulfide	79
61	DSC of Generated Crystalline Antimony Trisulfide	80



## SECTION I INTRODUCTION

Antimony sulfides have received attention in such areas as semiconductors, paints, polymers and lubrication. They exist in a number of different stoichiometry - crystalline  $\text{Sb}_2\text{S}_3$ , amorphous  $\text{Sb}_2\text{S}_3$ ,  $\text{Sb}_2\text{S}_4$  and  $\text{Sb}_2\text{S}_5$ . Crystalline  $\text{Sb}_2\text{S}_3$ , stibnite, is a black material consisting of ribbon-like  $(\text{Sb}_4\text{S}_6)_n$  chains. Several studies on the electrical conductivity of  $\text{Sb}_2\text{S}_3$  have been carried out in relation to usage in semiconductor systems (1 & 2). The amorphous form of  $\text{Sb}_2\text{S}_3$  is orange in color and has been said to contain excess sulfur. The structure of orange  $\text{Sb}_2\text{S}_3$ , somewhat ambiguous, was examined in a recent study (3) by x-ray powder diffraction and found not to be entirely amorphous. Thermogravimetric studies on amorphous  $\text{Sb}_2\text{S}_3$ , reveal a weight loss between 130 and 190 °C. This loss has been attributed to both removal of water and sulfur, and to sulfur oxidation (4). A transition from orange to black  $\text{Sb}_2\text{S}_3$  occurs when the amorphous form is heated under nitrogen to 270 °C. Treatment with dilute hydrochloric acid will also transform the orange form to black.

Antimony tetrasulfide, brick-red in color and amorphous in structure (6) has been studied as an extreme pressure and an antiwear additive to greases (7). It has also been looked at as a

bonded solid lubricant (8). Thermally,  $\text{Sb}_2\text{S}_4$  is reported to melt at  $510^\circ\text{C}$  and when heated for extended periods of time in nitrogen at  $525^\circ\text{C}$ , give off sulfur to form  $\text{Sb}_2\text{S}_3$ .

The pentasulfide is reddish orange in color. As with amorphous  $\text{Sb}_2\text{S}_3$ , the pentasulfide contains excess elemental sulfur. Actually, there is some doubt as to the existence of the pentasulfide. Long et al., (5) examined stibnite, amorphous  $\text{Sb}_2\text{S}_3$ , and  $\text{Sb}_2\text{S}_5$  by Mossbauer spectroscopy. Their results indicated that in all cases, antimony was present in the +3 oxidation state. Also, there was little difference in the isomer shifts or the widths at half maximum between amorphous  $\text{Sb}_2\text{S}_3$  and  $\text{Sb}_2\text{S}_5$ .

Our laboratory has been involved in a study of tribological properties of solid lubricant compacts made from mixtures of various antimony sulfides and molybdenum disulfide (9). Preliminary results have indicated that the antimony sulfides can improve the tribological performance of  $\text{MoS}_2$ ; however, the beneficial effects of the sulfides show a temperature dependence. This result has stimulated the following investigation of the thermal and oxidative properties of  $\text{Sb}_2\text{S}_3$ ,  $\text{Sb}_2\text{S}_4$ , and  $\text{Sb}_2\text{S}_5$ .

## SECTION II EXPERIMENTAL

1. Chemicals: Antimony trisulfide and antimony pentasulfide were obtained from Fisher Scientific (reagent grade) and used as received. Antimony tetrasulfide was obtained from Dr J. King of Penwalt Corp and also used as received. The oxides of antimony--trioxide, tetra-oxide and penta-oxide were from Alpha Chemicals (ultrapure 99.99 percent). The dimorphs of the trioxide were obtained by the following method. Samples of the trioxide were placed in a platinum cylinder, sealed in quartz under argon (0.2 atm) and heated to a specific temperature for 2 hours then rapidly cooled to room temperature. To obtain the cubic form, the sample was heated to 590 °C and the orthorhombic 620 °C. Reagent grade sulfur was purchased from Fisher Scientific. All materials were sieved through a 30-micron filter to ensure uniform particle size.

2. Infrared Spectroscopy: Infrared data were collected on a Nicolet 740 spectrometer. Samples were run as polyethylene disks. Each sample was run for a total of 64 scans at 4 cm<sup>-1</sup> resolution.

3. Thermal analysis: Thermal experiments were performed on a Dupont 2100 thermal analysis system consisting of thermogravimetric analysis (TGA), differential scanning calorimetry (DSC), and high temperature differential thermal

analysis (DTA). In TGA experiments, sample sizes were kept between 20 and 25 mg, and run in platinum pans under dynamic atmospheres (200 ml/min). DSC was performed on samples ranging from 3 to 4 mg for  $\text{Sb}_2\text{S}_5$ ,  $\text{Sb}_2\text{S}_4$ , and the antimony oxides. Due to the increased density of  $\text{Sb}_2\text{S}_3$ , sample sizes were between 5 and 6 mg to insure complete coverage of the sample pan. Samples were run in aluminum hermetically sealed pans with inverted lids. Pinholes were placed in the lids to allow equilibration with the DSC environment. Flow rates were kept high (250 ml/min) to purge the system of corrosive gases formed during heating. Samples run under nitrogen were allowed to equilibrate for a minimum of 15 minutes. For DTA experiments, alumina sample cups were used with sample sizes kept between 10 and 20 mg. In all thermal experiments, unless otherwise stated, temperature scan rates were 20 °C per minute.

### SECTION III RESULTS AND DISCUSSION

#### 1.0 Antimony trisulfide ( $\text{Sb}_2\text{S}_3$ )

Antimony trisulfide is a black solid, thermally stable to  $575^\circ\text{C}$  under an inert atmosphere as evidenced by TGA. (See Figure 1.) At temperatures above  $575^\circ\text{C}$ ,  $\text{Sb}_2\text{S}_3$  undergoes a reaction with the TGA's platinum sample pan resulting in a rapid weight loss. When  $\text{Sb}_2\text{S}_3$  is heated in the presence of air, a series of reactions occur. Four distinct areas of weight change are observed: weight losses between  $300$  and  $425^\circ\text{C}$ ;  $425$  and  $500^\circ\text{C}$ ;  $525$  and  $600^\circ\text{C}$ ; and a slight increase from  $600$  to  $625^\circ\text{C}$ .

Examining the oxidation via high temperature DTA, one finds at least two exotherms -  $446$  and  $604^\circ\text{C}$ . (See Figure 2.) The  $446^\circ\text{C}$  peak is asymmetric and has a shoulder at  $400^\circ\text{C}$  indicating the presence of multiple overlapping exotherms. This exotherm lies in the temperature region as the first two areas of weight loss ( $300$  and  $500^\circ\text{C}$ ) in the TGA. The exotherm at  $604^\circ\text{C}$  coincides with the third weight loss and the small weight gain in the TGA. This peak agrees with the literature value for the oxidation of  $\text{Sb}_2\text{O}_3$  to  $\text{Sb}_2\text{O}_4$  (10). On going from  $\text{Sb}_2\text{O}_3$  to  $\text{Sb}_2\text{O}_4$ , one would expect a weight gain in the TGA; however, a loss is observed followed by a small gain and then stabilization. This is explained by a combination of  $\text{Sb}_2\text{O}_3$  sublimation and oxidation which forms a layer of  $\text{Sb}_2\text{O}_4$  retarding further oxidation and

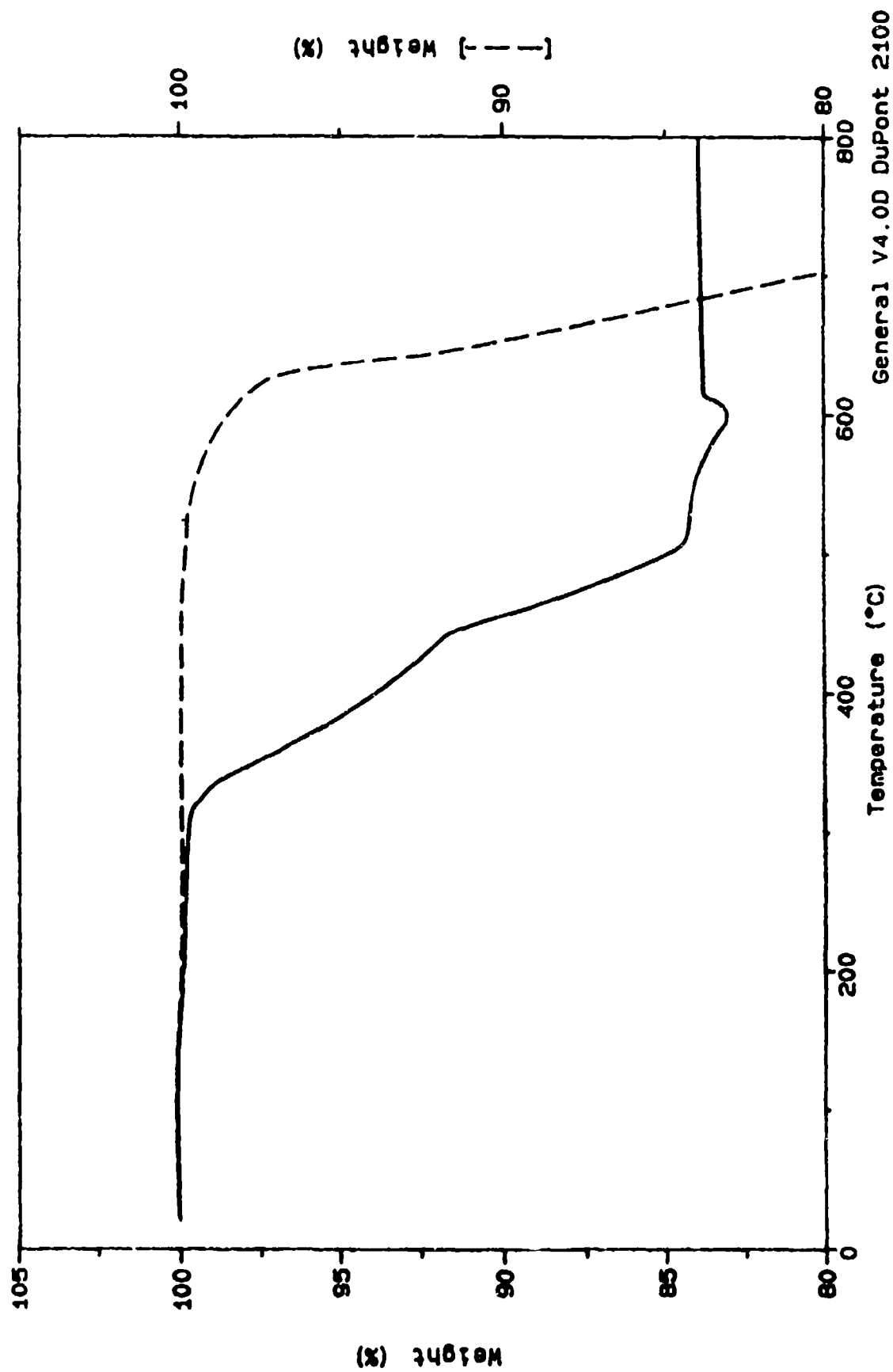


Figure 1. TGA of  $Sb_2S_3$  (—) Air; (---)  $N_2$ .

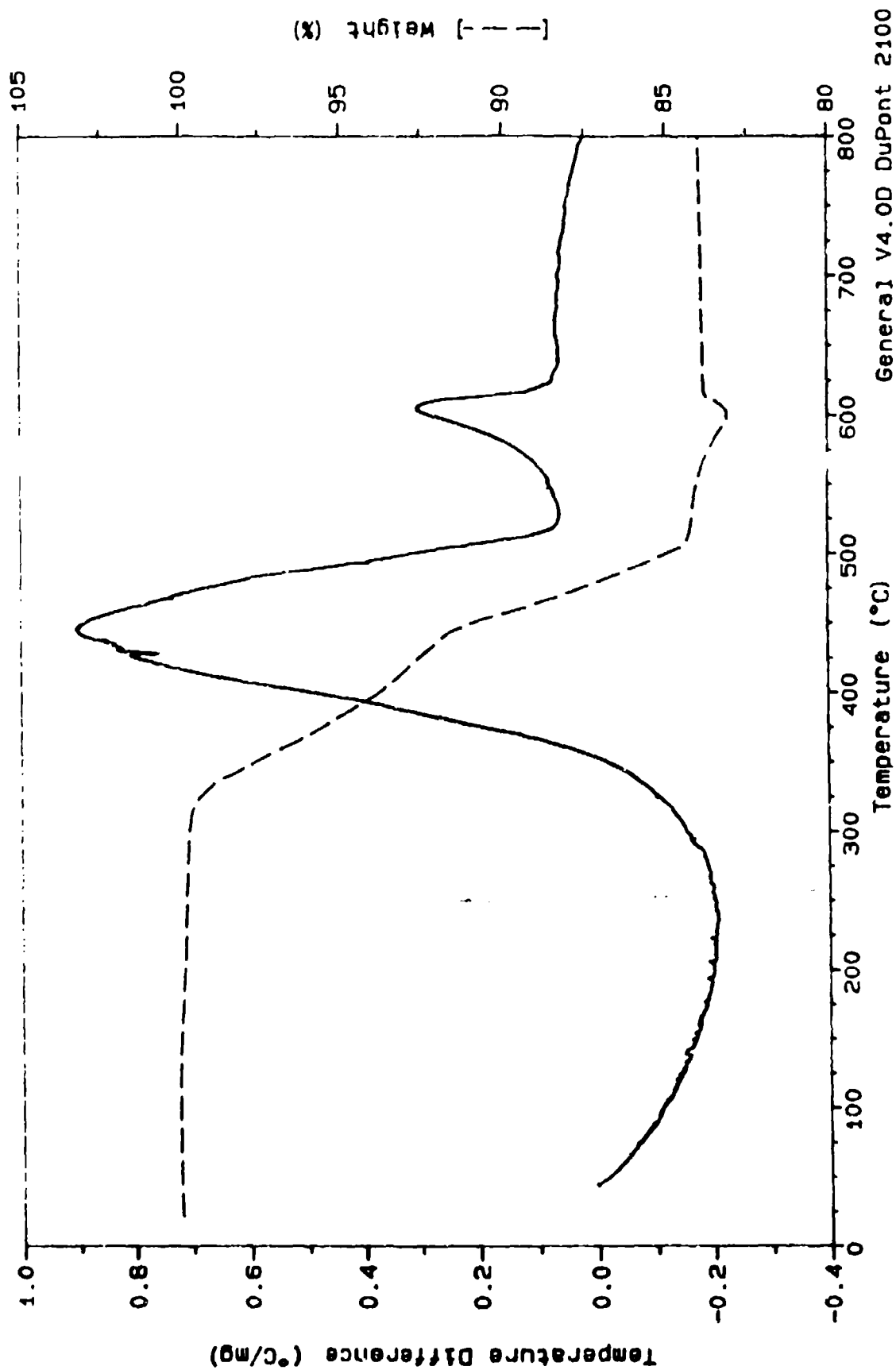


Figure 2. DTA of  $\text{Sb}_2\text{S}_3$  (—) Air; TGA (----) Air.

sublimation. Centers (11) has shown that the oxidation of cubic  $\text{Sb}_2\text{O}_3$  occurs by a sublimation controlled mechanism.

Assignment of the 604 °C exotherm to the oxidation of  $\text{Sb}_2\text{O}_3$  to  $\text{Sb}_2\text{O}_4$  indicates that the previous exotherm at 400 °C and the weight losses between 300 and 500 °C must correspond to the oxidation of  $\text{Sb}_2\text{S}_3$  to  $\text{Sb}_2\text{O}_3$ . The complex nature of both the TGA and the DTA curves points to a multistep process. When the oxidation is examined by DSC - a more sensitive technique at lower temperatures than the DTA (Figure 3), two peaks are observed: 434 °C with shoulders at 360 °C; 407 °C; and 473 °C with shoulders at 484 °C and 495 °C. When a smaller sample size is used (1.8 mg), the peaks are further resolved. (See Figure 4.) The first exotherm shifts to 394 °C with a shoulder at 356 °C, and the higher temperature peak splits into two - 463 and 476 °C with a shoulder at 491 °C.

In an attempt to better understand the oxidation of  $\text{Sb}_2\text{S}_3$ , a series of isothermal TGAs (3h in air or nitrogen) were run at various temperatures corresponding to different portions of the DSC/DTA curves. The products were then examined by fourier transform infrared (FTIR) spectroscopy. Figure 5 shows the far IR spectra of  $\text{Sb}_2\text{S}_3$  and  $\text{Sb}_2\text{S}_3$  thermally stressed at 275 °C in  $\text{N}_2$ .  $\text{Sb}_2\text{S}_3$  has characteristic bands at 336, 274, 242, and 138  $\text{cm}^{-1}$ . Thermal stressing results in no observable changes to the IR spectrum.



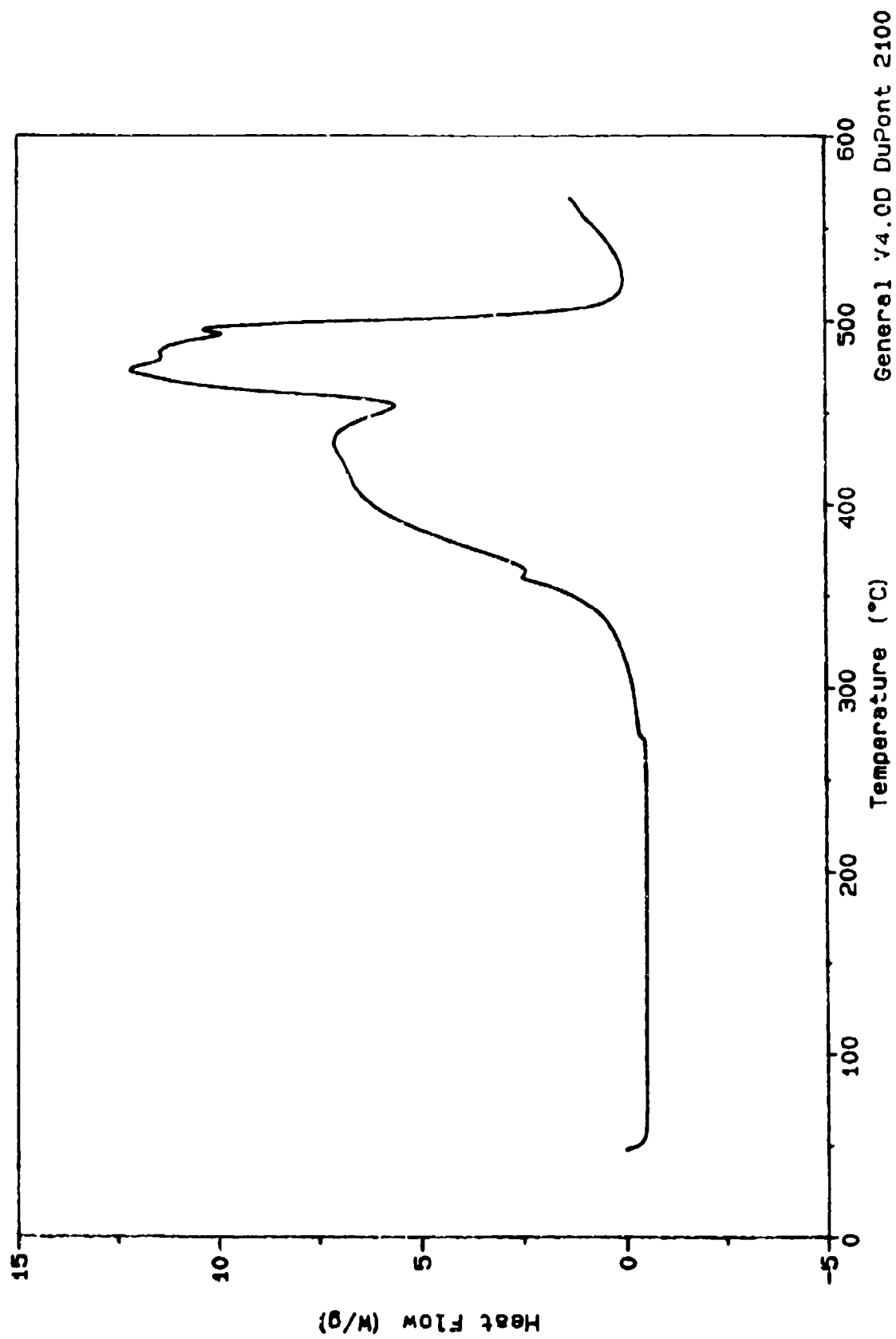


Figure 3. DSC of  $\text{Sb}_2\text{S}_3$  in Air.

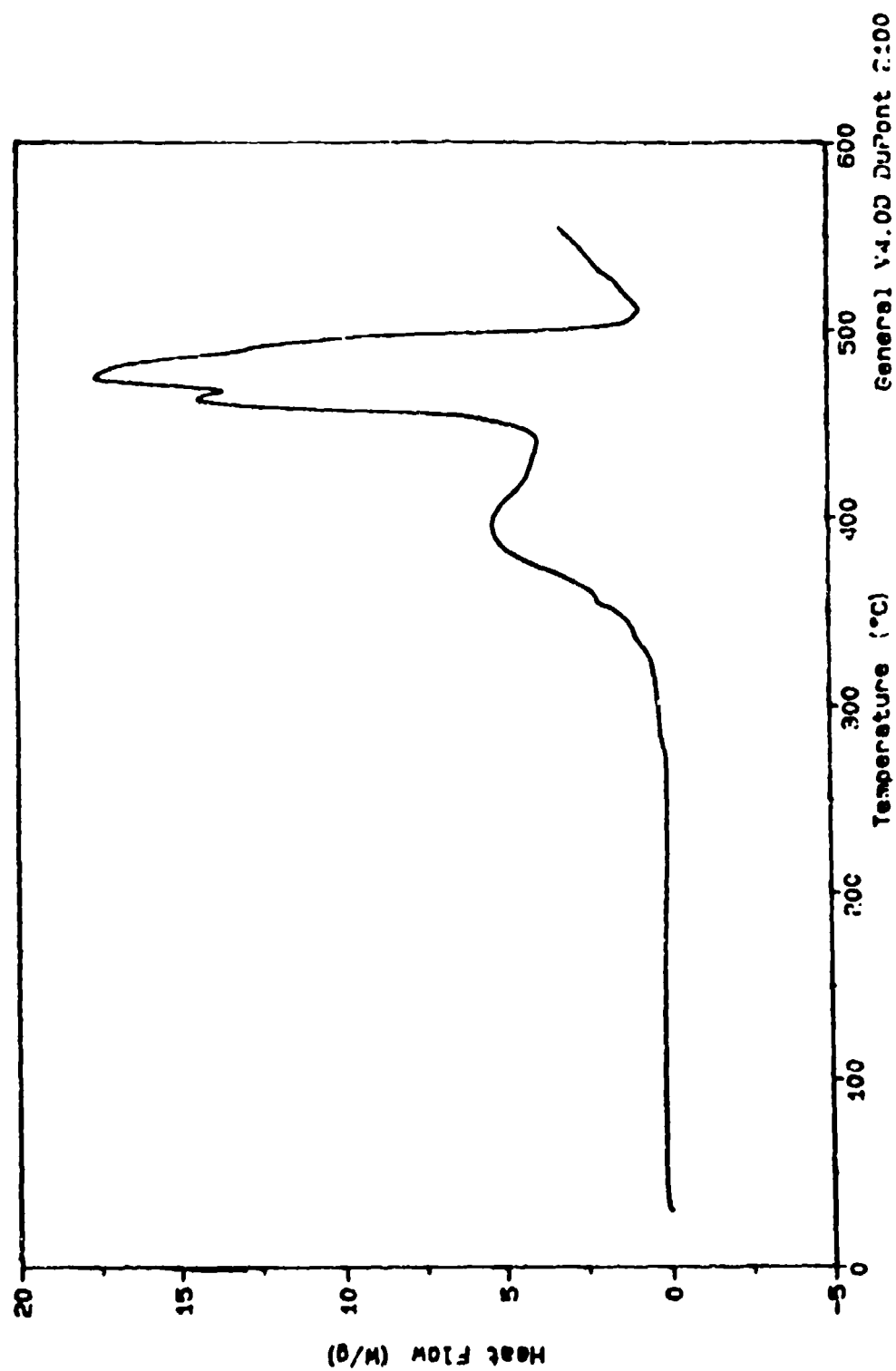


Figure 4. DSC of 1.8 mg Sample of  $\text{Sb}_2\text{S}_3$ .

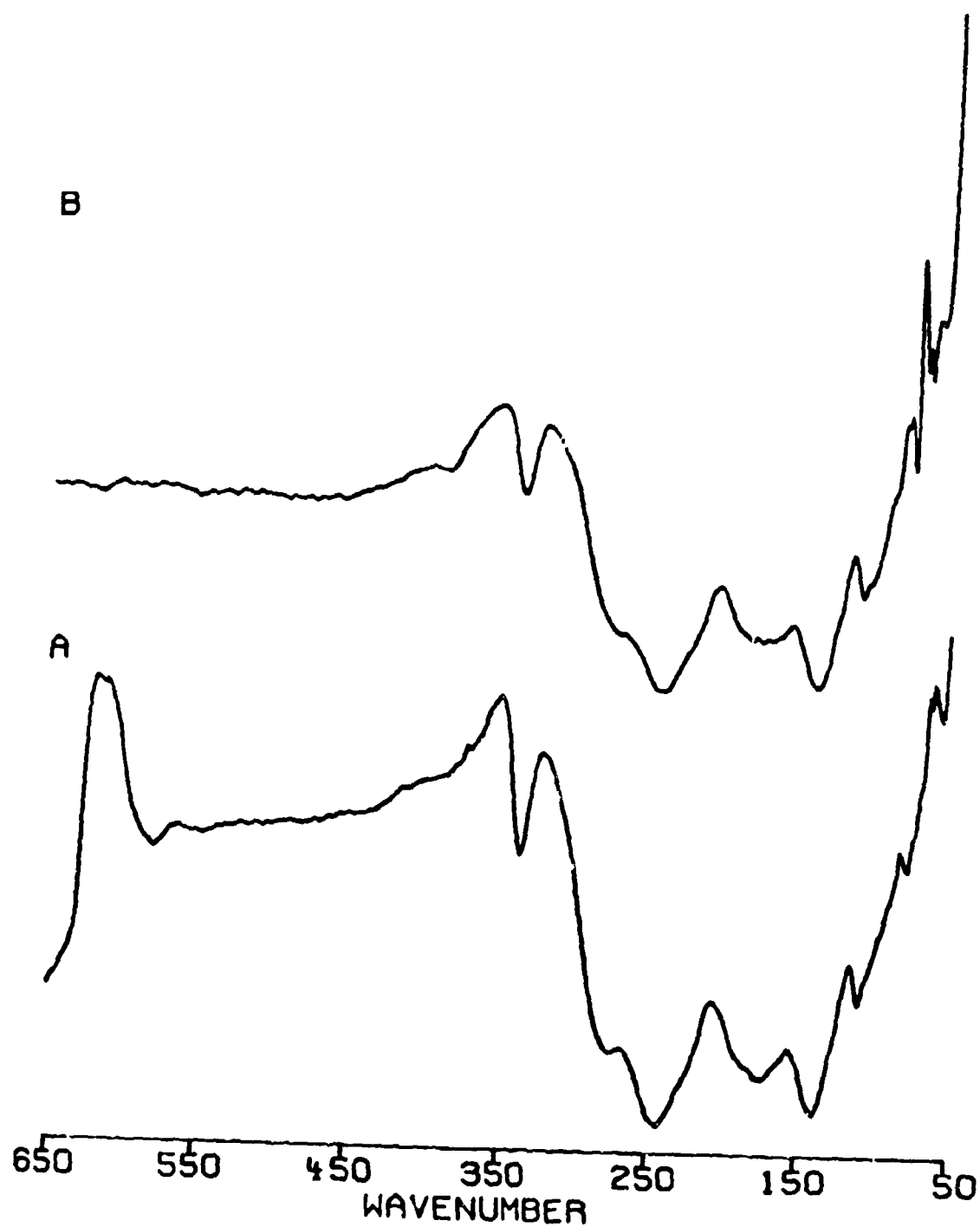


Figure 5. Far IR of  $\text{Sb}_2\text{S}_3$  (A) Virgin; (B) Heated at 275°C in  $\text{N}_2$ .

When  $\text{Sb}_2\text{S}_3$  is heated in air at 400 and 480 °C, a number of changes occur. (See Figure 6.) The characteristic bands of  $\text{Sb}_2\text{S}_3$  disappear and are replaced with bands at 384, 259, and 180  $\text{cm}^{-1}$ . Heating at 525 °C (Figure 7) produces the same spectrum as the samples heated at 400 and 480 °C; however, heating at 800 °C results in the production of a new material showing bands at 529, 443, 365, and 287  $\text{cm}^{-1}$ .

Comparing the spectra of the oxidation products in Figures 6 & 7 with those of the known antimony oxides - cubic and orthorhombic  $\text{Sb}_2\text{O}_3$ ,  $\text{Sb}_2\text{O}_4$ , and  $\text{Sb}_2\text{O}_5$  (Figures 8 & 9), one finds that oxidation at temperatures below the 504 °C exotherm leads to the formation of cubic  $\text{Sb}_2\text{O}_3$  and temperatures above 600 °C forms  $\text{Sb}_2\text{O}_4$ .

Examination of these samples in the mid IR, reveals an interesting band at about 1100  $\text{cm}^{-1}$  for the samples heated in air at temperatures below 600 °C. (See Figures 10 & 11.) This band is absent in virgin  $\text{Sb}_2\text{S}_3$  and the sample heated to 800 °C. It is also absent in the nitrogen heated  $\text{Sb}_2\text{S}_3$ . (See Figure 12.) In addition, the band is not seen in any of the oxides. (See Figures 13 & 14.) This band is characteristic of sulfate containing compounds (12) and suggests that  $\text{Sb}_2\text{S}_3$  oxidation goes through a sulfate containing intermediate.

Results of a DSC experiment carried out under nitrogen are shown in Figure 15. A broad endotherm at 510 °C with a shoulder at 491 °C (corresponding to the melting of  $\text{Sb}_2\text{S}_3$ ) is observed.

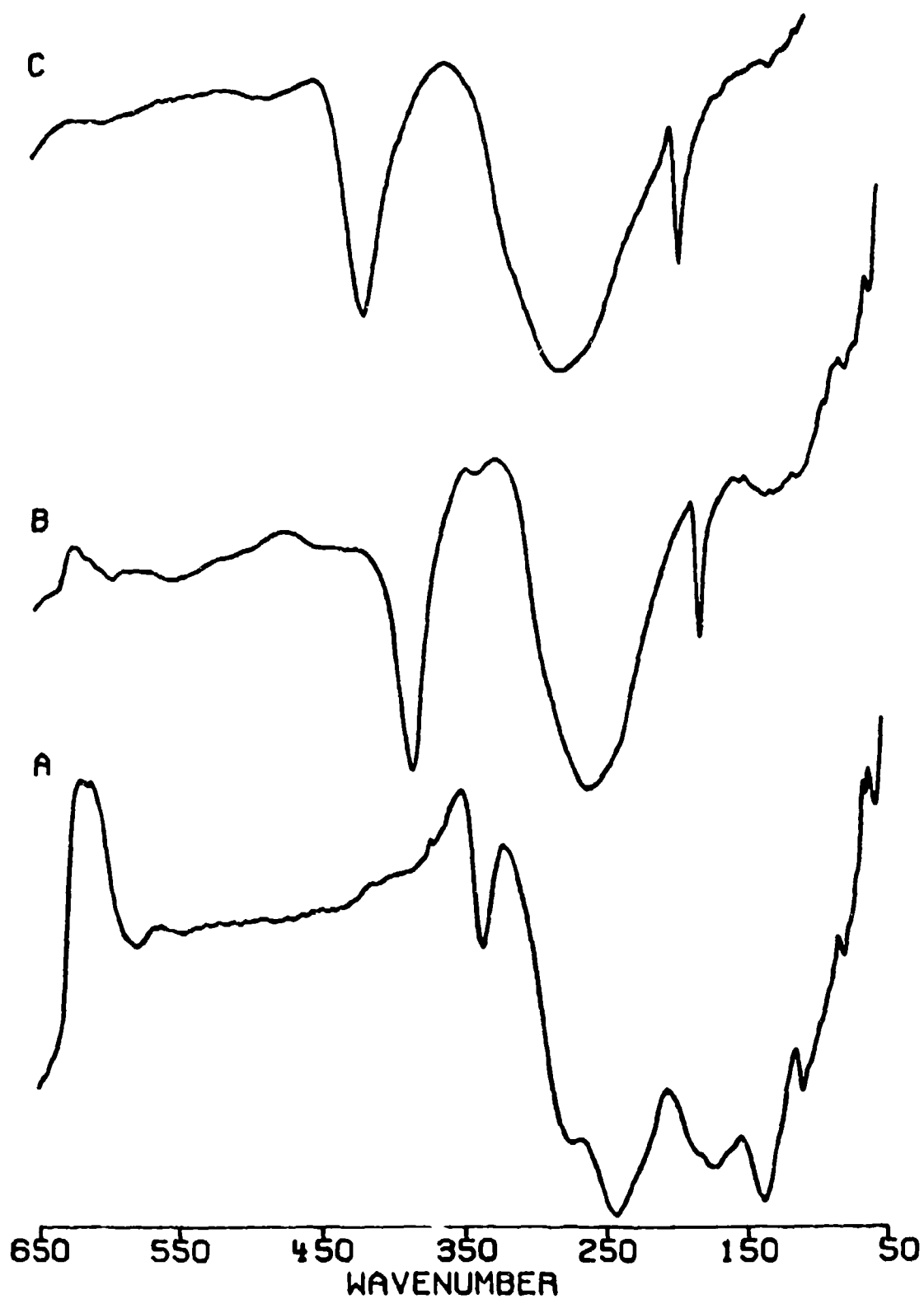


Figure 6. Far IR of Oxidized  $\text{Sb}_2\text{S}_3$  (A) Virgin; (B) 400°C in Air;  
(C) 480°C in Air.

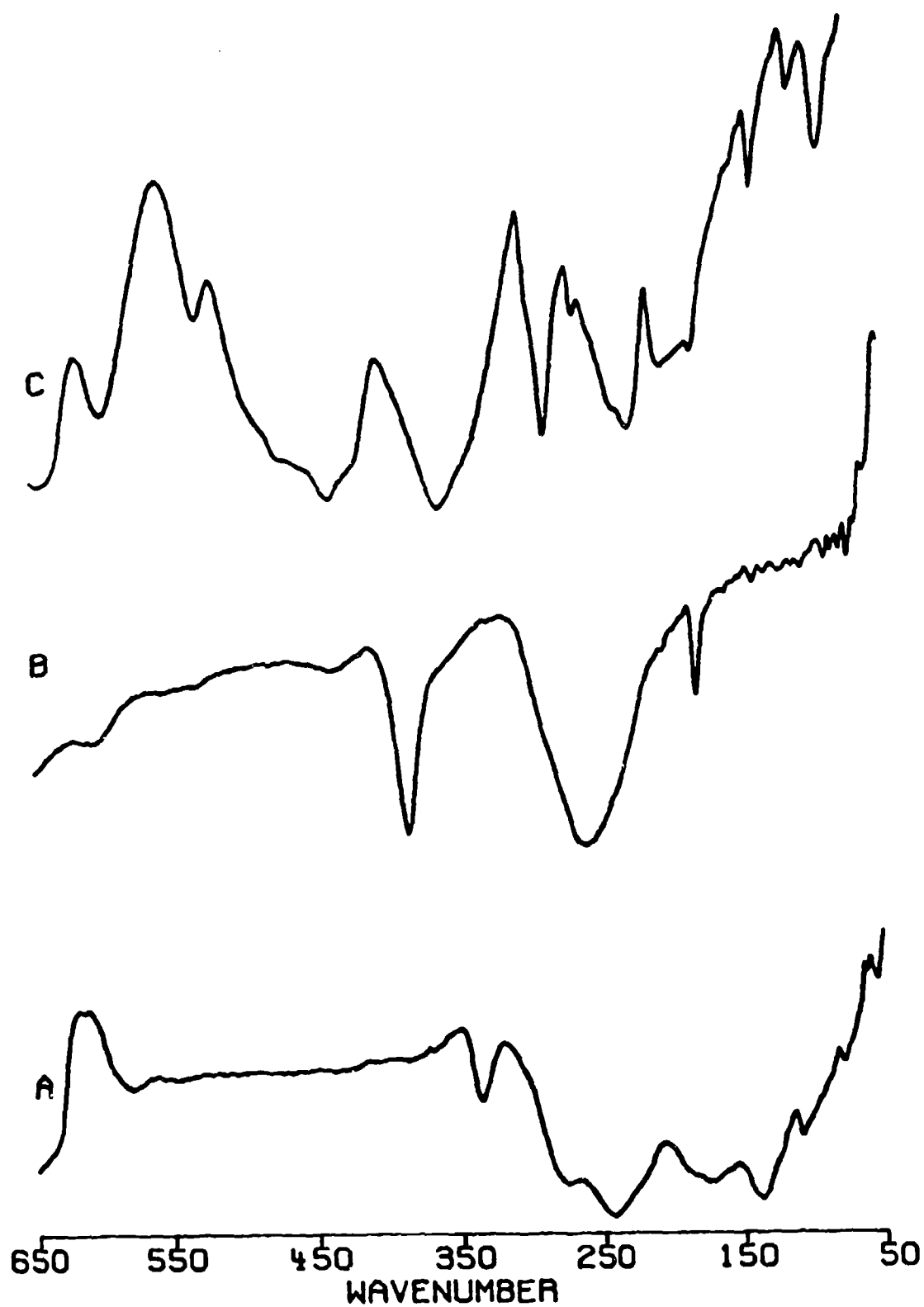


Figure 7. Far IR of Oxidized  $\text{Sb}_2\text{S}_3$  (A) Virgin; (B) 525°C in Air;  
(C) 800°C in Air.

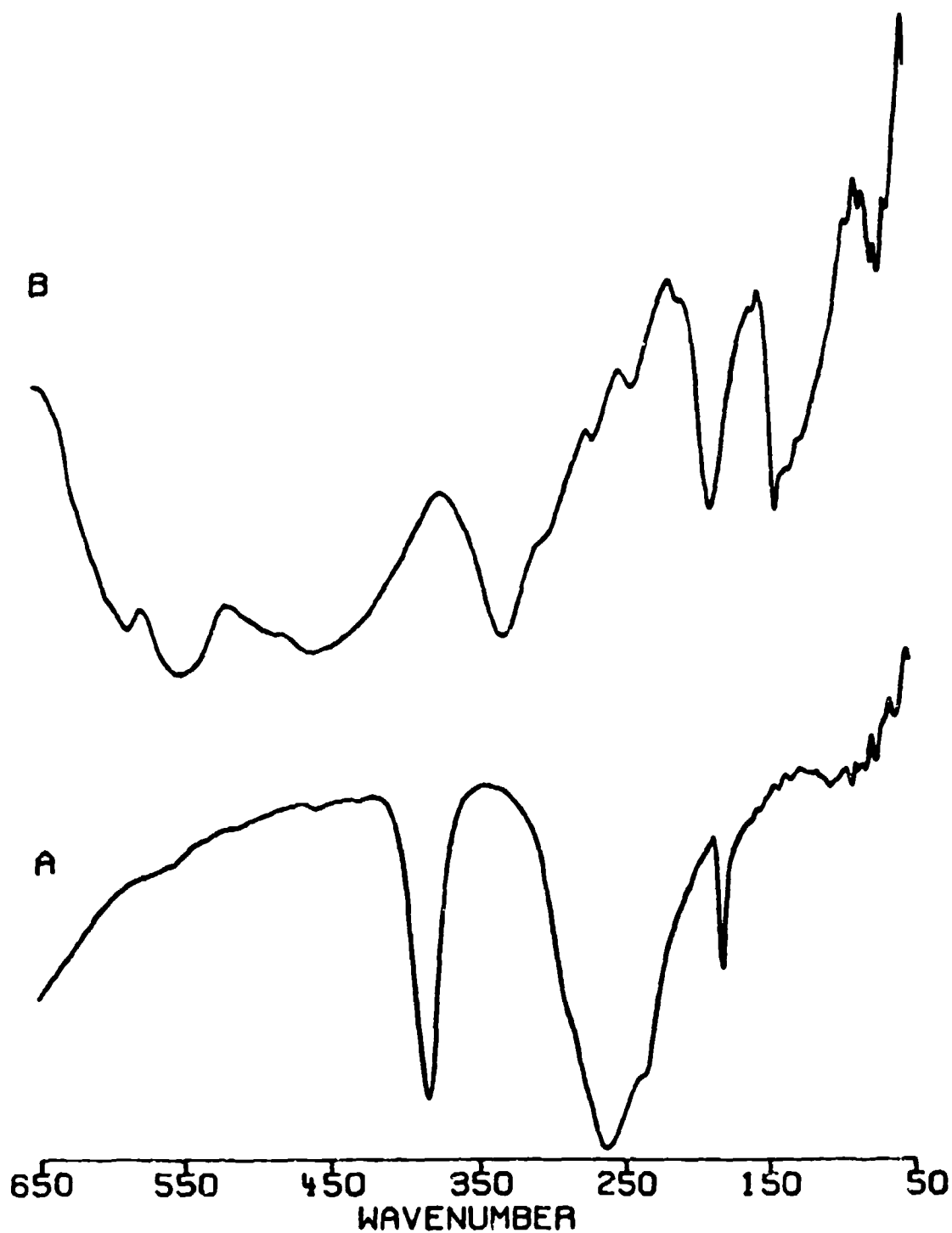


Figure 8. Far IR of Antimony Oxides (A) Cubic  $\text{Sb}_2\text{O}_3$ ; (B) Orthorhombic  $\text{Sb}_2\text{O}_3$ .

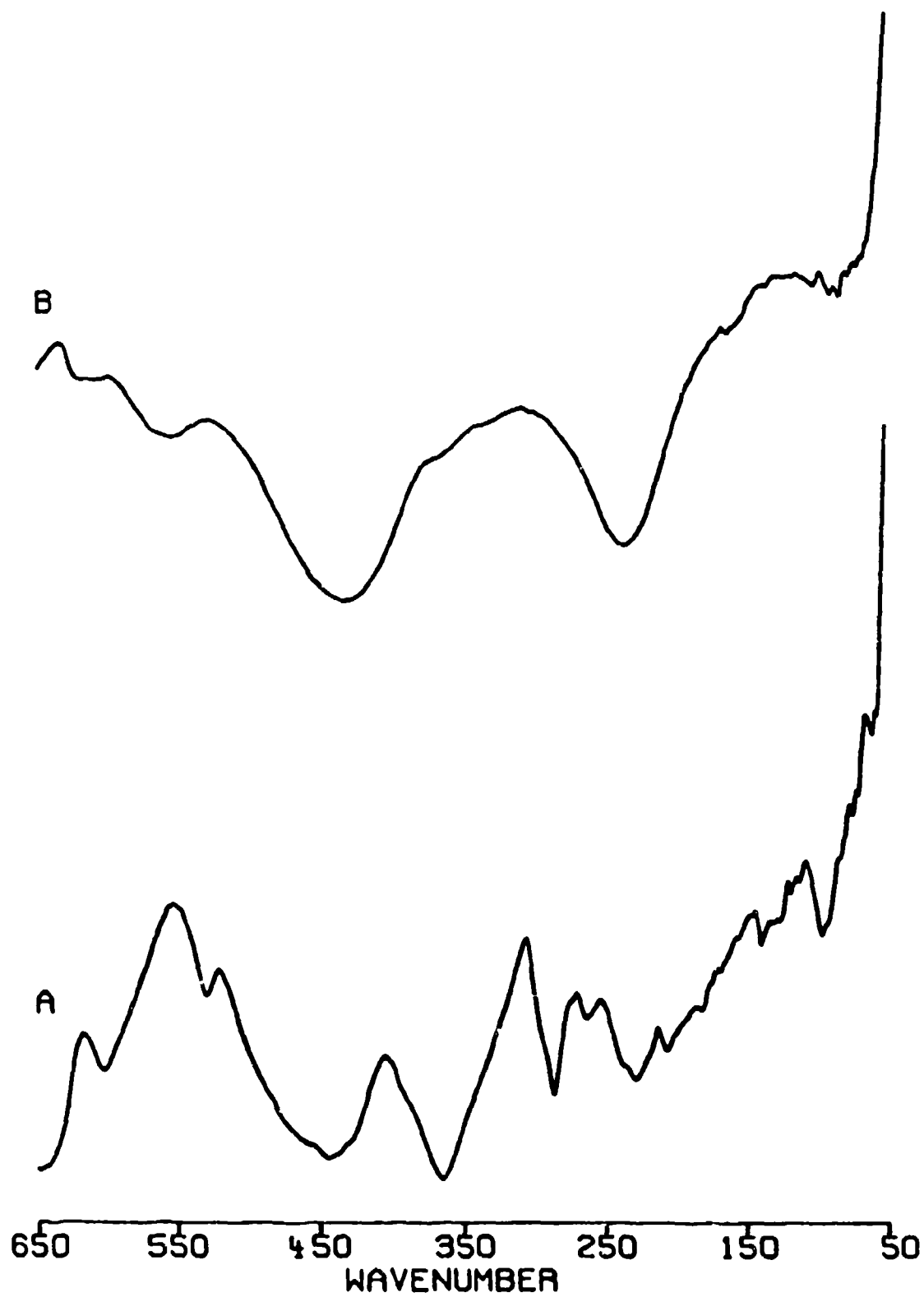


Figure 9. Far IR of Antimony Oxides (A)  $\text{Sb}_2\text{O}_4$ ; (B)  $\text{Sb}_2\text{O}_5$ .



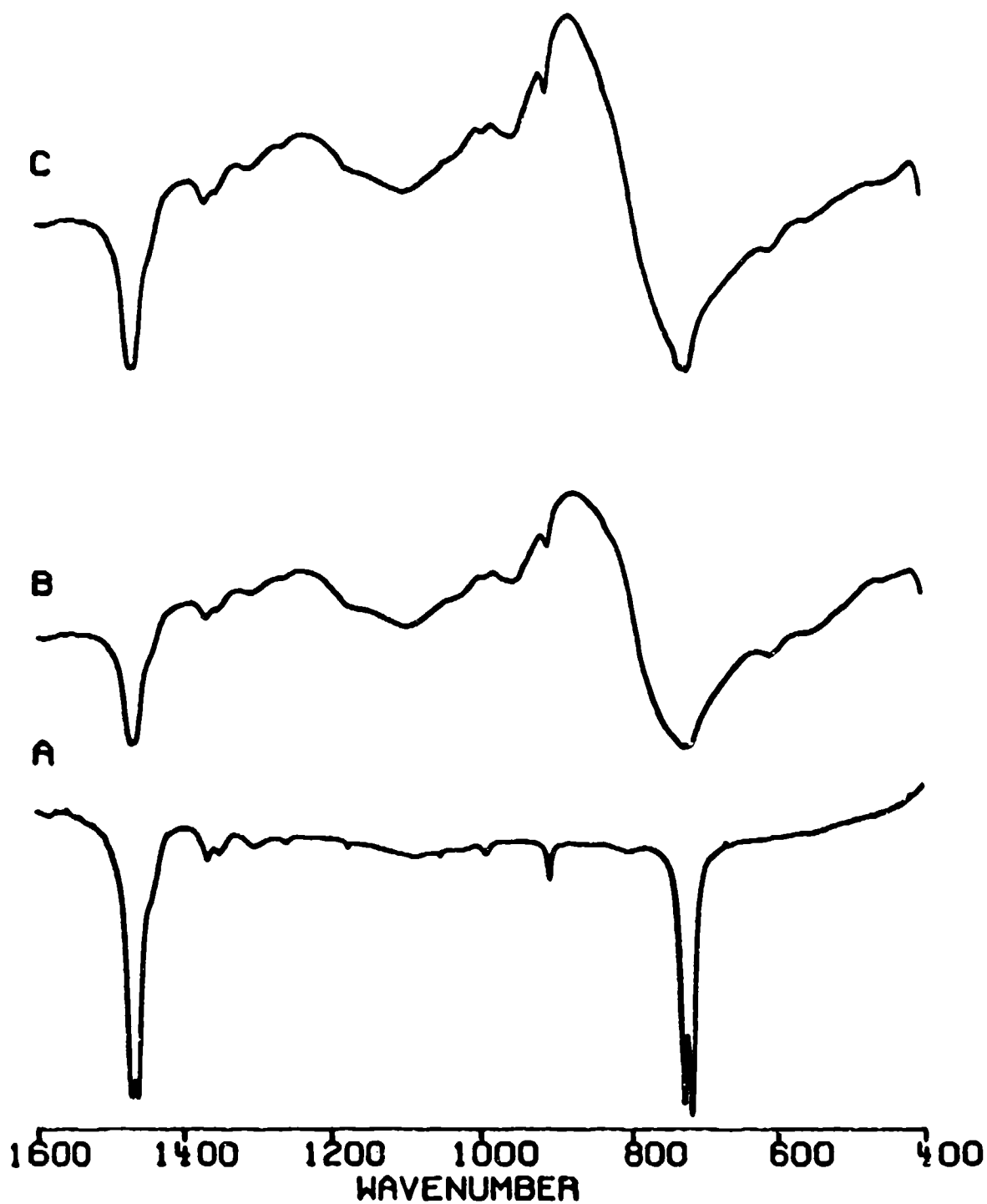


Figure 10. Mid IR of Antimony Trisulfide (A) Virgin; (B) 400°C in Air; (C) 430°C in Air.

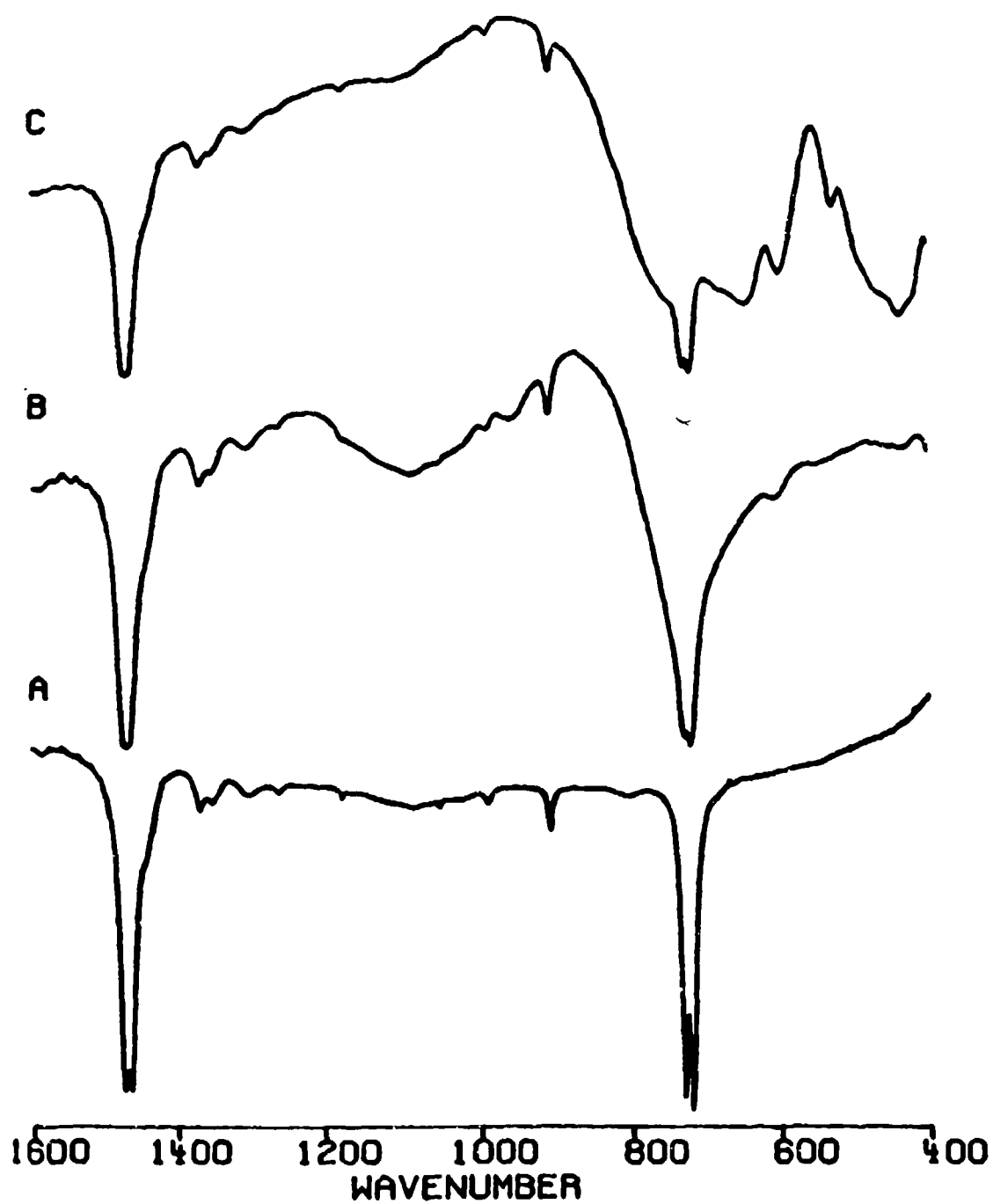


Figure 11. Mid IR of Antimony Trisulfide (A) Virgin; (B) 525°C in Air; (C) 800°C in Air.

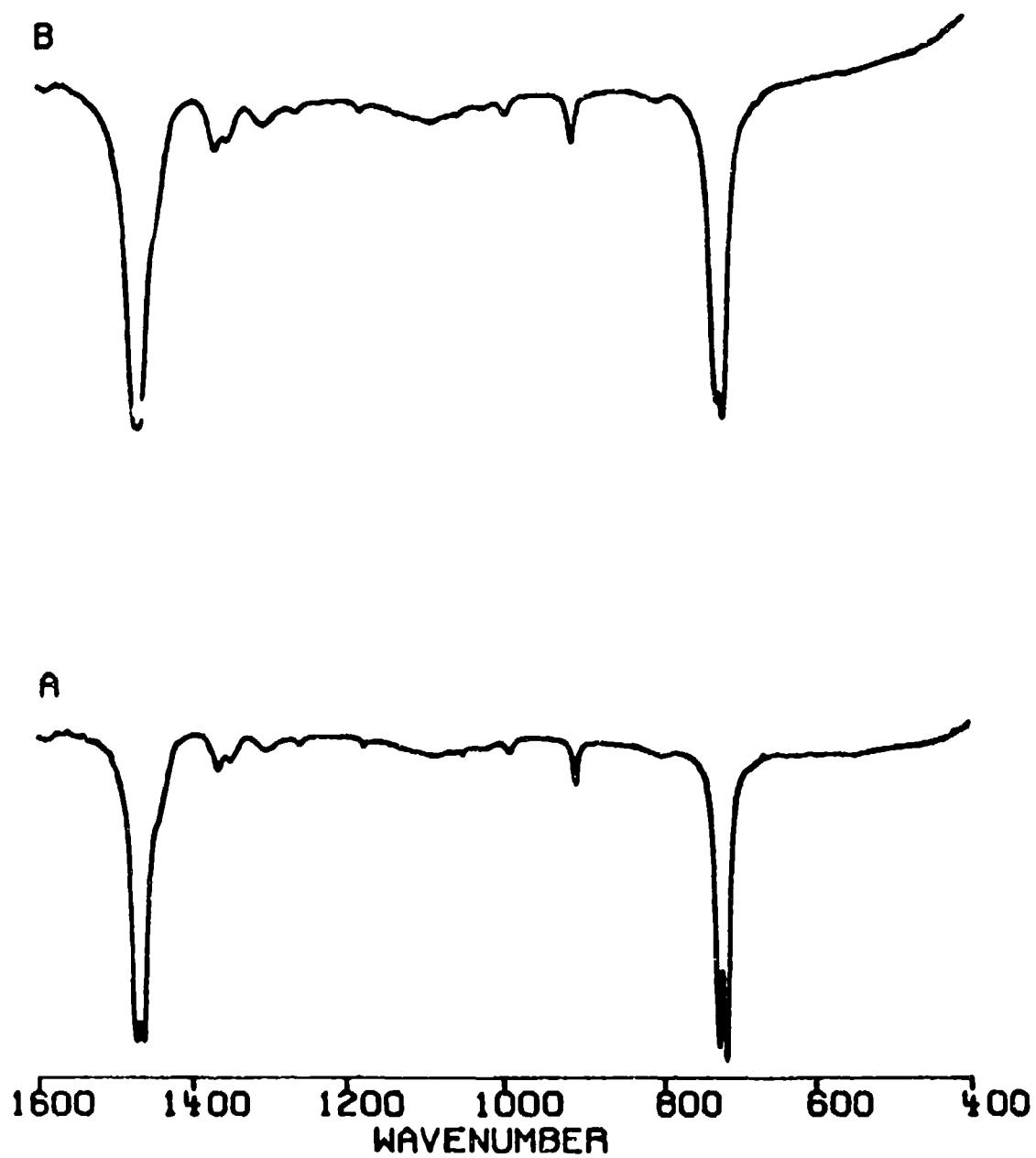


Figure 12. Mid IR of Antimony Trisulfide (A) Virgin; (B) 275°C in N<sub>2</sub>.

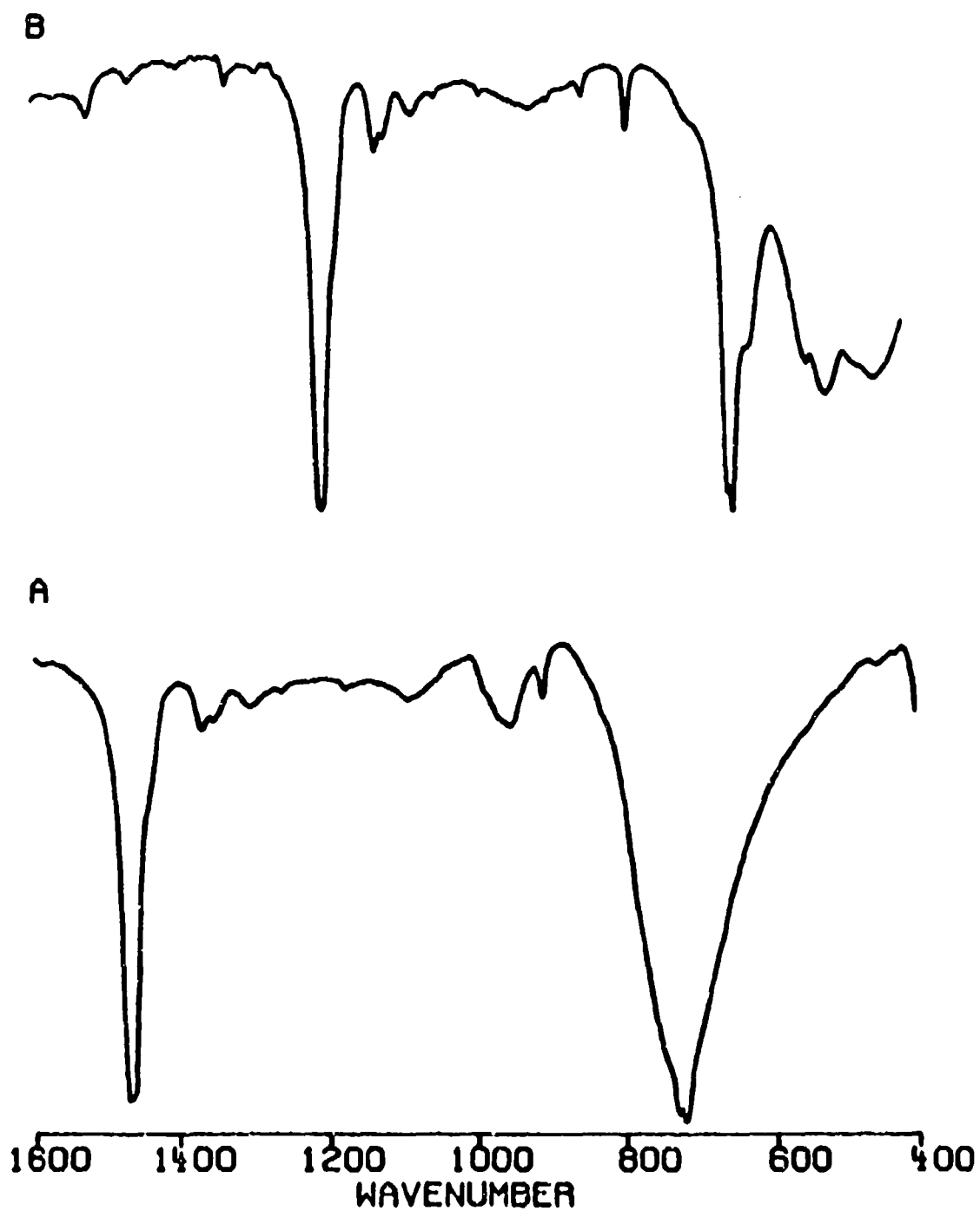


Figure 13. Mid IR of Antimony Oxides (A) Cubic  $\text{Sb}_2\text{O}_3$ ;  
(B) Orthorhombic  $\text{Sb}_2\text{O}_3$ .

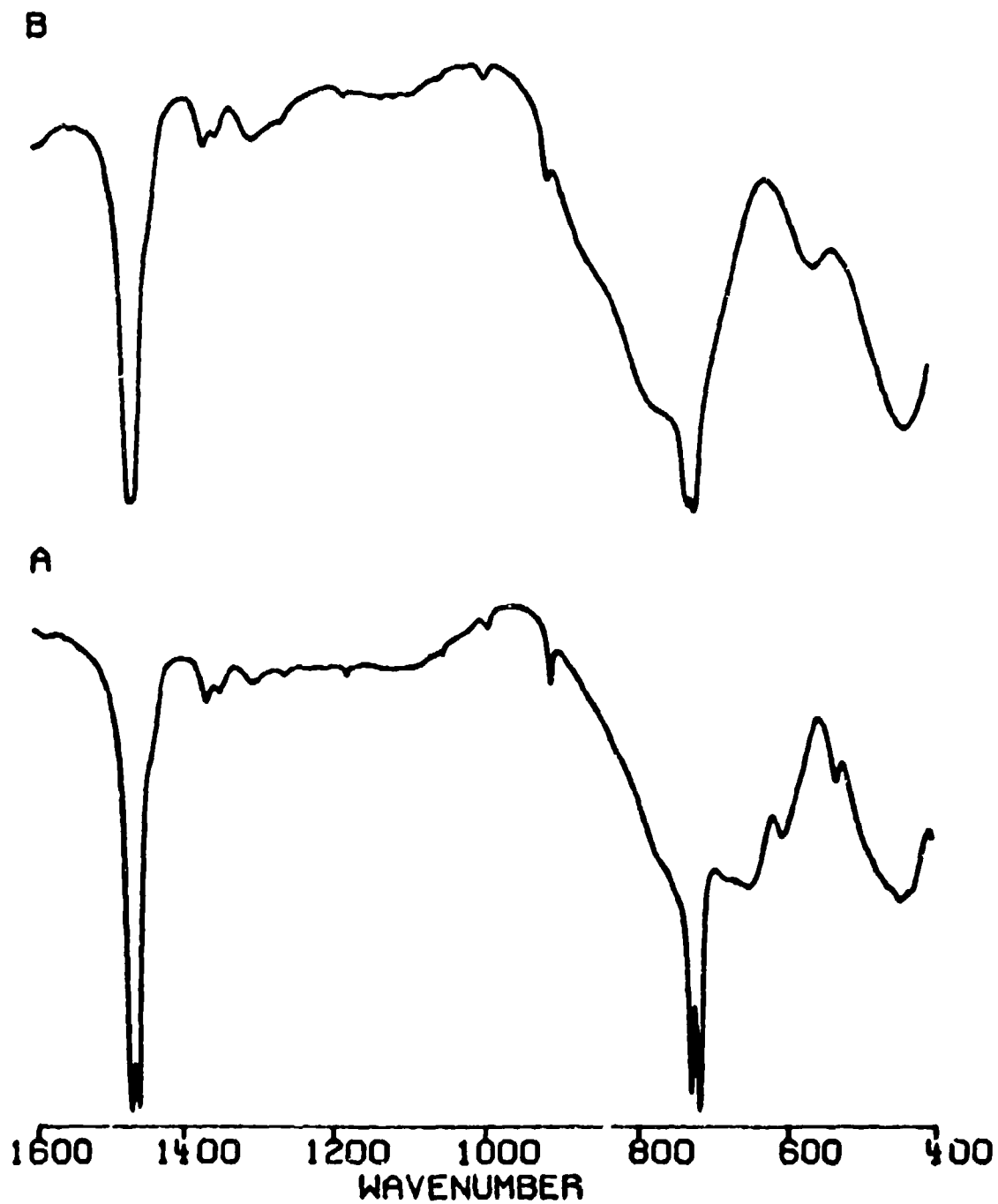


Figure 14. Mid IR of Antimony Oxides (A)  $\text{Sb}_2\text{O}_4$ ; (B)  $\text{Sb}_2\text{O}_5$ .

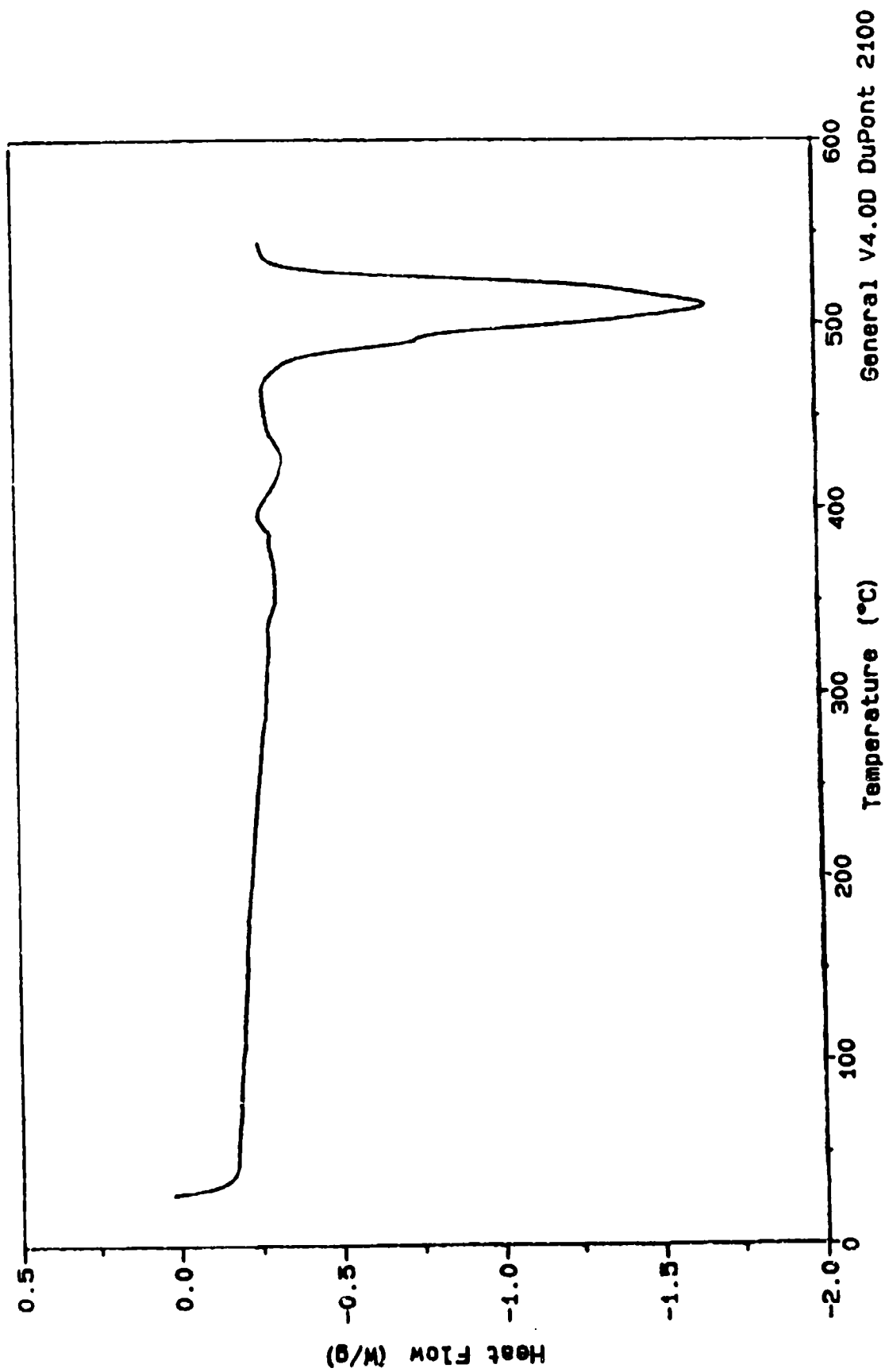


Figure 15. DSC of  $\text{Sb}_2\text{S}_3$  in  $\text{N}_2$ .

This is lower than the literature value of 566 °C (13) and somewhat broader than one would expect for a melting. One possible explanation may be a reaction with the sample pan similar to that seen in TGA experiments. To test this, a sample was run in a gold pan. (See Figure 16.) The endotherm was sharper; however, the shoulder at 491 °C remained - indicating some reaction with the aluminum pan. Melting endotherms in general are dependent on factors such as particle size and structure. The presence of small amounts of amorphous  $\text{Sb}_2\text{S}_3$ , impurities, thermal decompositions and/or reaction with the sample pan could contribute to broadening of melting endotherms.

When  $\text{Sb}_2\text{S}_3$  is run in the DSC to temperatures above the melt, rapidly cooled to room temperature and rerun, the following curve is obtained. (See Figure 17.) The rapidly cooled  $\text{Sb}_2\text{S}_3$  has a glass transition at 232 °C followed by a heat of crystallization (69.1 J/g) at 318 °C. The melting endotherm splits into two distinct peaks - 497 and 514 °C with a shoulder at 522 °C. Repeating the cooling procedure and rerunning in air (Figure 18), yields the same glass transition and crystallization followed by oxidation. The two peaks at 488 and 507 °C are the result of a combination of the oxidation exotherms and the melting of unoxidized  $\text{Sb}_2\text{S}_3$ . (See Figure 19.) When  $\text{Sb}_2\text{S}_3$  is allowed to cool slowly from a melt, it solidifies into a crystalline form as evidenced from the lack of a glass transition or crystallization exotherm. (See Figure 20.)

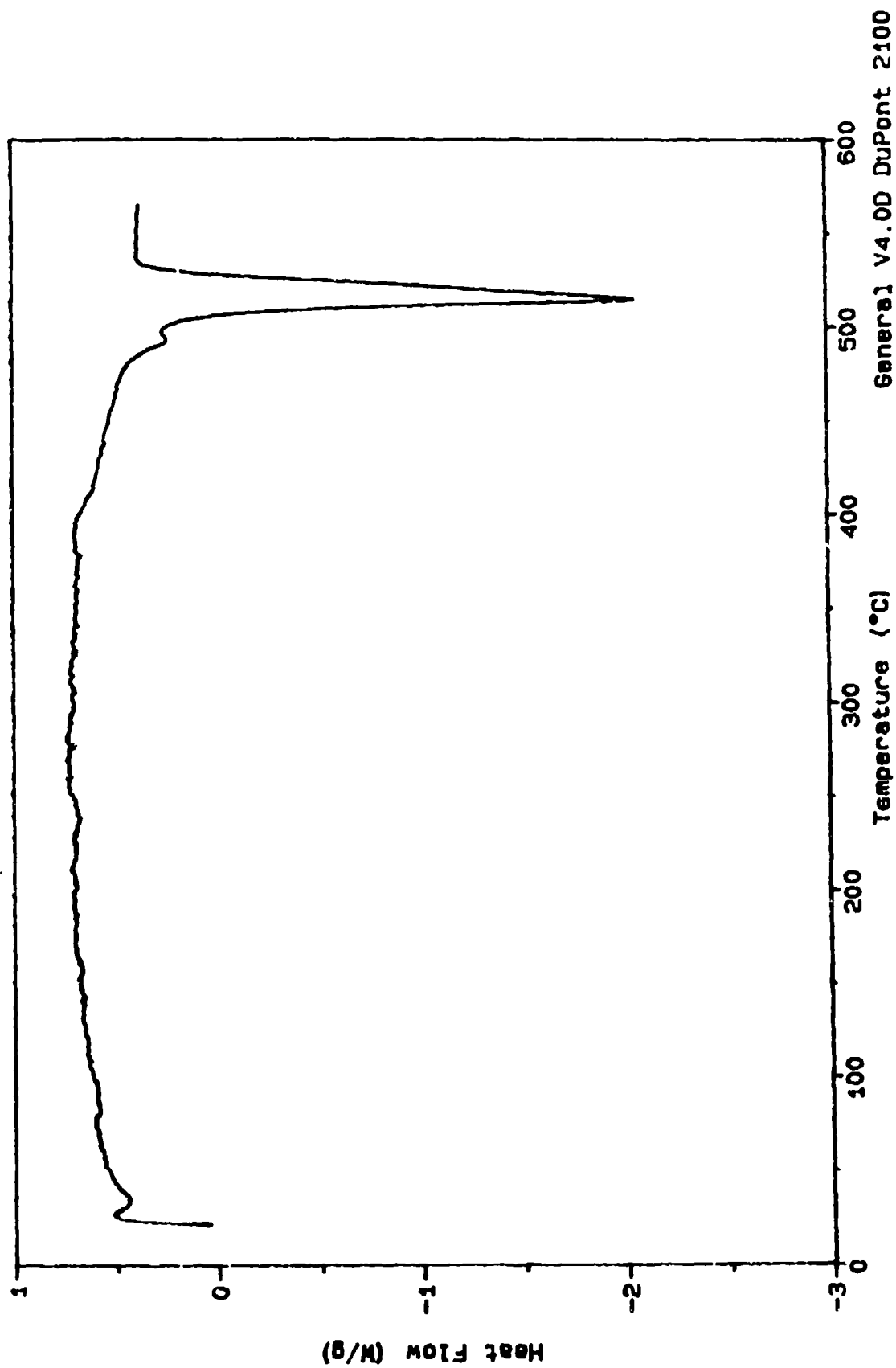


Figure 16. DSC of  $\text{Sb}_2\text{S}_3$  in  $\text{N}_2$ , Cold Sample Pan.



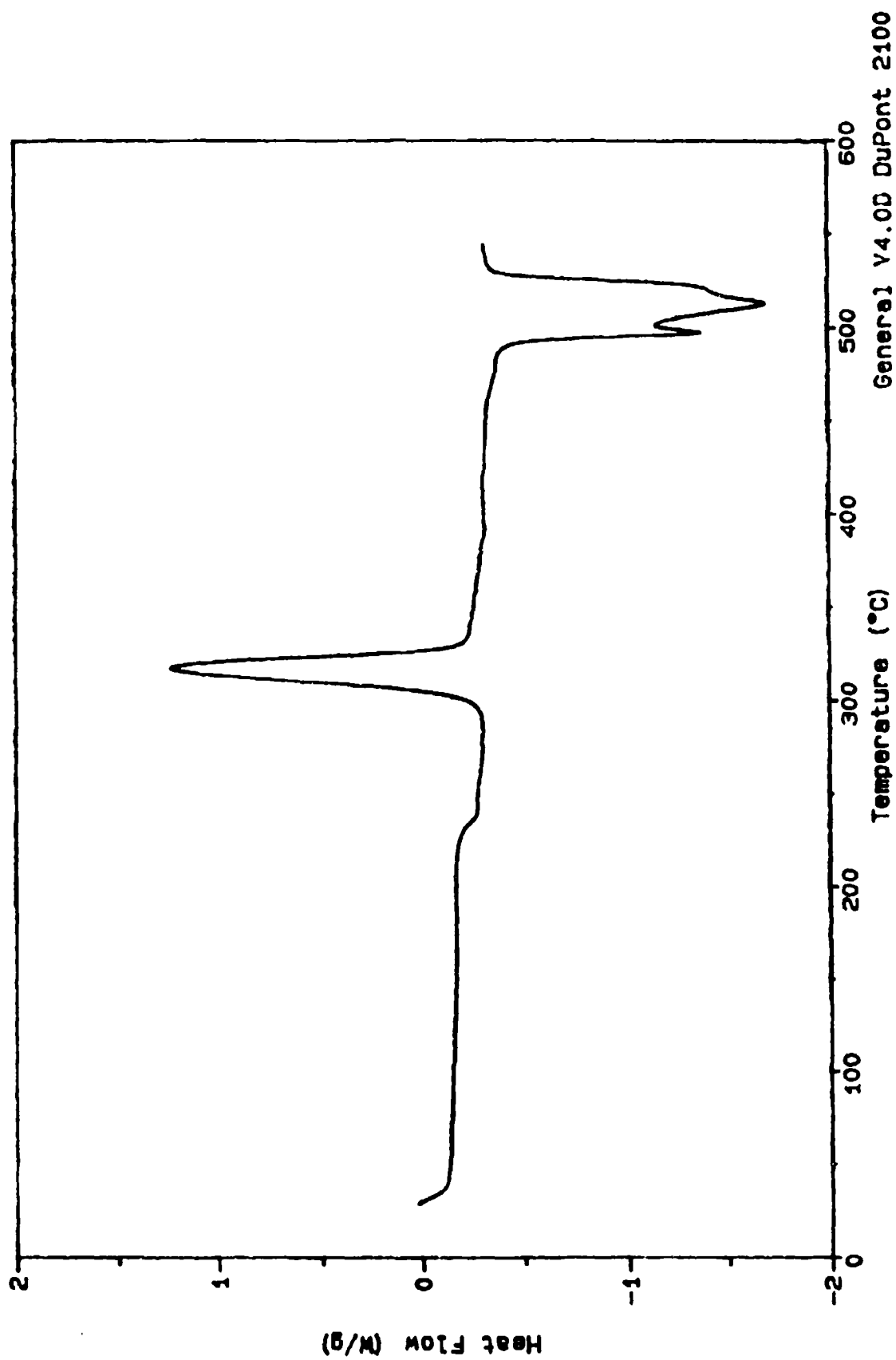


Figure 17. DSC of Amorphous  $\text{Sb}_2\text{S}_3$ , (Rapidly Cooled from Melt), in  $\text{N}_2$ .

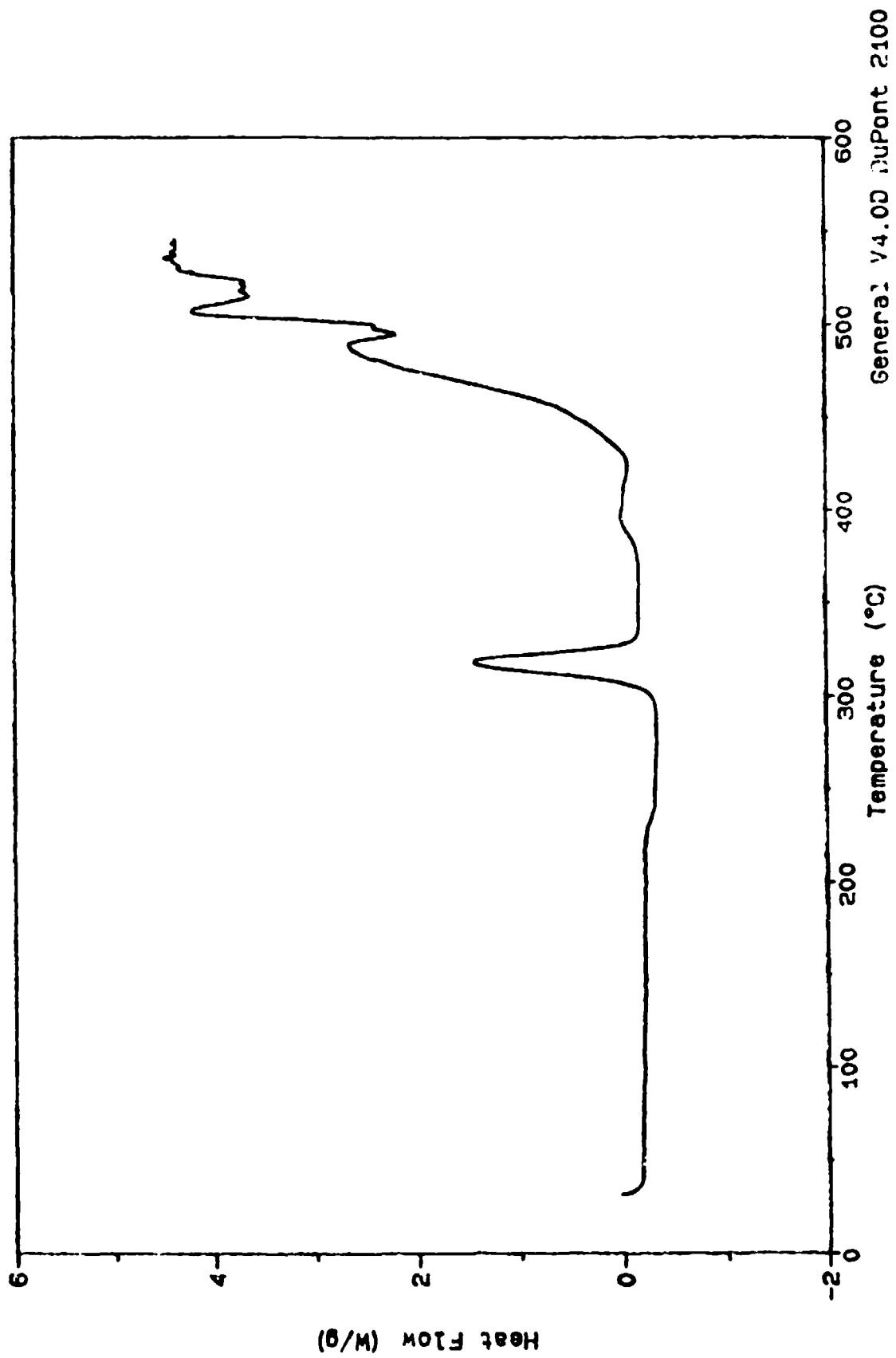
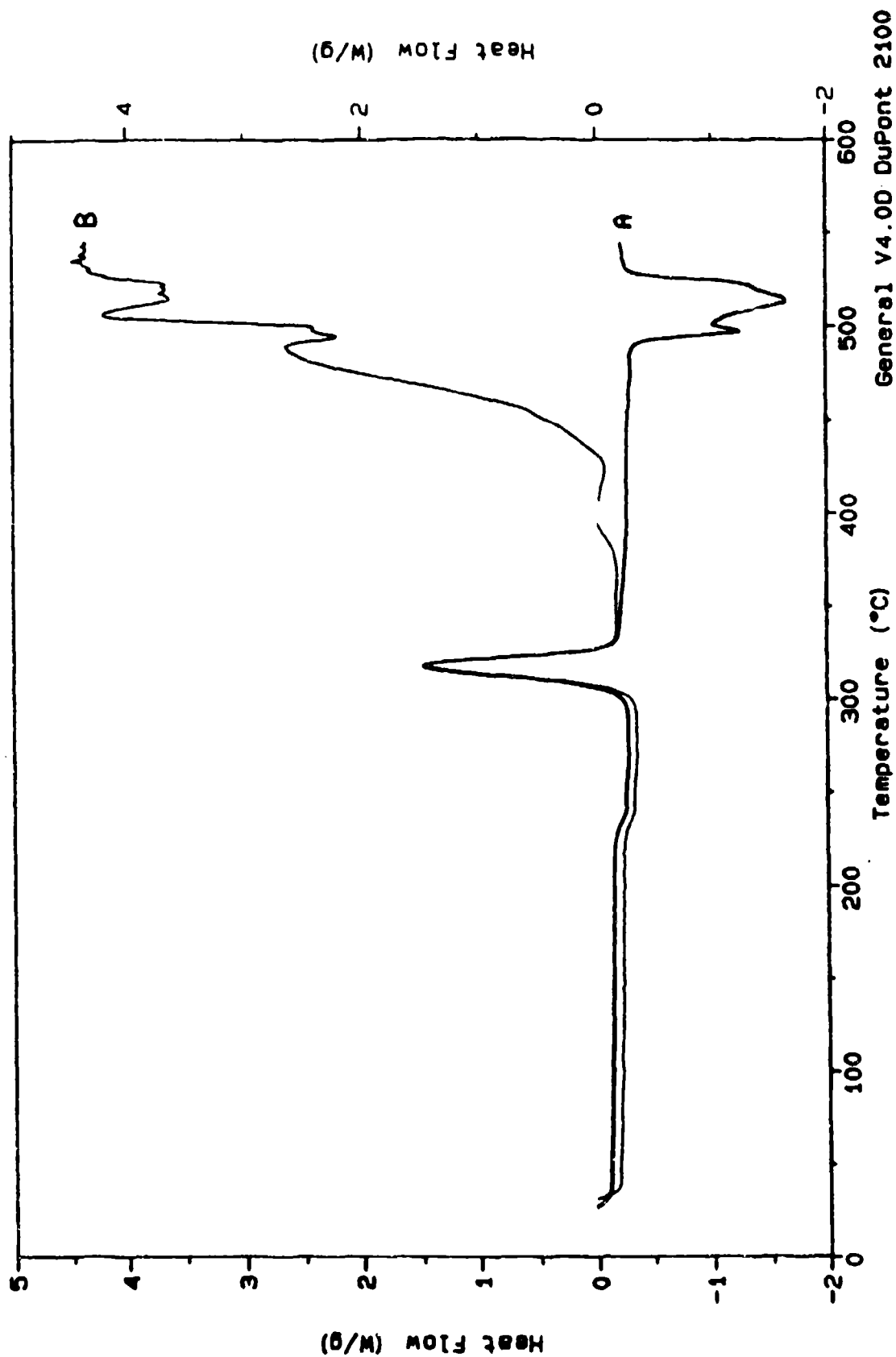


Figure 18. DSC of Amorphous  $\text{Sb}_2\text{S}_3$  in Air.



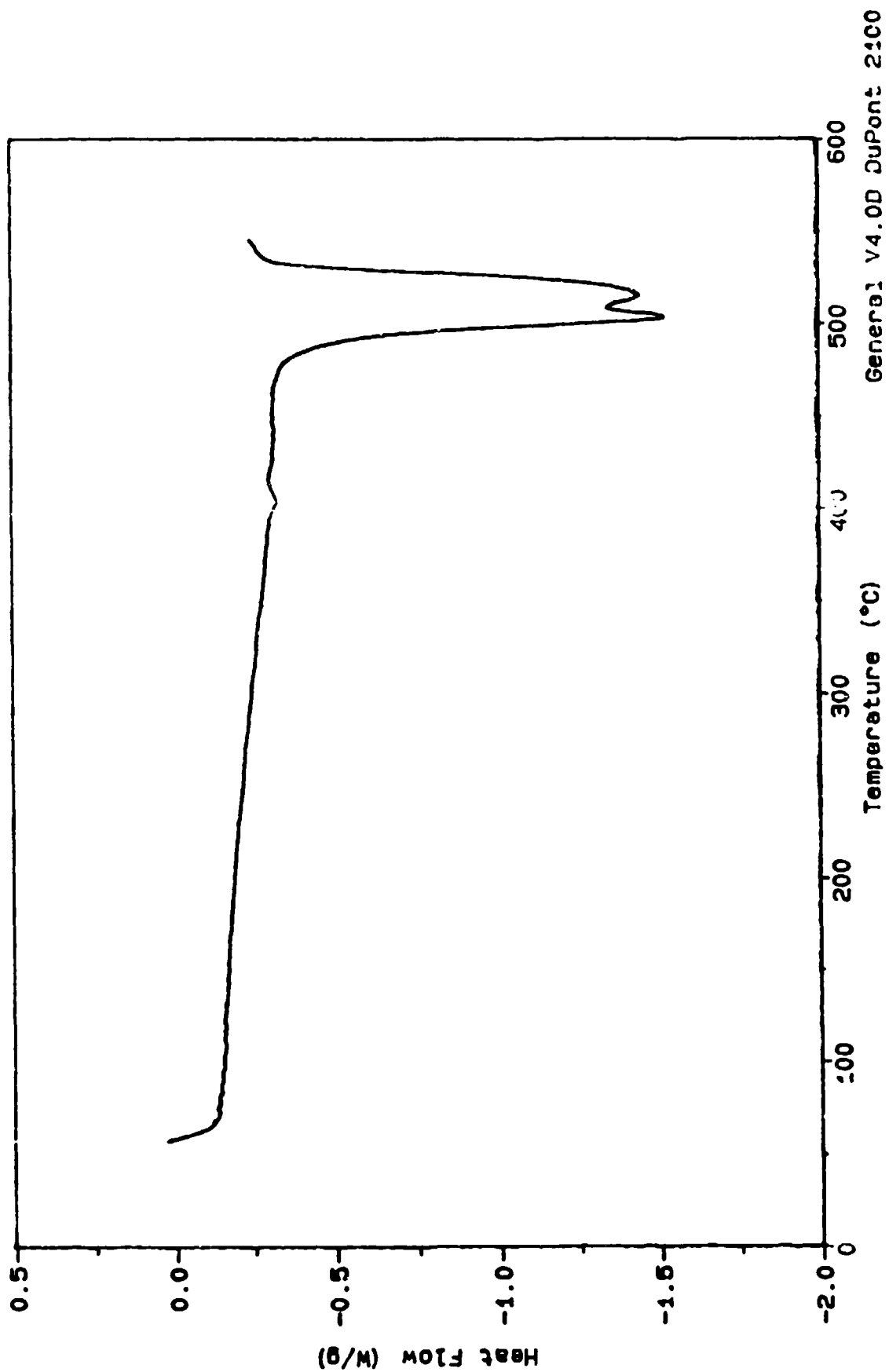


Figure 20. DSC of Crystalline  $\text{Sb}_2\text{S}_3$  in Air (Slow Cooled from Melt).

Since the following sections will deal with antimony sulfides of higher sulfur to antimony ratios ( $\text{Sb}_2\text{S}_4$  and  $\text{Sb}_2\text{S}_5$ ), the effects of elemental sulfur on  $\text{Sb}_2\text{S}_3$ 's thermal and oxidative properties were examined. Figure 21 shows the DSC curve of  $\text{Sb}_2\text{S}_3$  mixed with enough elemental sulfur to equal that found in  $\text{Sb}_2\text{S}_4$ . Under nitrogen, the melting of the alpha and beta forms of sulfur can be seen (105 and 116 °C respectively) followed by volatilization at 287 °C. The added sulfur does have an effect on the  $\text{Sb}_2\text{S}_3$ , as demonstrated by the increase in temperature of the melt to 525 °C.

When the  $\text{Sb}_2\text{S}_3$  with sulfur is run in air, different results are obtained. As shown in Figure 22, the presence of sulfur causes some changes in the 350 to 525 °C region. There appears to be more contribution from the 434 °C exotherm and less from the one at 473 °C. In addition, a new exotherm is observed at 272 °C. This area corresponds to the oxidation of sulfur. (See Figure 23.) The intensity changes in the remaining two exotherms may result from a reaction between  $\text{Sb}_2\text{S}_3$  and  $\text{SO}_2$  generated by oxidation of the added sulfur to produce more of the sulfate containing species identified in the mid IR spectra of air stressed  $\text{Sb}_2\text{S}_3$  samples.

## 2.0 Antimony tetrasulfide ( $\text{Sb}_2\text{S}_4$ )

Antimony tetrasulfide does not possess the same thermal stability as the trisulfide. Heating  $\text{Sb}_2\text{S}_4$  in the TGA under a nitrogen atmosphere results in a 8.7 percent weight loss between

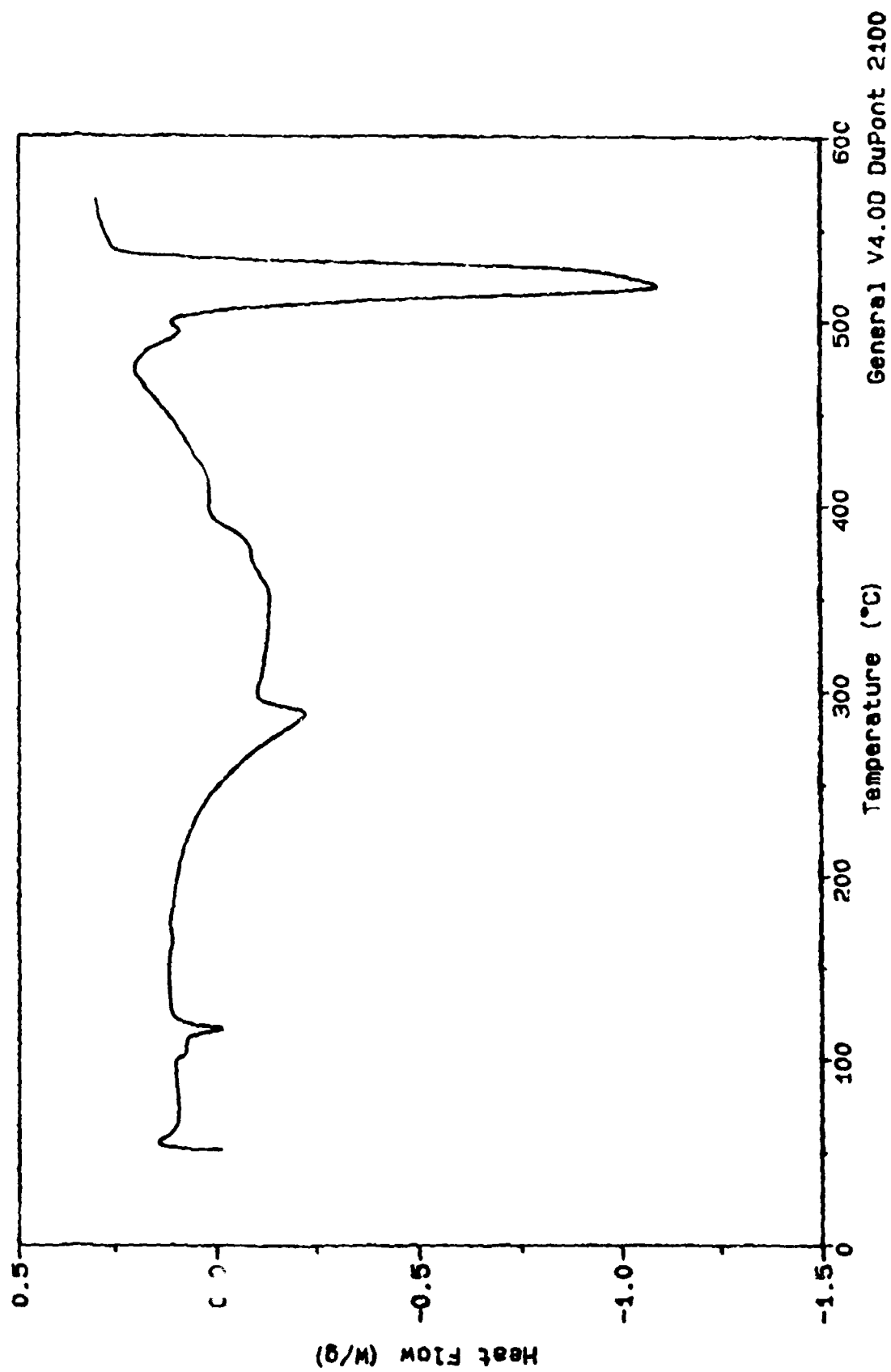


Figure 21. DSC of  $\text{Sb}_2\text{S}_3$  and Sulfur in  $\text{N}_2$ .

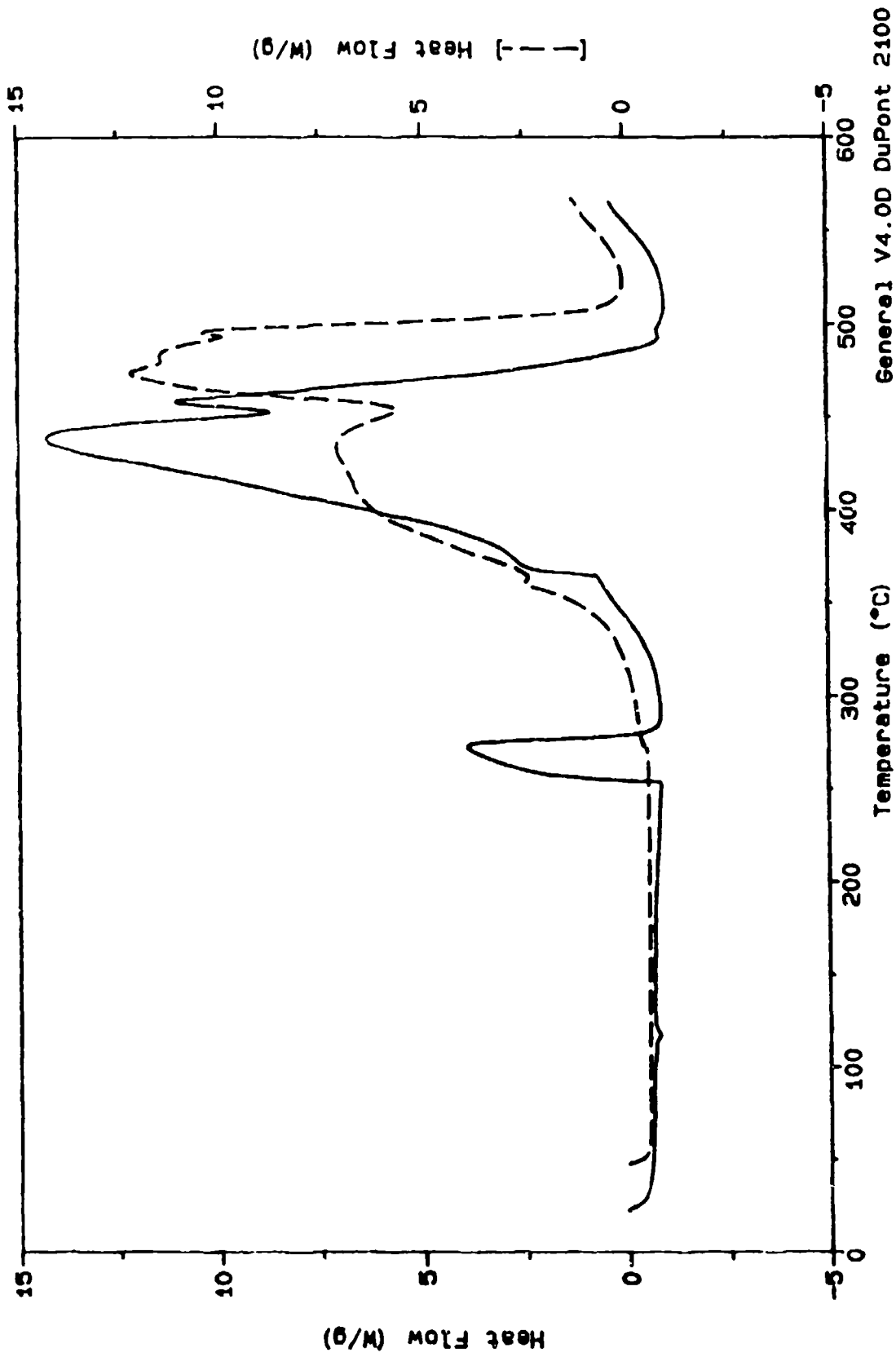


Figure 22. DSC of  $\text{Sb}_2\text{S}_3$  and Sulfur in Air.

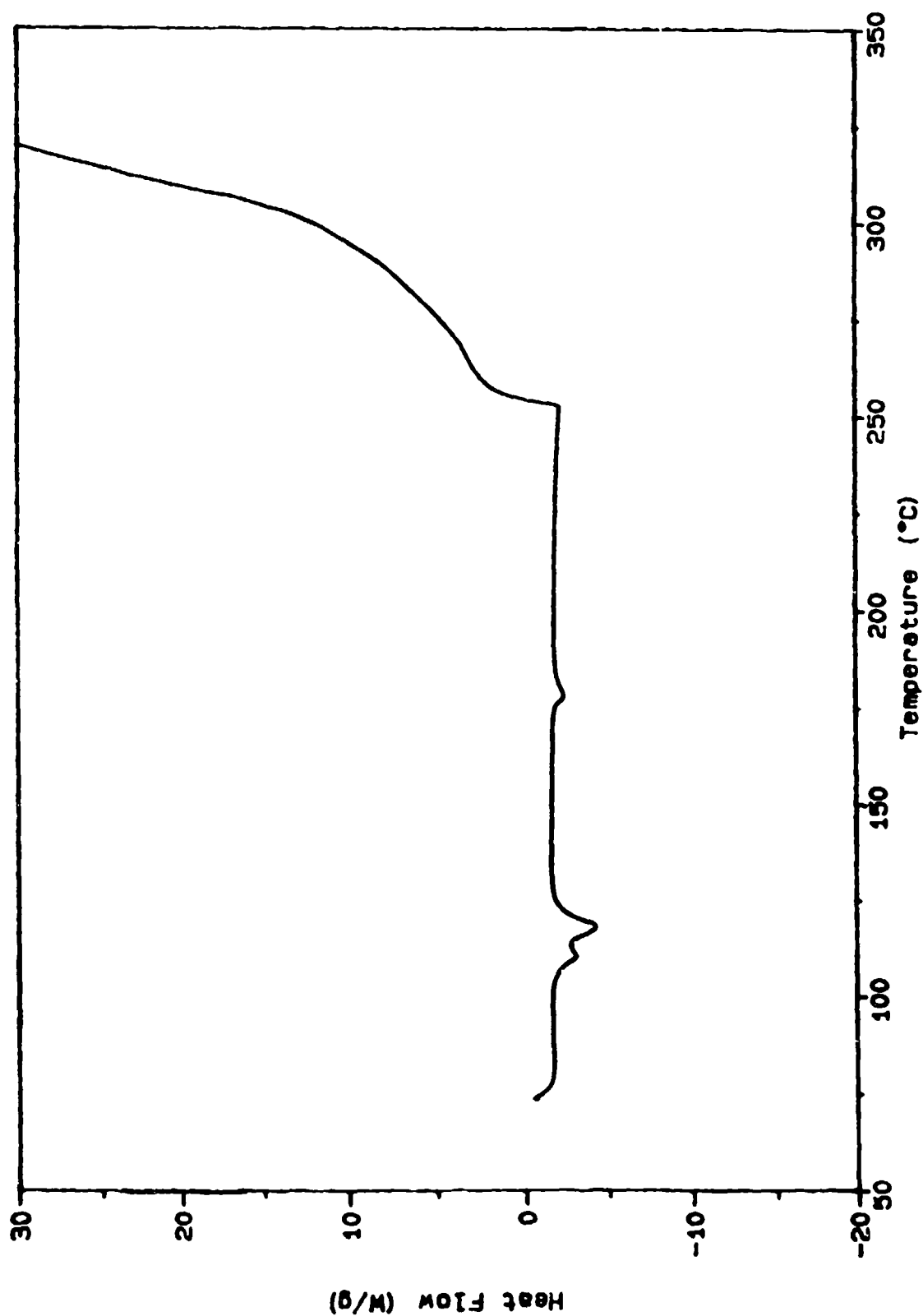


Figure 23. DSC of Sulfur in  $N_2$ .



195 and 230 °C. (See Figure 24.) After the initial loss, the sample weight remains constant to 600 °C. Although not shown, at temperatures beyond 600 °C a rapid weight loss occurs and evidence of reaction between the sample and the platinum sample pan can be seen. If heating is stopped before reaction with the platinum sample pan can occur, one sees that the  $\text{Sb}_2\text{S}_4$  changes color from brick red to black. This color change along with the 8.7 percent weight loss, suggests that sulfur is being lost to yield  $\text{Sb}_2\text{S}_3$ . (See Reaction 1.) The theoretical weight loss for reaction 1 is 8.6 percent.



The Far IR spectrum of the above product along with those of  $\text{Sb}_2\text{S}_3$  and  $\text{Sb}_2\text{S}_4$  are shown in Figure 25.  $\text{Sb}_2\text{S}_4$  has one broadband at 280  $\text{cm}^{-1}$  and a shoulder at 150  $\text{cm}^{-1}$ . The sample heated under nitrogen to 275 °C, displays a spectrum almost identical to  $\text{Sb}_2\text{S}_3$ . This is in agreement with King and Asmerom (6), who reported that prolonged heating of  $\text{Sb}_2\text{S}_4$  at 525 °C resulted in a 8.6 percent weight loss and formation of  $\text{Sb}_2\text{S}_3$  (determined by x-ray analysis).

Differential scanning calorimetry of  $\text{Sb}_2\text{S}_4$  in nitrogen (Figure 26) shows several features not seen with  $\text{Sb}_2\text{S}_3$ . There is an exotherm at 210 °C (40 J/g) with a small shoulder at 170 °C, followed by a small endotherm at 302 °C. The melting endotherm is also sharper than that observed for the trisulfide and occurs at 548 °C, which is 38°C higher.

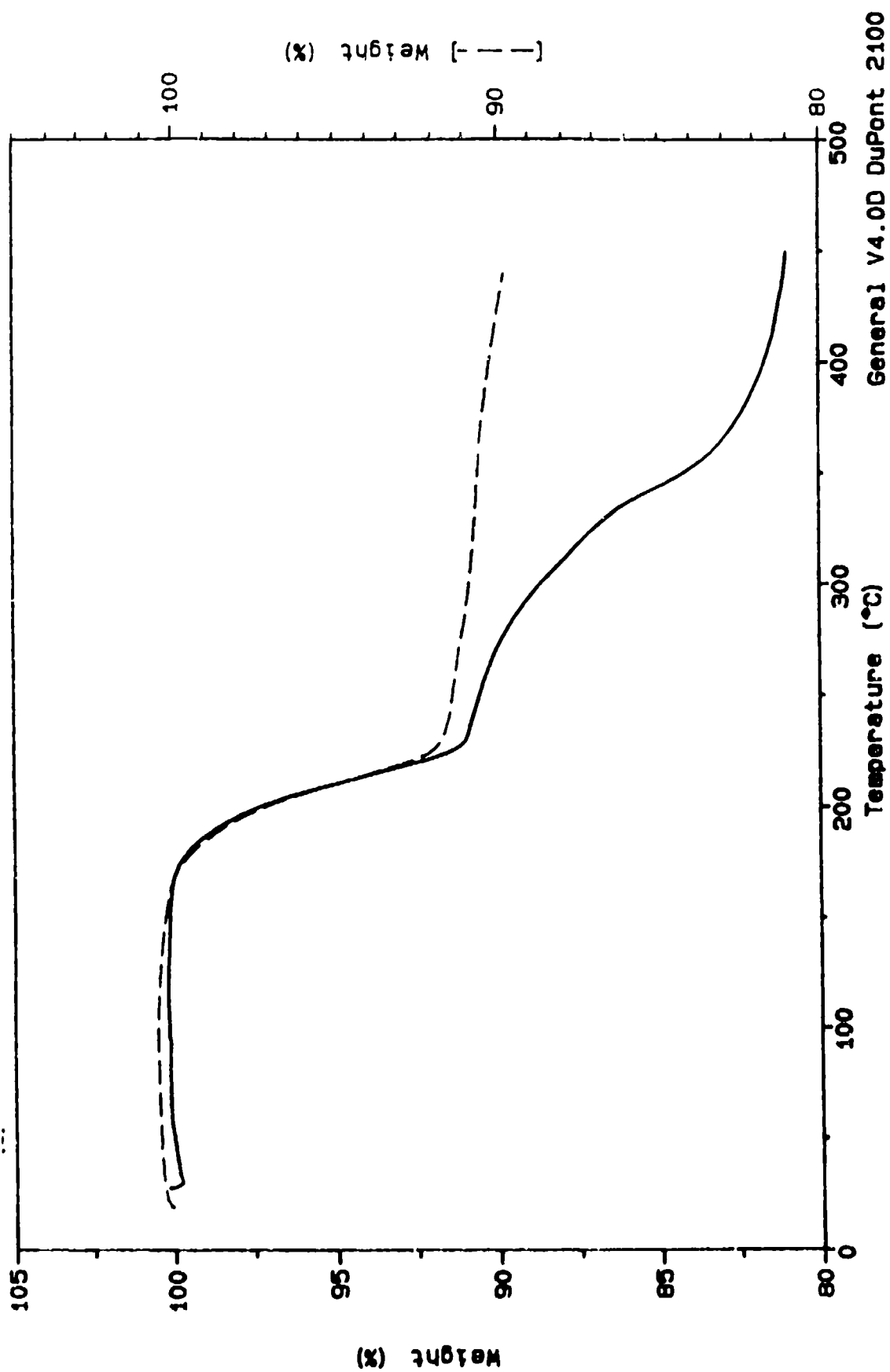


Figure 24. TGA of  $\text{Sb}_2\text{S}_4$  (—) in Air; (---) in  $\text{N}_2$ .

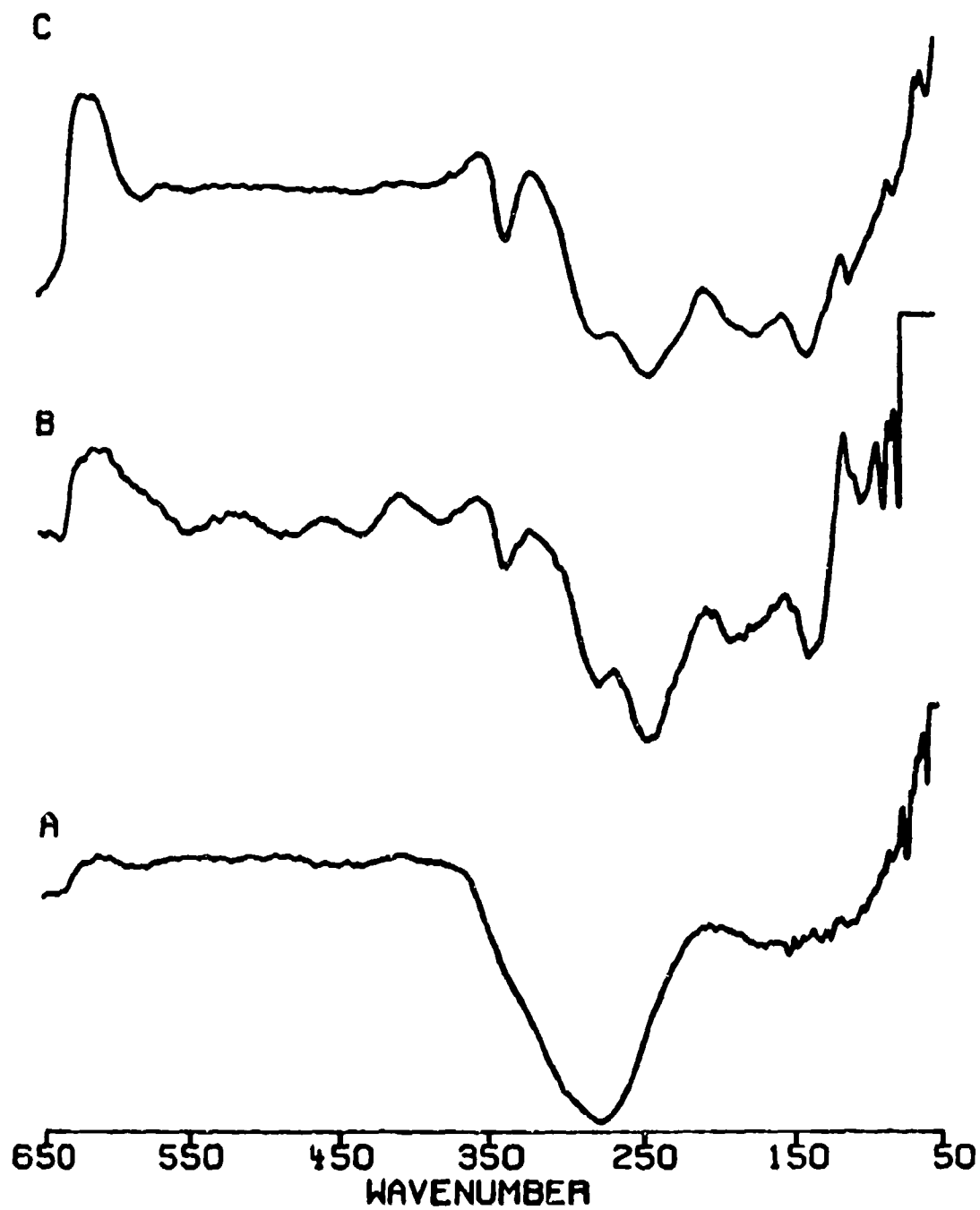


Figure 25. Far IR of  $\text{Sb}_2\text{S}_4$  (A) Virgin; (B) Heated 275°C in  $\text{N}_2$ ;  
(C)  $\text{Sb}_2\text{S}_3$  (Virgin).

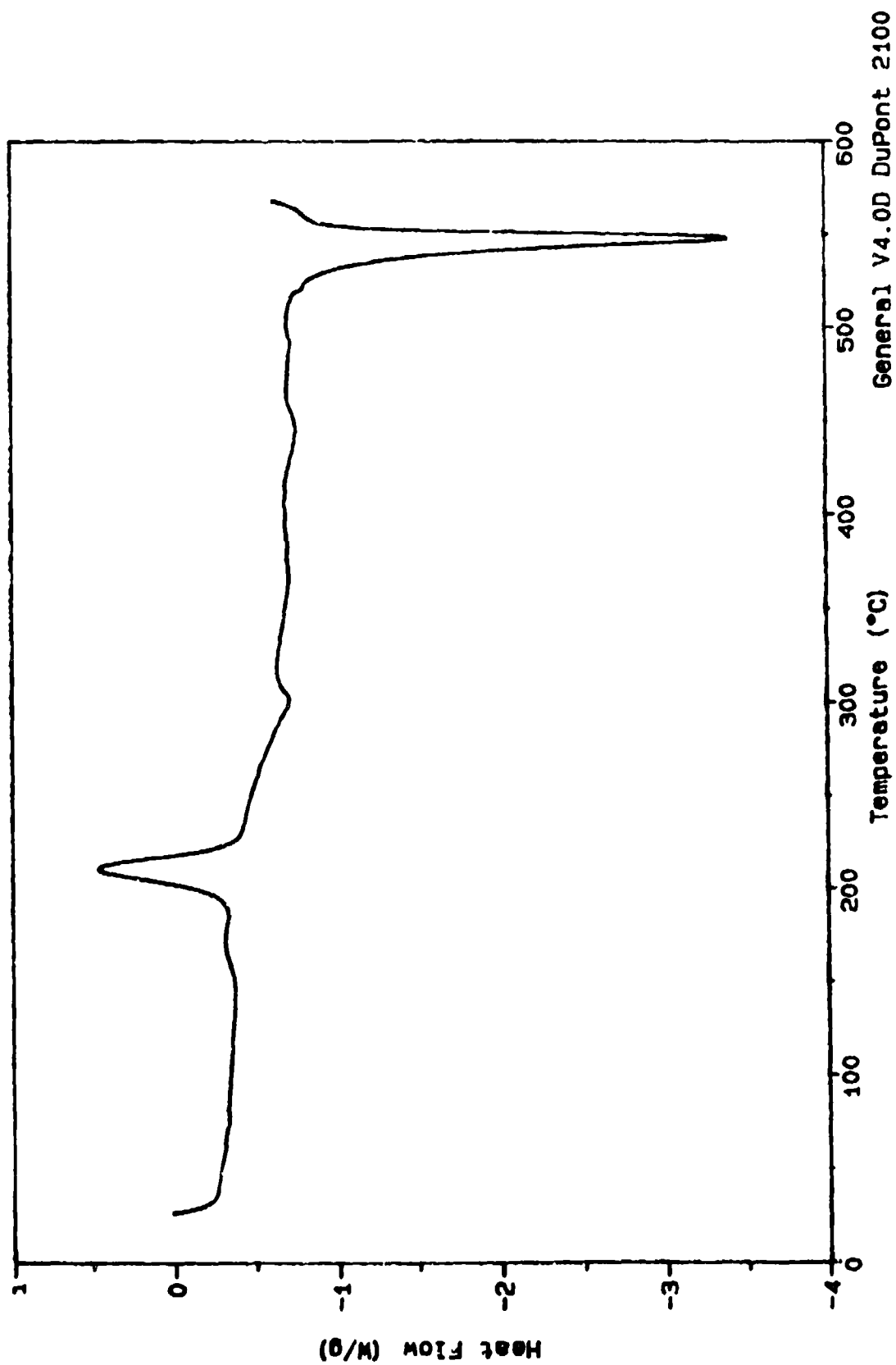


Figure 26. DSC of  $\text{Sb}_2\text{S}_4$  in  $\text{N}_2$ .

When DSC and TGA curves are overlaid, (Figure 27), one sees that the exotherm and the 8.7 percent weight loss occur concurrently. This exotherm is most likely associated with a structural rearrangement occurring along with the release of sulfur. Further evidence for this assignment is found by running a sample in the DSC through the 210 °C peak, rapidly cooling and rerunning. (See Figure 28.) One can see the melting of the released sulfur. (See the alpha and beta forms.)

Returning to Figure 26, the small endotherm at 302 °C can now be identified as the volatilization of released sulfur. The melting of  $\text{Sb}_2\text{S}_3$  generated by reaction 1 (548 °C) is closer to the literature value of  $\text{Sb}_2\text{S}_3$ . This may result from a combination of several factors - particle size and crystal structure of the  $\text{Sb}_2\text{S}_3$  formed, side reactions and purity. Also as seen in the previous section, when elemental sulfur was added to  $\text{Sb}_2\text{S}_3$ , melting occurred at higher temperatures. The free sulfur generated in reaction 1 may contribute in the same way to yield the higher value.

Differential thermal analysis performed in air, produces the thermogram in Figure 29. Several exotherms are observed: 212, 269, 369, and 581 °C. These are associated with reaction 1, the

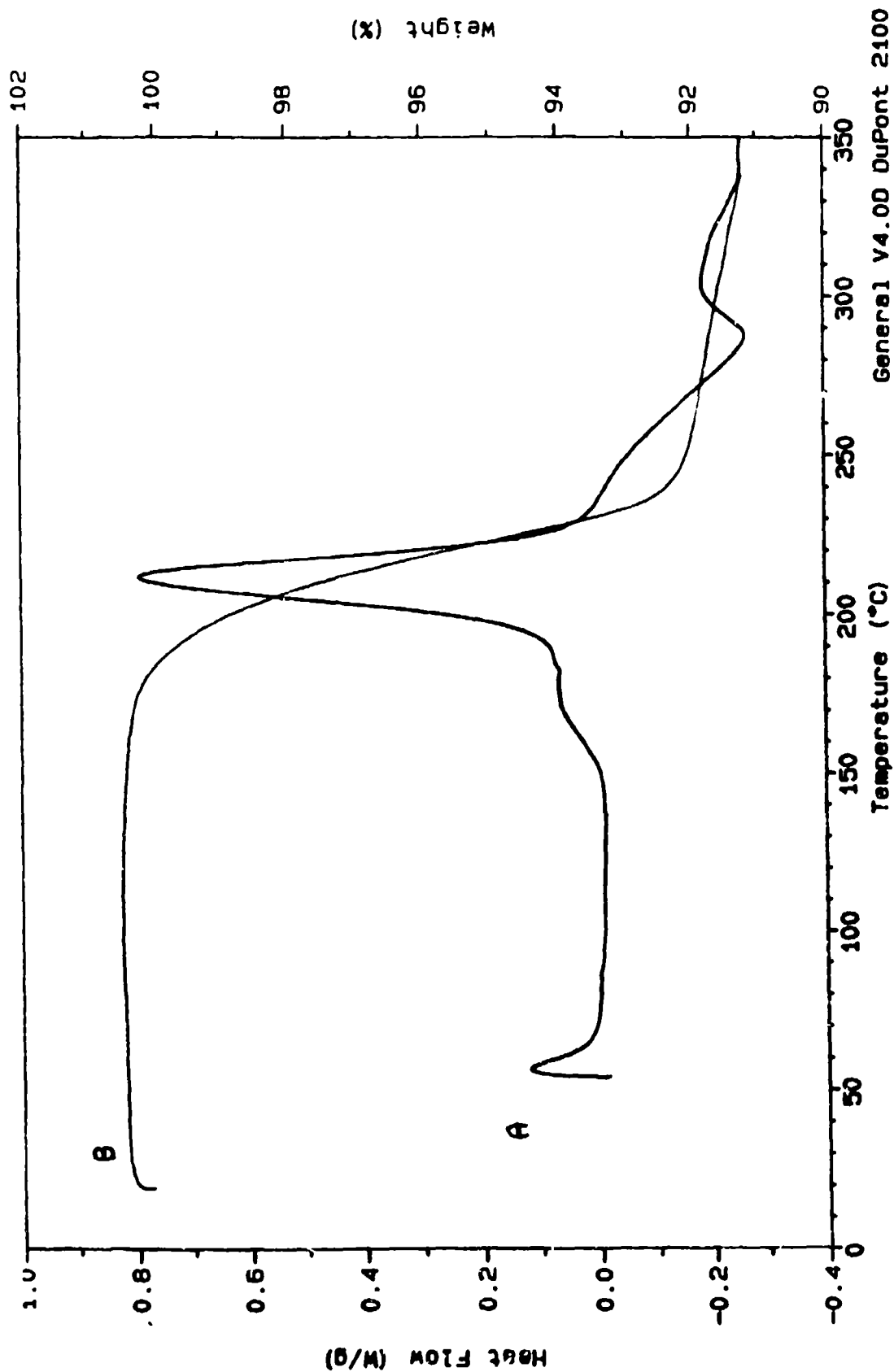


Figure 27. Comparison of (A) DSC and (B) TGA of  $\text{Sb}_2\text{S}_4$  in  $\text{N}_2$ .

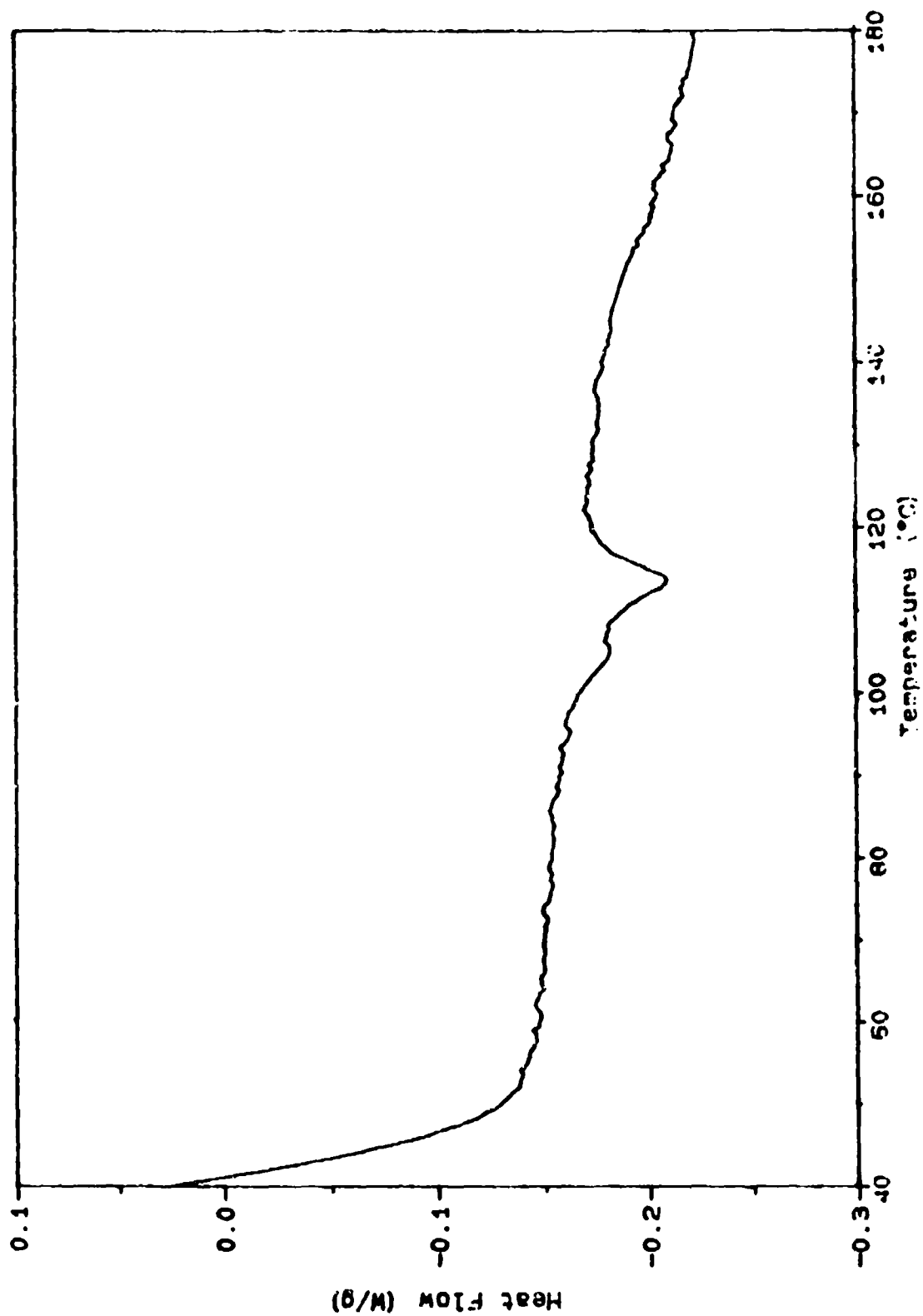


Figure 28. DSC of Released Sulfur ( $\text{Sb}_2\text{S}_4$  previously heated to  $250^\circ\text{C}$  in  $\text{N}_2$ ).

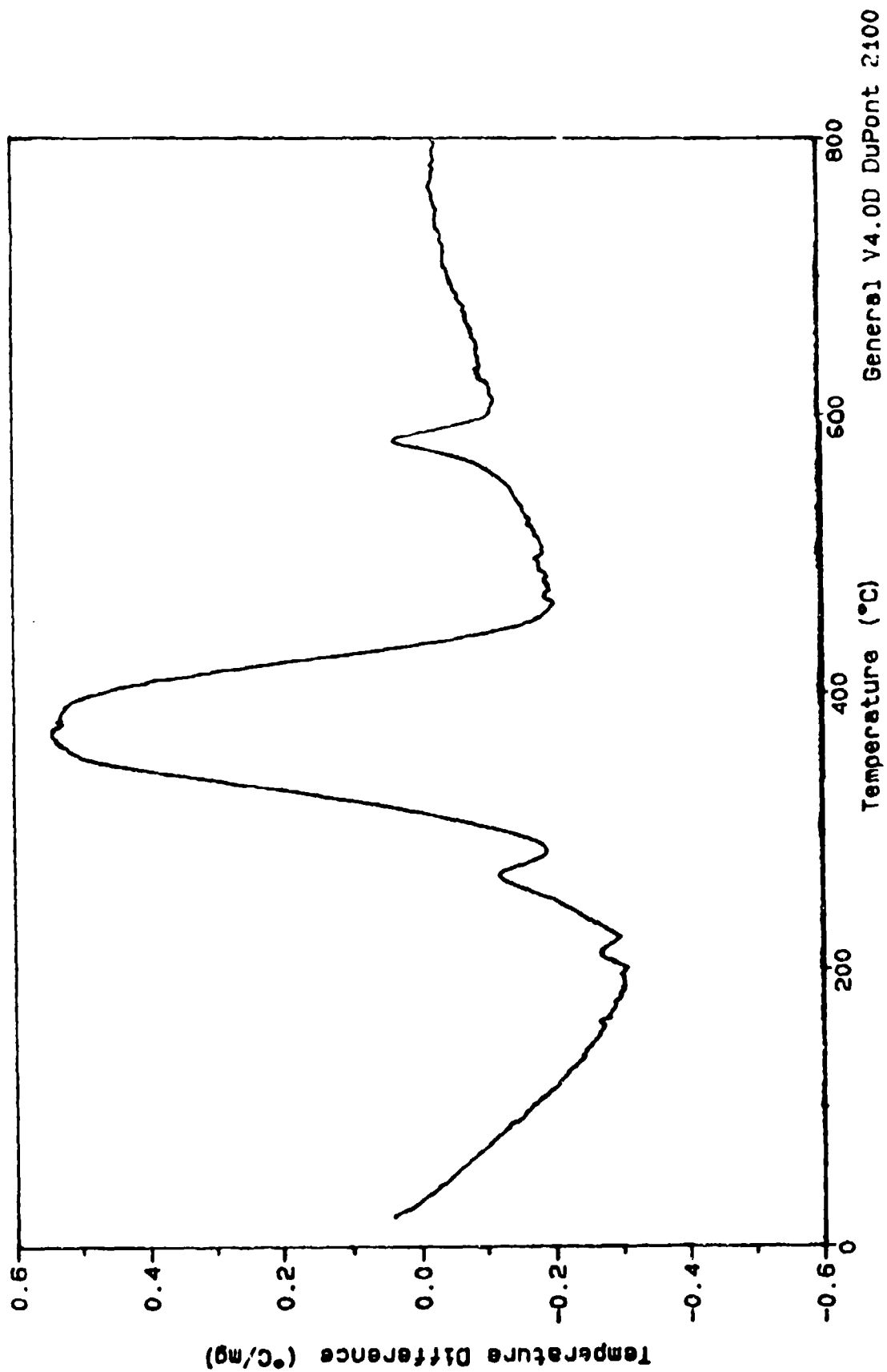


Figure 29. DSC of  $\text{Sb}_2\text{S}_4$  in Air.



oxidation of the released sulfur, oxidation of  $\text{Sb}_2\text{S}_3$  and finally the oxidation of  $\text{Sb}_2\text{O}_3$  to  $\text{Sb}_2\text{O}_4$ . (See below.)

Isothermal TGA in air followed by IR analysis reveals a process similar to that of  $\text{Sb}_2\text{S}_3$ 's oxidation. Exposure to temperatures below  $581^\circ\text{C}$  (temperature of the last exotherm) results in the formation of cubic  $\text{Sb}_2\text{O}_3$ . (See Figure 30.) At  $525^\circ\text{C}$ , the major species is  $\text{Sb}_2\text{O}_3$ ; however, the presence of shoulders at  $442$  and  $286^\circ\text{C}$  indicates the beginning of  $\text{Sb}_2\text{O}_4$  formation. Above  $600^\circ\text{C}$  (Figure 31), an IR spectrum corresponding to  $\text{Sb}_2\text{O}_4$  is seen. As with  $\text{Sb}_2\text{S}_3$ , mid-IR analysis reveals the  $1100\text{ cm}^{-1}$  band typical of a sulfate containing species, for samples heated in air at  $425$ ,  $525$ , and  $650^\circ\text{C}$ . (See Figures 32 & 33.) Virgin  $\text{Sb}_2\text{S}_4$  and  $\text{Sb}_2\text{S}_4$  heated under nitrogen do not display this band. (See Figure 34.) This band is also absent in the sample heated in air to  $1050^\circ\text{C}$ , indicating the sulfate is not stable at elevated temperatures.

When  $\text{Sb}_2\text{S}_4$  is heated under nitrogen in the DSC above its melting point (a temperature where  $\text{Sb}_2\text{S}_3$  should be present as a result of reaction 1), rapidly cooled and rerun, the thermogram in Figure 35 is obtained. A glass transition at  $227^\circ\text{C}$  is seen along with two overlapping exotherms at  $279$  and  $293^\circ\text{C}$ . This indicates the formation of amorphous  $\text{Sb}_2\text{S}_3$ . The two exotherms point to the possibility of two distinct structures being formed. The melting endotherm on the second run is broader than the first and is lowered to  $541^\circ\text{C}$ . Slow cooling from the melt and rerunning shows

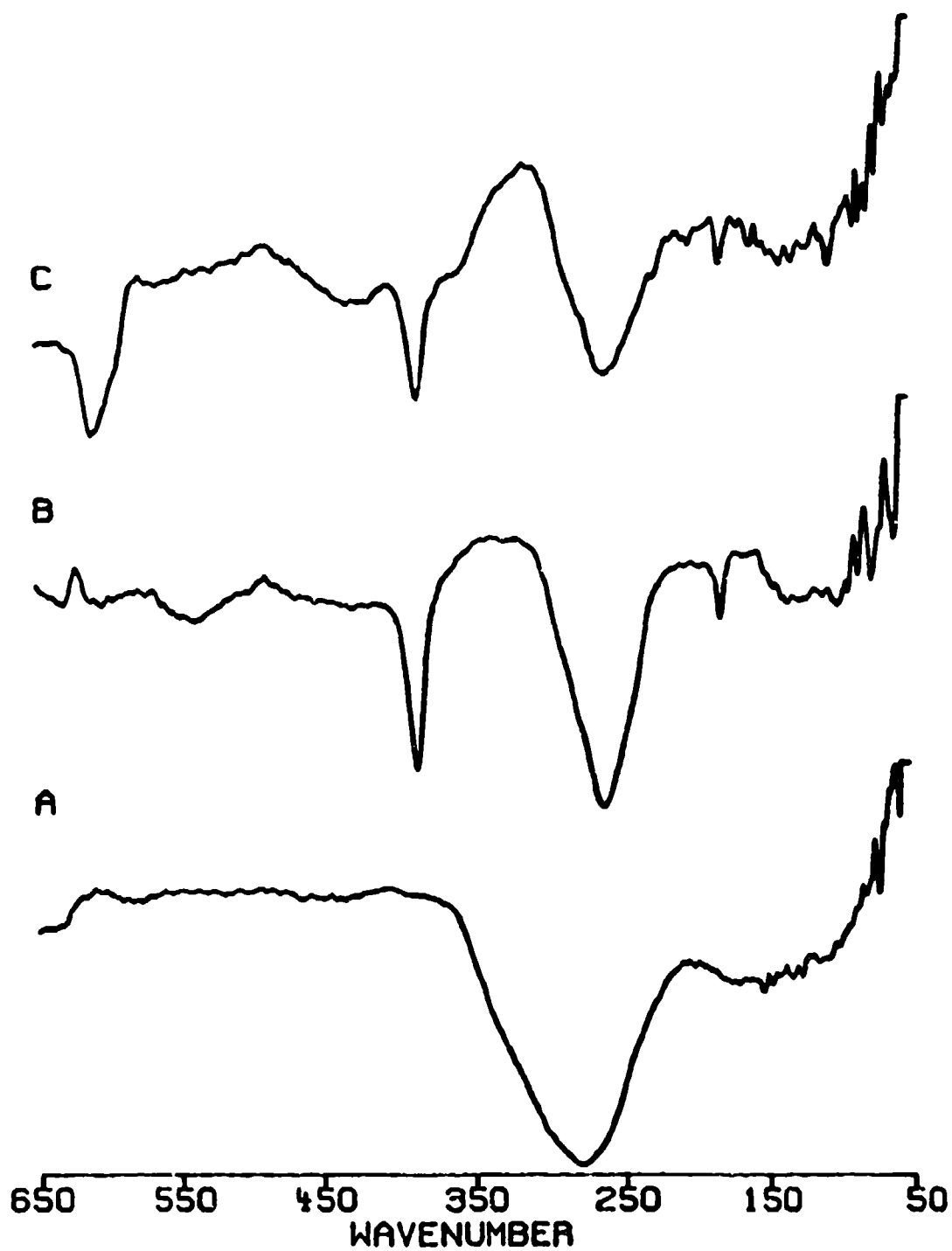


Figure 30. Far IR of  $\text{Sb}_2\text{S}_4$  (A) Virgin; (B) 425°C in Air;  
(c) 525°C in Air.

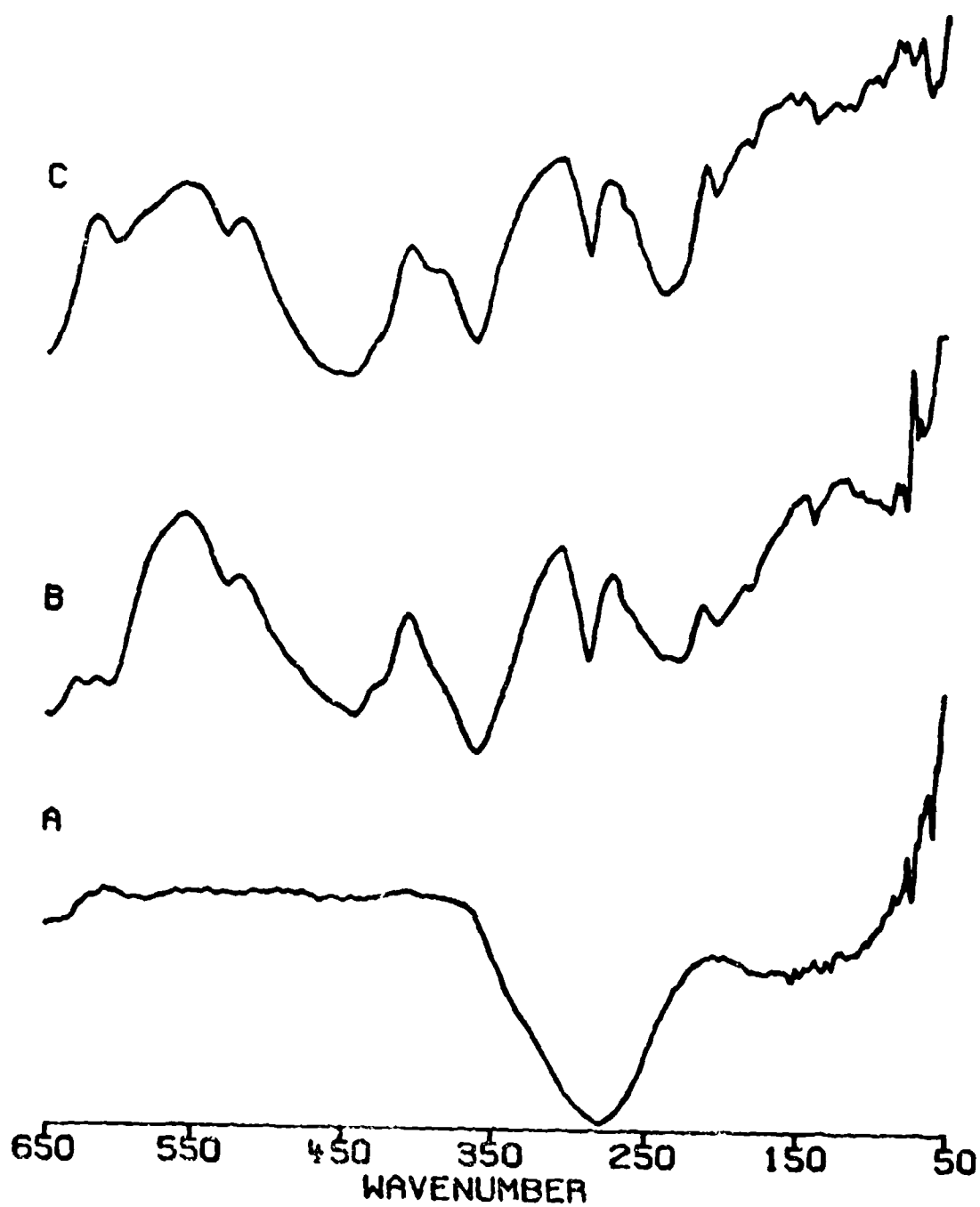


Figure 31. Far IR of  $\text{Sb}_2\text{S}_4$  (A) Virgin; (B) 650°C in Air; (C) 1050°C in Air.



Figure 32. Mid IR of  $\text{Sb}_2\text{S}_4$  (A) Virgin; (B) 425°C in Air;  
(C) 525°C in Air.



Figure 33. Mid IR of  $\text{Sb}_2\text{S}_4$  (A) Virgin; (B) 650°C in Air; (C) 1050°C in Air.

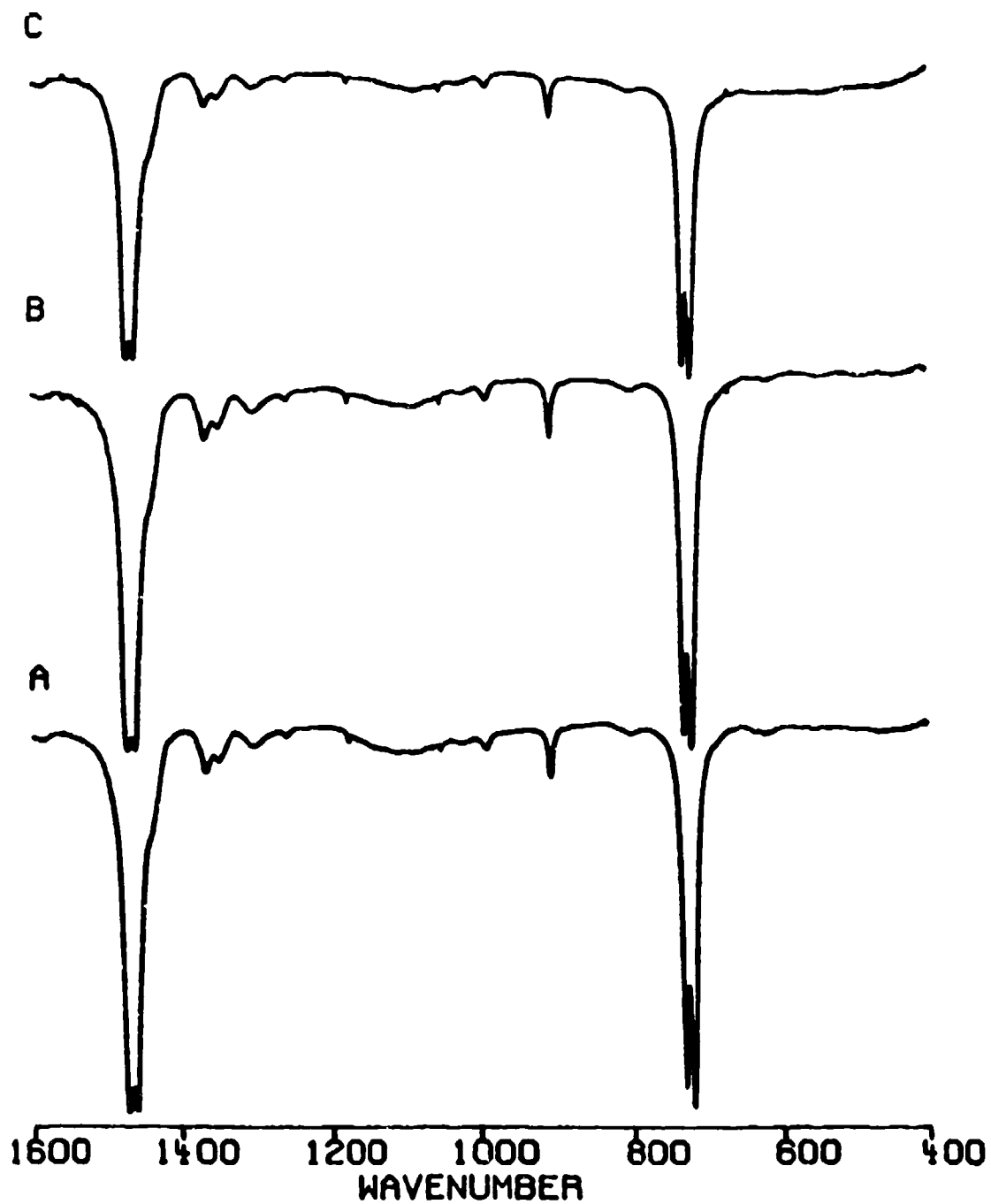


Figure 34. Mid IR of  $\text{Sb}_2\text{S}_4$  (Virgin) (A) Virgin; (B) 230°C in  $\text{N}_2$ ; (C)  $\text{Sb}_2\text{S}_3$ .

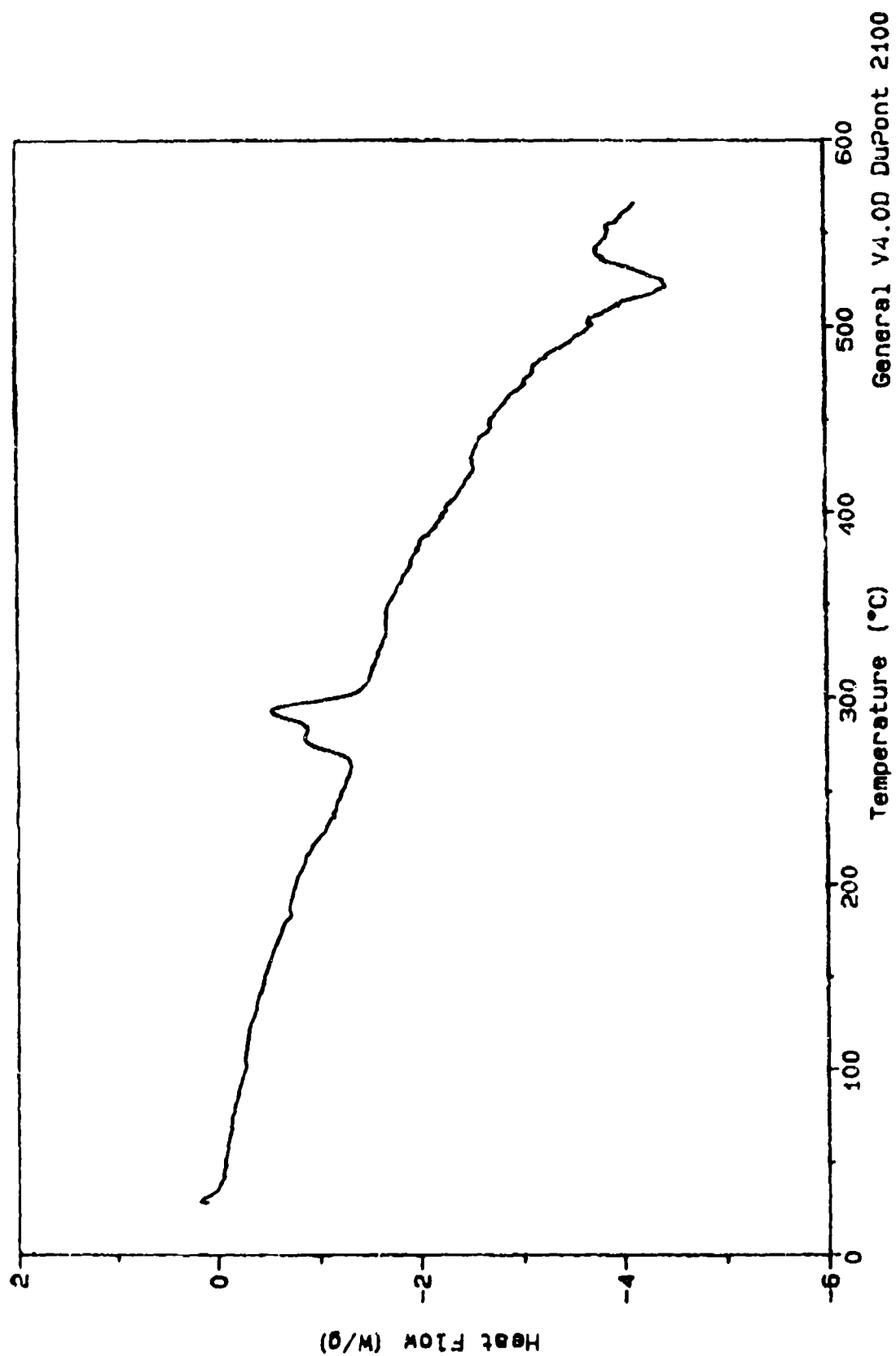


Figure 35. DSC of generated  $\text{Sb}_2\text{S}_3$  ( $\text{Sb}_2\text{S}_4$  rapidly cooled from melt in  $\text{N}_2$ ).

no glass transitions or heats of crystallization, indicating crystalline  $\text{Sb}_2\text{S}_3$  formed. (See Figure 36.) Melting occurs at  $545^\circ\text{C}$  and the endotherm is broader and less intense than in the first run - indicating there may be some decomposition or side reactions. Also a small endotherm at  $450^\circ\text{C}$  is unseen in any of the previous experiments.

Addition of elemental sulfur to  $\text{Sb}_2\text{S}_4$  in an amount equal to that found in antimony pentasulfide produced some interesting effects. Figure 37 shows the results of DSC performed under anaerobic conditions on  $\text{Sb}_2\text{S}_4$  + sulfur, along with those of  $\text{Sb}_2\text{S}_4$ . The most pronounced effect is a lowering in temperature of the exotherm associated with the release of sulfur to form  $\text{Sb}_2\text{S}_3$ . Unlike  $\text{Sb}_2\text{S}_3$ , there is no increase in the melting point on the addition of elemental sulfur. When the experiment is carried out in air (Figure 38), the same shift in the  $210^\circ\text{C}$  exotherm is observed; however, the oxidations of sulfur and the generated  $\text{Sb}_2\text{S}_3$  occur at slightly higher temperatures.

### 3.0 Antimony pentasulfide ( $\text{Sb}_2\text{S}_5$ )

As previously mentioned, antimony pentasulfide, a reddish brown solid, contains antimony in the +3 oxidation state along with considerable amounts of excess sulfur. In order to examine the effects of excess sulfur contained in  $\text{Sb}_2\text{S}_5$ , samples were extracted with  $\text{CS}_2$  and parallel studies were conducted with extracted and unextracted  $\text{Sb}_2\text{S}_5$ .



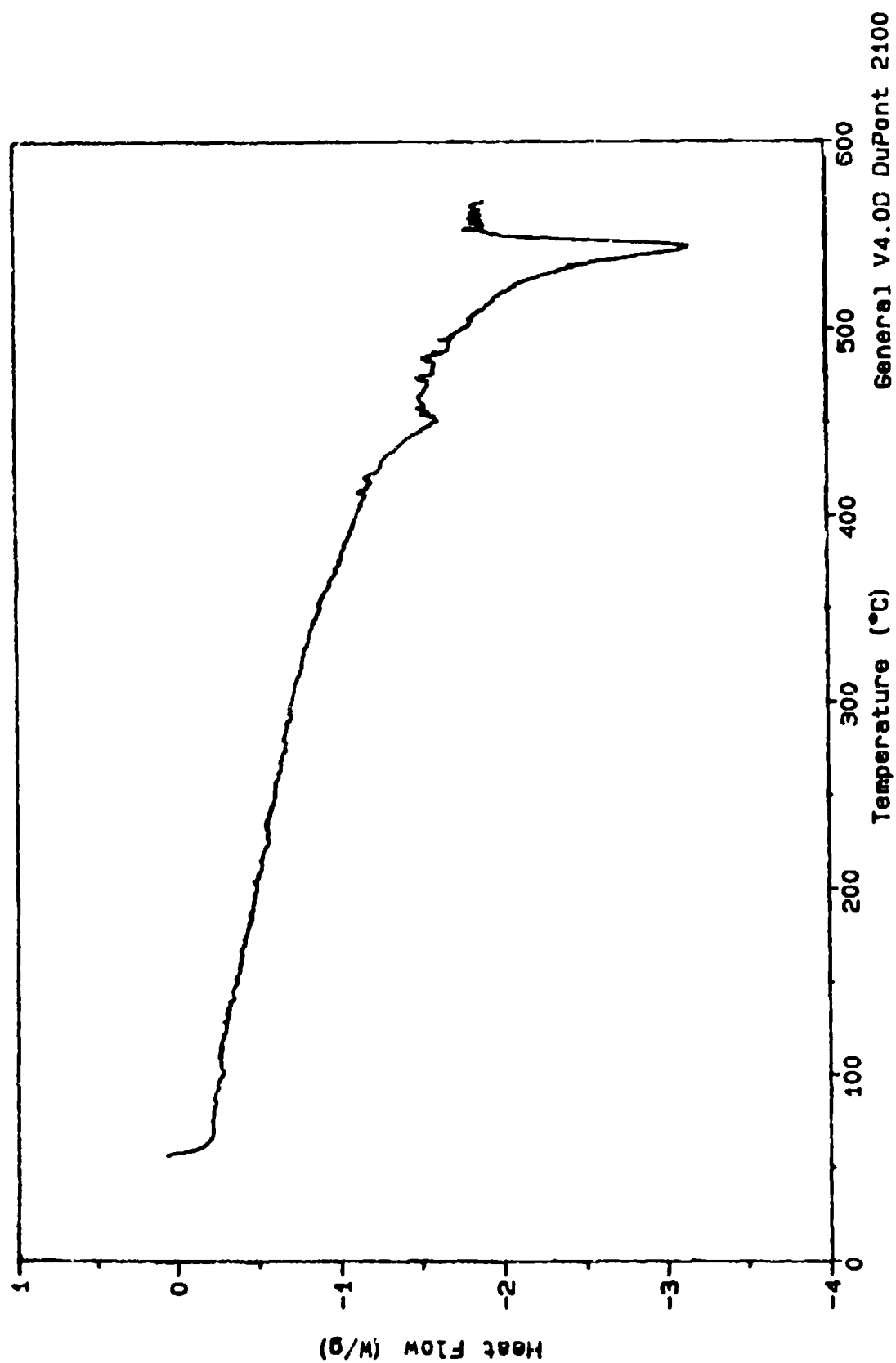


Figure 36. DSC of Generated  $\text{Sb}_2\text{S}_3$  ( $\text{Sb}_2\text{S}_4$  slow cooled from melt in  $\text{H}_2$ ).

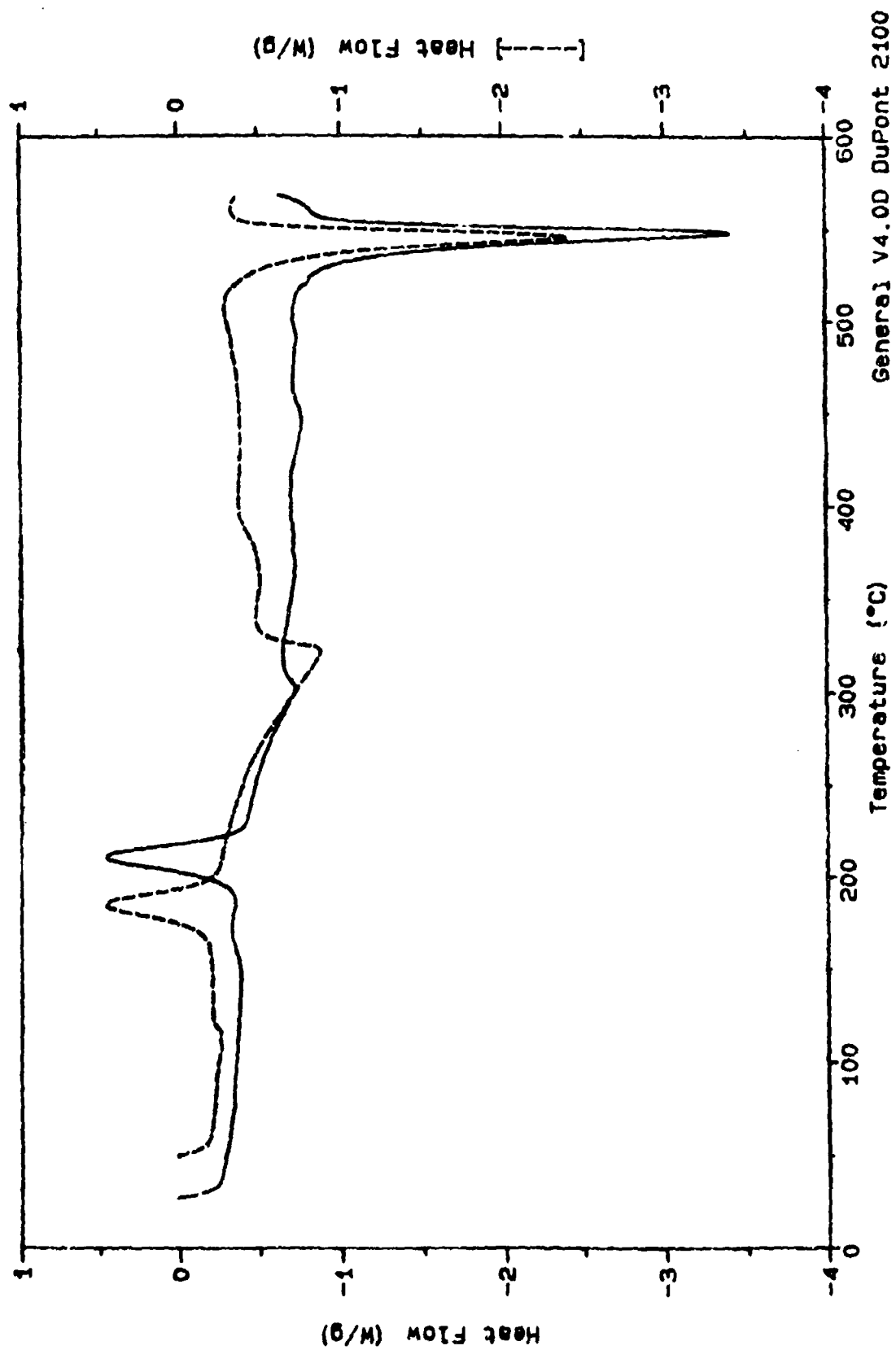


Figure 37. DSC of (—)  $\text{Sb}_2\text{S}_4$ ; (---) Sulfur in  $\text{N}_2$ .

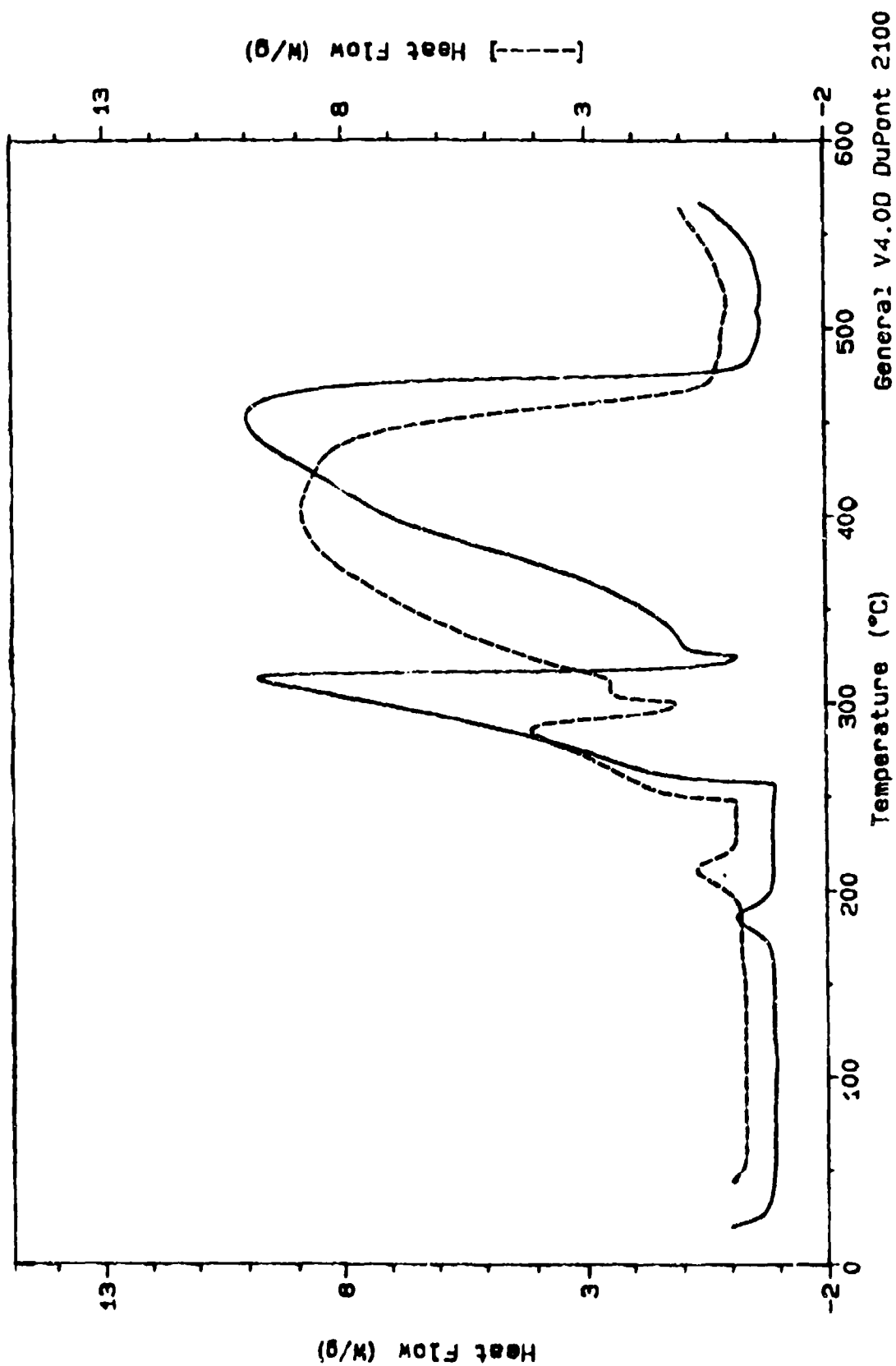


Figure 38. DSC of (—)  $\text{Sb}_2\text{S}_4$  and Sulfur; (---)  $\text{Sb}_2\text{S}_4$  in Air.

When extracted with  $\text{CS}_2$  in a Soxhlet extraction apparatus,  $\text{Sb}_2\text{S}_5$  experienced a 15 percent weight loss. This loss equalled the weight of sulfur recovered from evaporation of the  $\text{CS}_2$ . Determination of antimony concentration by permanganate titration (14) gave 69.5 percent for extracted  $\text{Sb}_2\text{S}_5$  and 57.59 percent for unextracted  $\text{Sb}_2\text{S}_5$ . Theoretical values for  $\text{Sb}_2\text{S}_5$ , and  $\text{Sb}_2\text{S}_3$  are 60.30, and 71.69 percent respectively. The observed value for extracted  $\text{Sb}_2\text{S}_5$  is closer to the theoretical value for  $\text{Sb}_2\text{S}_3$  (71.9 percent) than  $\text{Sb}_2\text{S}_5$  (60.3 percent); however, the color of the material remains reddish brown. This tends to support the theory that  $\text{Sb}_2\text{S}_5$  is really amorphous  $\text{Sb}_2\text{S}_3$  with excess sulfur.

Far IR spectra of unextracted and extracted  $\text{Sb}_2\text{S}_5$ , along with  $\text{Sb}_2\text{S}_4$  are shown in Figure 39. All three display similar patterns - a broadband centered around 290  $\text{cm}^{-1}$  with a shoulder at about 150  $\text{cm}^{-1}$ . Band maxima are at 292, 285, and 179  $\text{cm}^{-1}$ , respectively. These results indicate that removal of excess sulfur is producing a structure similar to  $\text{Sb}_2\text{S}_4$ .

Thermogravimetric analysis in nitrogen (Figure 40) shows a 16 percent weight loss occurring between 193 and 239  $^{\circ}\text{C}$ . Unlike  $\text{Sb}_2\text{S}_4$ , this weight loss does not occur in a single step. The curve is asymmetric and the derivative spectrum shows two peaks. This suggests that the excess sulfur is coordinated in the antimony sulfide in two distinct ways. From 200  $^{\circ}\text{C}$  on, the sample shows the same thermal stability as  $\text{Sb}_2\text{S}_3$  and  $\text{Sb}_2\text{S}_4$  - ultimately

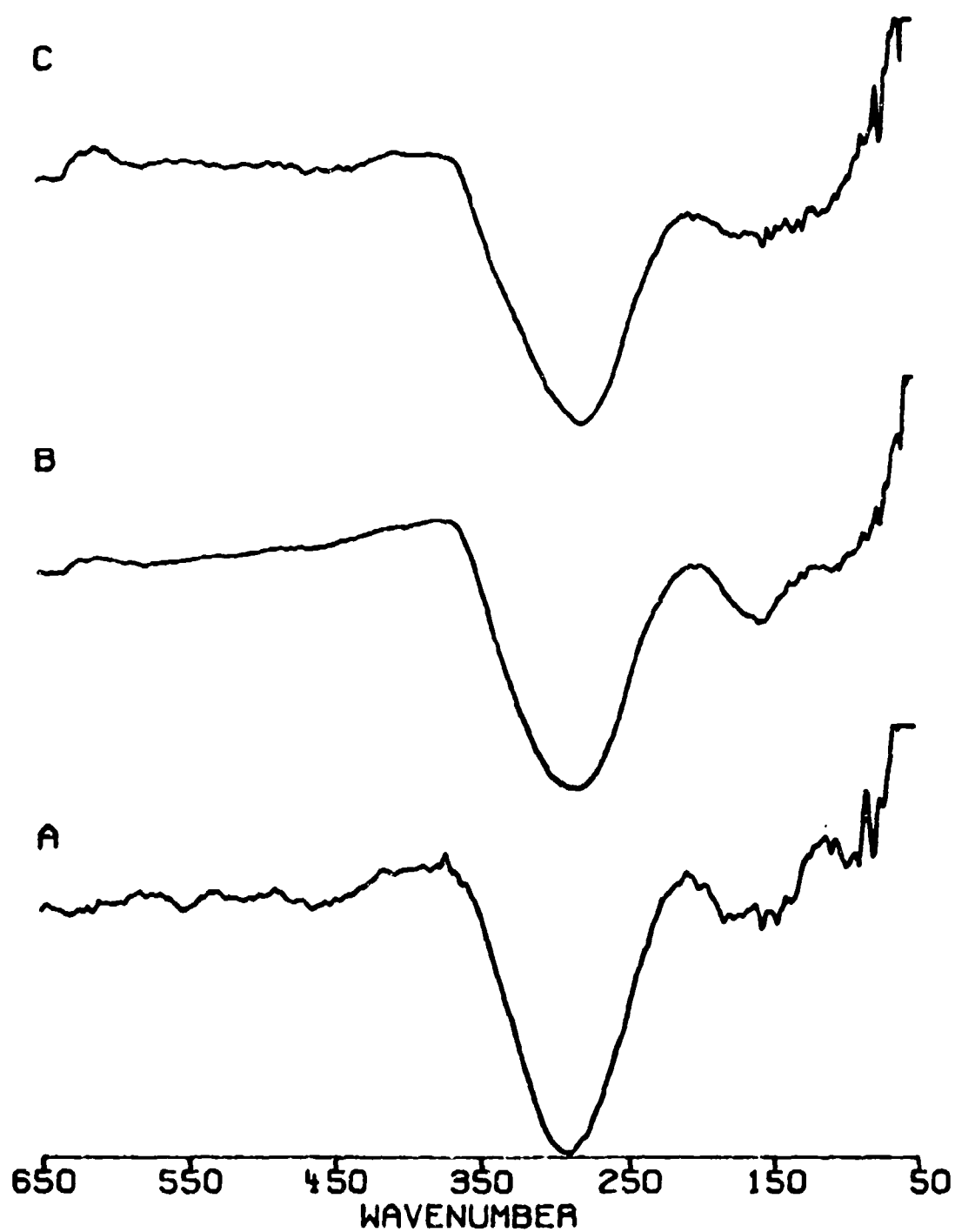


Figure 39. Far IR of  $\text{Sb}_2\text{S}_5$  (A)  $\text{Sb}_2\text{S}_5$ ; (B)  $\text{Sb}_2\text{S}_5$  extracted;  
(C)  $\text{Sb}_2\text{S}_4$ .

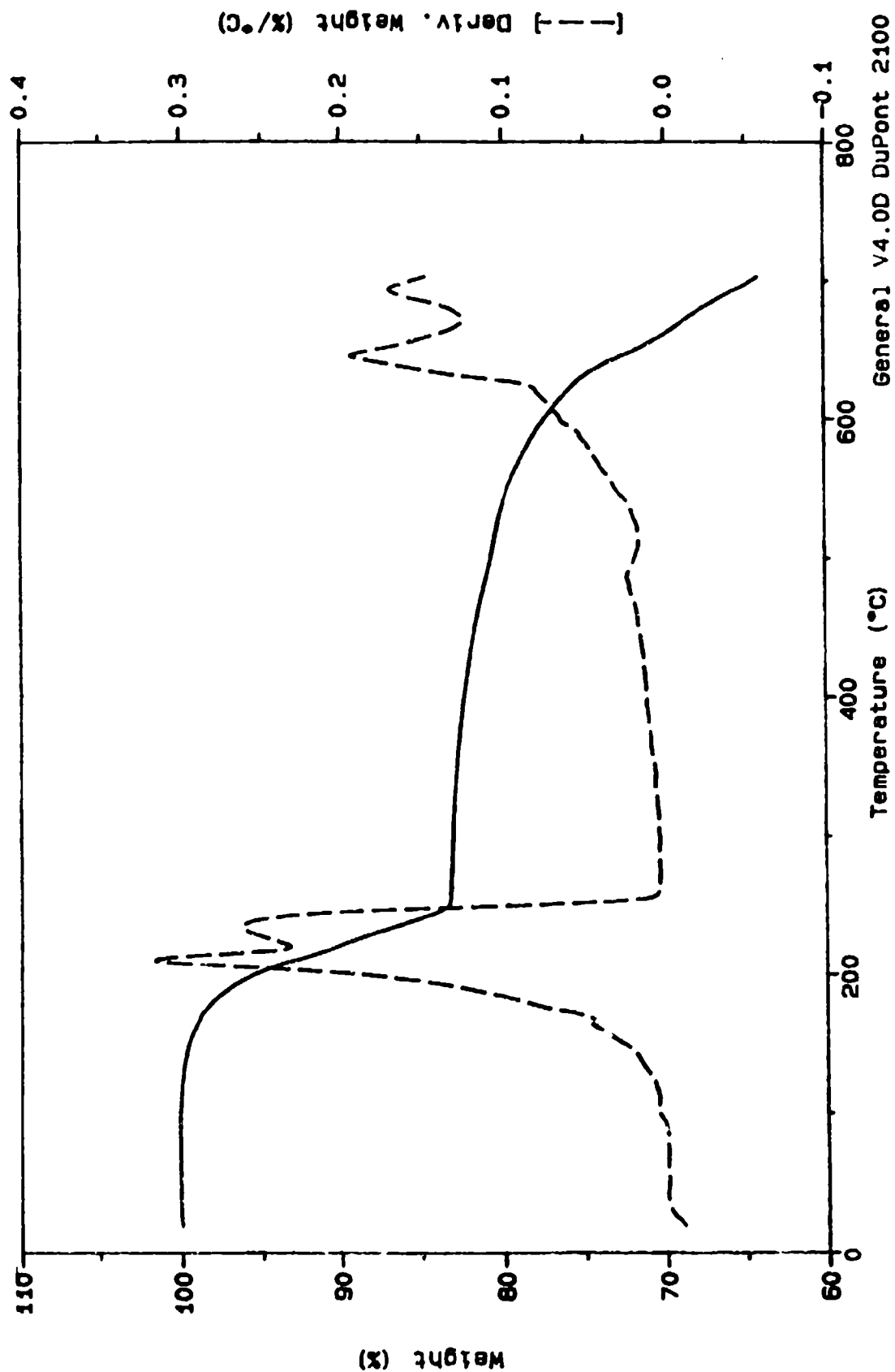


Figure 40. TGA of  $\text{Sb}_2\text{S}_5$  (—) % wt loss; (----) 1st derivative.

reacting with the platinum pan at temperatures above 600 °C. The initial weight loss is close to that predicted for reaction 2 (16 percent vs 15.9 percent). It is also close to the amount of sulfur obtained by extraction.



Results of DSC on  $\text{Sb}_2\text{S}_5$  under nitrogen are shown in Figure 41.  $\text{Sb}_2\text{S}_5$  behaves in the same manner as  $\text{Sb}_2\text{S}_4$  with the exception of the presence of excess sulfur as seen by the melting endotherm at 115 °C. (Note: only the beta form is observed.) The first exotherm occurs at 231 °C (15 J/g) followed by the melt at 553 °C which is 5 °C higher than the one for  $\text{Sb}_2\text{S}_4$ . Again, this increase may be due to a combination of factors - generated particle size, crystallinity and/or reactions with the sample pan. When DSC and TGA curves are overlaid (Figure 42), one sees that the exotherm coincides with the second portion of the weight loss. This supports the idea that the excess sulfur is present (or bound) within the antimony sulfide in two distinct ways.

Isothermal TGA experiments support the loss of sulfur to produce  $\text{Sb}_2\text{S}_3$ . When  $\text{Sb}_2\text{S}_5$  is heated under nitrogen to 270 °C (just beyond the 231 °C exotherm) and the product is examined by IR, a spectrum matching that of  $\text{Sb}_2\text{S}_3$  is observed. (See Figure 43.)

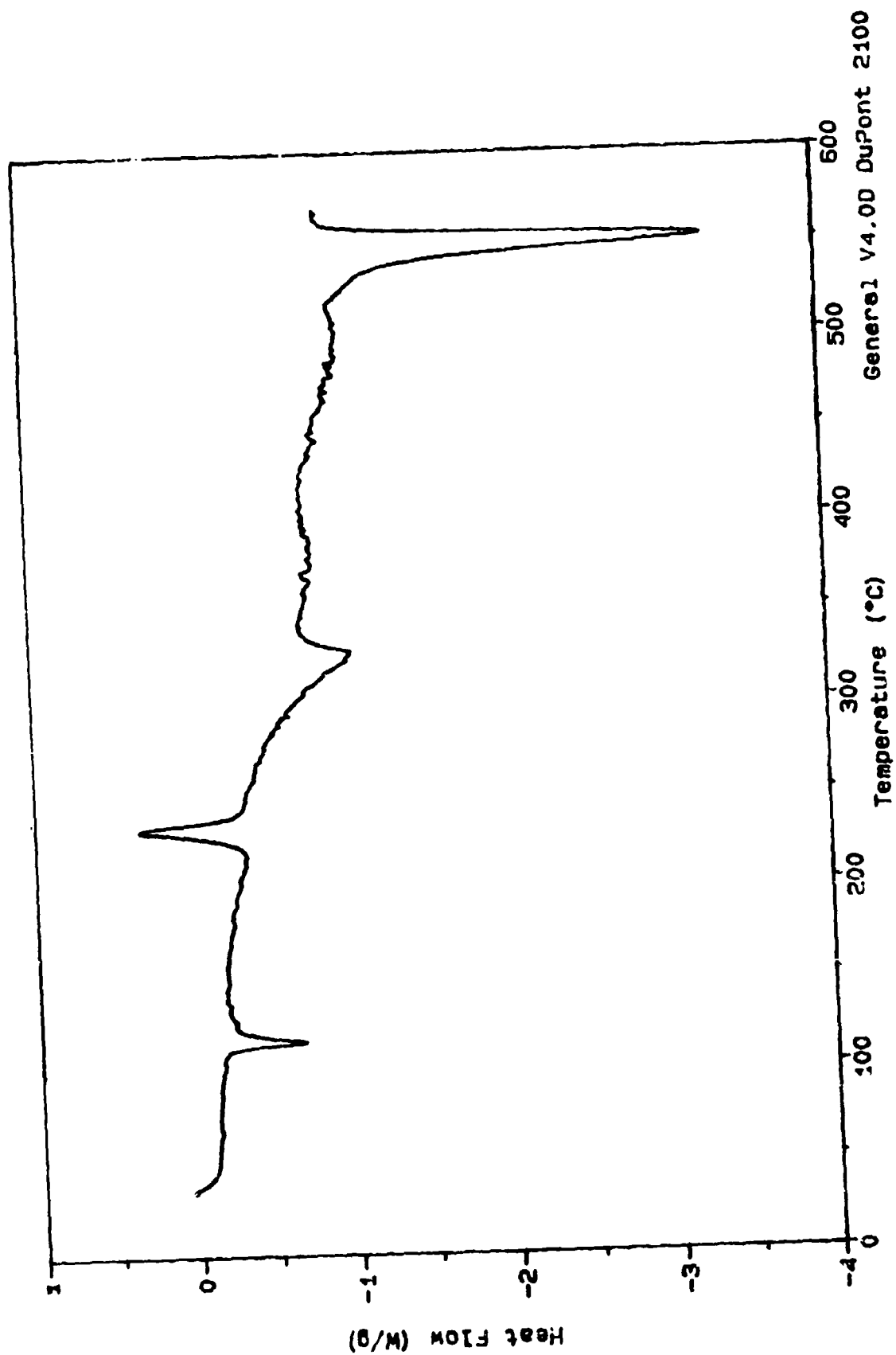


Figure 41. DSC of  $\text{Sb}_2\text{S}_5$  in  $\text{N}_2$ .



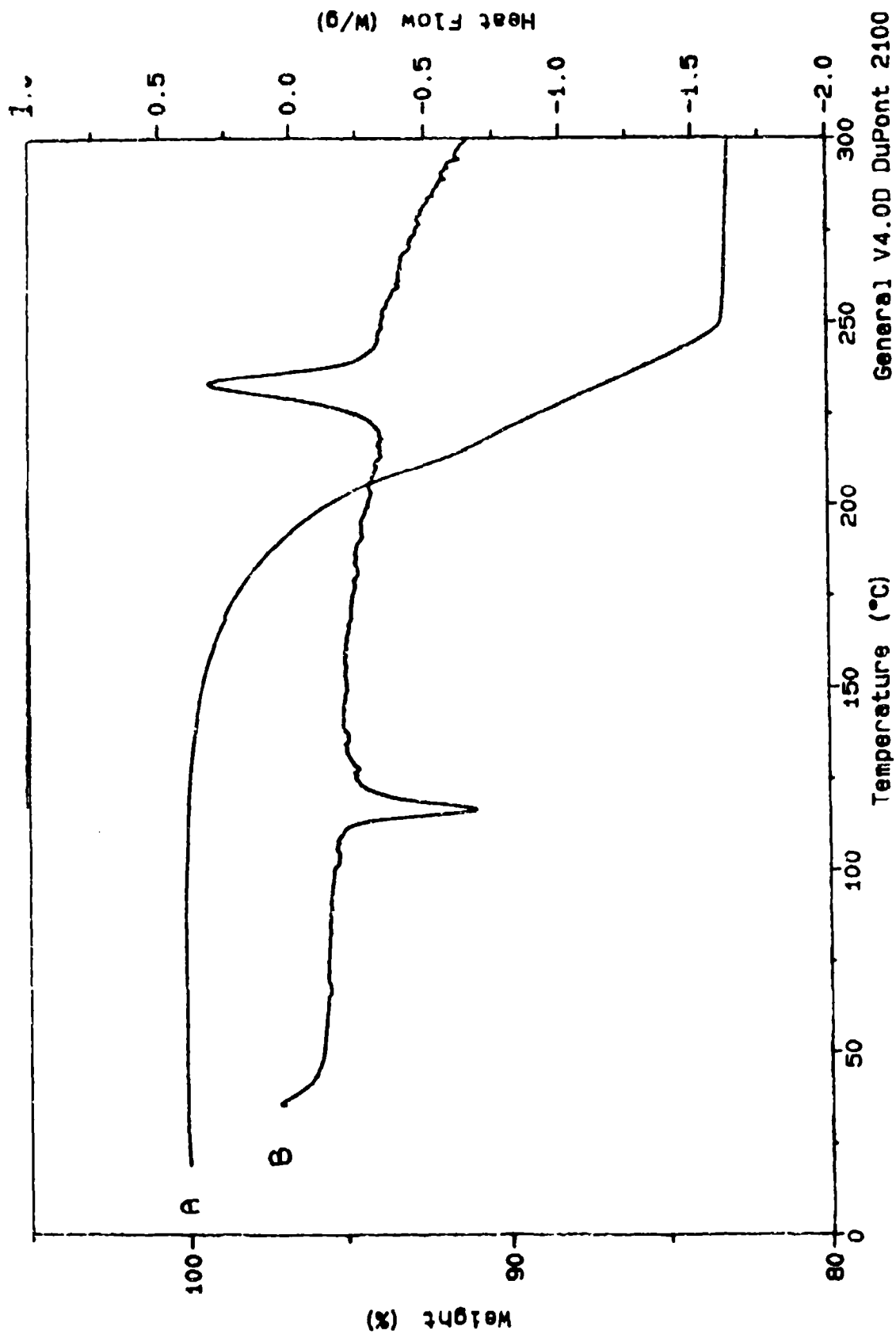


Figure 42. DSC - TGA Comparison of  $\text{Sb}_2\text{S}_5$  (A) TGA (B) DSC (Both in  $\text{N}_2$ ).

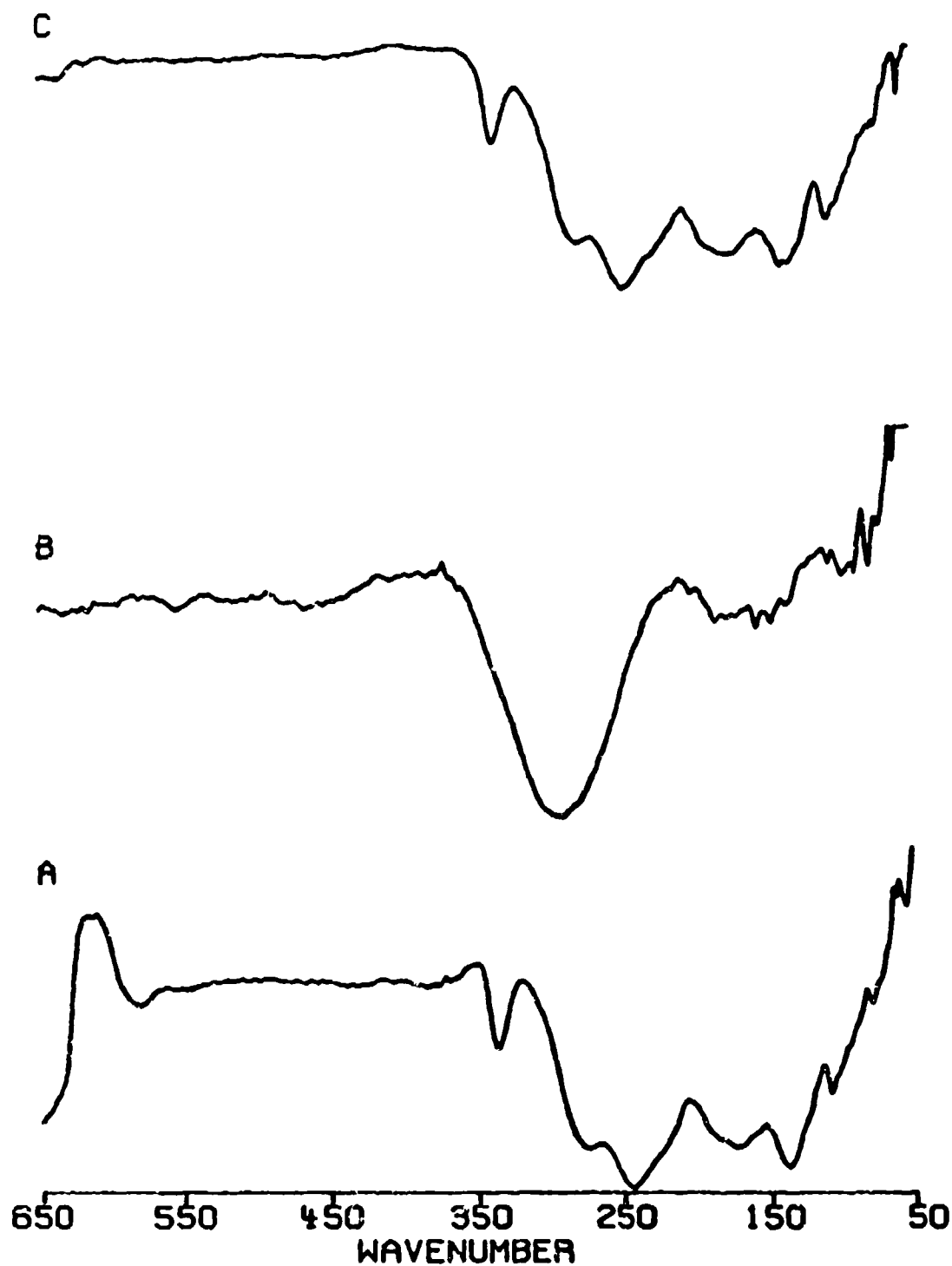


Figure 43. Far IR of  $\text{Sb}_2\text{S}_5$  (A)  $\text{Sb}_2\text{S}_3$ ; (B)  $\text{Sb}_2\text{S}_5$ ; (C)  $\text{Sb}_2\text{S}_5$  at 270°C in  $\text{N}_2$ .

Like other antimony sulfides, the pentasulfide undergoes a complex oxidation. TGA (Figure 44) shows an initial weight loss occurring in a biphasic manner (as in nitrogen), followed by a series of incremental losses from 300 to 600 °C. This multistep oxidation can be seen in the DTA and DSC curves. (See Figures 45 & 46.) DTA results are similar to those of  $\text{Sb}_2\text{S}_4$ ; two large asymmetric exotherms (292 and 403 °C) followed by a smaller one at 604 °C. The larger exotherms are better resolved in the DSC. The 292 °C peak is shifted to 290 °C with shoulders at 259 and 280 °C. The 403 °C exotherm remains; however, a shoulder at 333 °C is observed.

Oxidation of the pentasulfide in the TGA, followed by IR analysis produced results similar to those for  $\text{Sb}_2\text{S}_4$  and  $\text{Sb}_2\text{S}_3$ . Figure 47 shows the Far IR spectra of  $\text{Sb}_2\text{S}_5$  heated in air to 400, 525 and 700 °C. At 400 °C, a combination of cubic  $\text{Sb}_2\text{O}_3$  and  $\text{Sb}_2\text{S}_3$  can be seen. The sample heated to 525 °C shows no signs of  $\text{Sb}_2\text{S}_3$ , but does reveal a combination of cubic  $\text{Sb}_2\text{O}_3$  (384 and 180  $\text{cm}^{-1}$ ) and  $\text{Sb}_2\text{O}_4$  (434 and 605  $\text{cm}^{-1}$ ). As with  $\text{Sb}_2\text{S}_3$  and  $\text{Sb}_2\text{S}_4$ , temperatures above 600 °C yield a spectrum matching  $\text{Sb}_2\text{O}_4$ . Mid IR analysis reveals the presence of the sulfate containing species common to only air heated samples. (See Figures 48 & 49.)

Heating  $\text{Sb}_2\text{S}_5$  to a melt in the DSC, rapidly cooling, and rerunning under nitrogen produces the thermogram shown in Figure 50. A glass transition at 228 °C followed by crystallization at 271 °C (35 J/g) indicates that amorphous  $\text{Sb}_2\text{S}_3$  formed from rapid

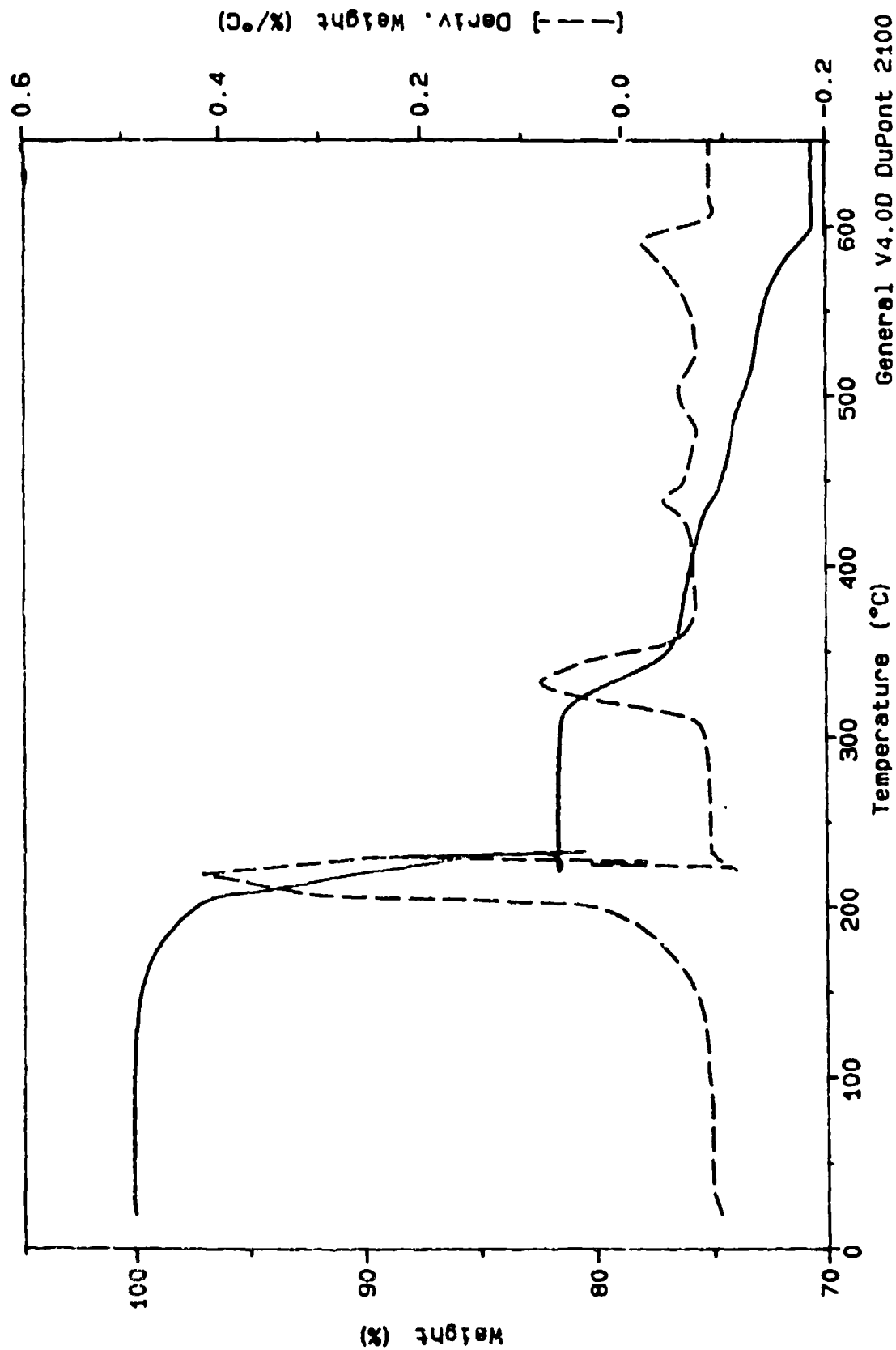


Figure 44. TGA of  $\text{Sb}_2\text{S}_5$  in Air.

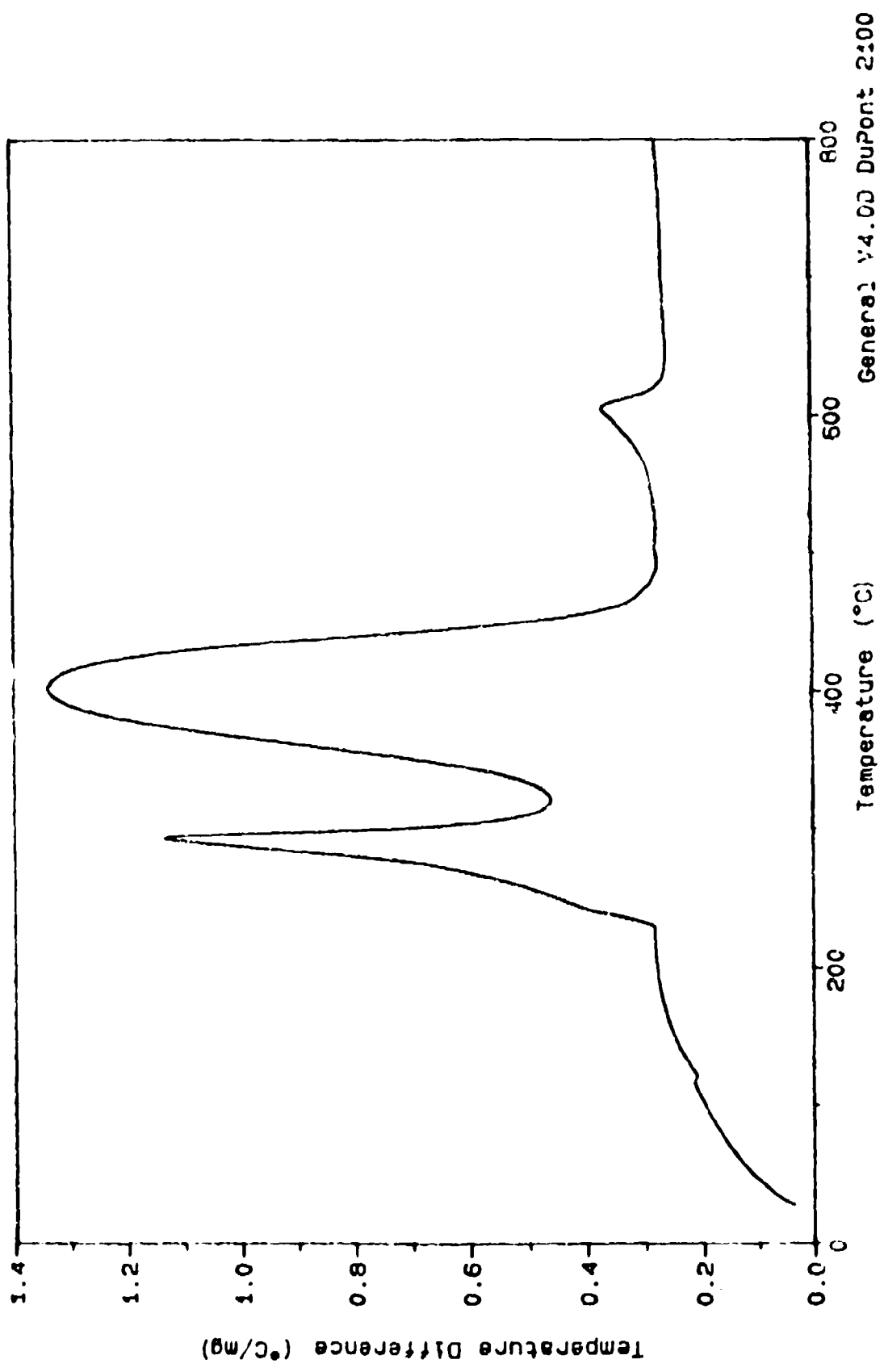


Figure 45. DTA of  $\text{Sb}_2\text{S}_5$  in Air.

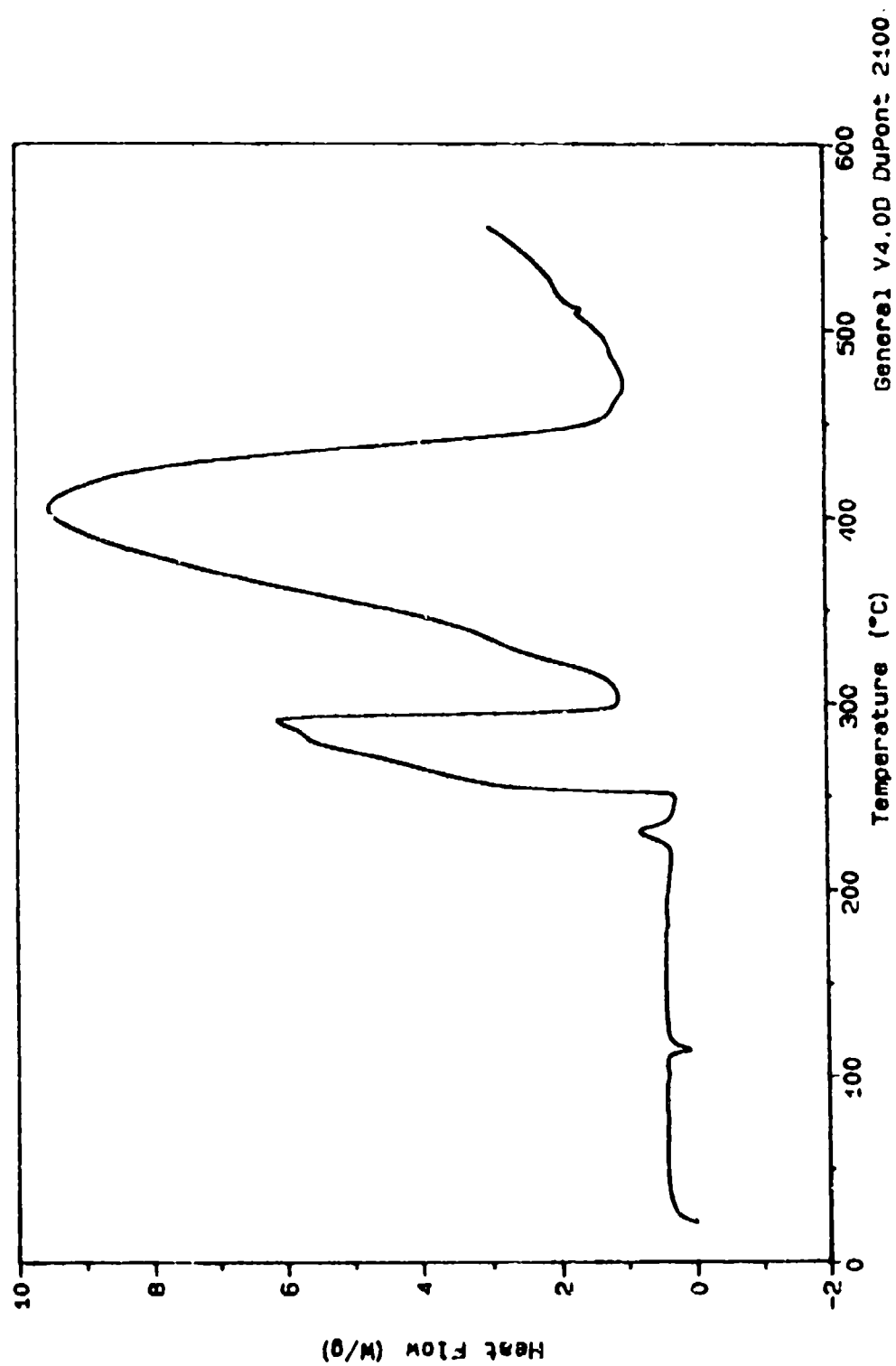


Figure 46. DSC of  $\text{Sb}_2\text{S}_5$  in Air.

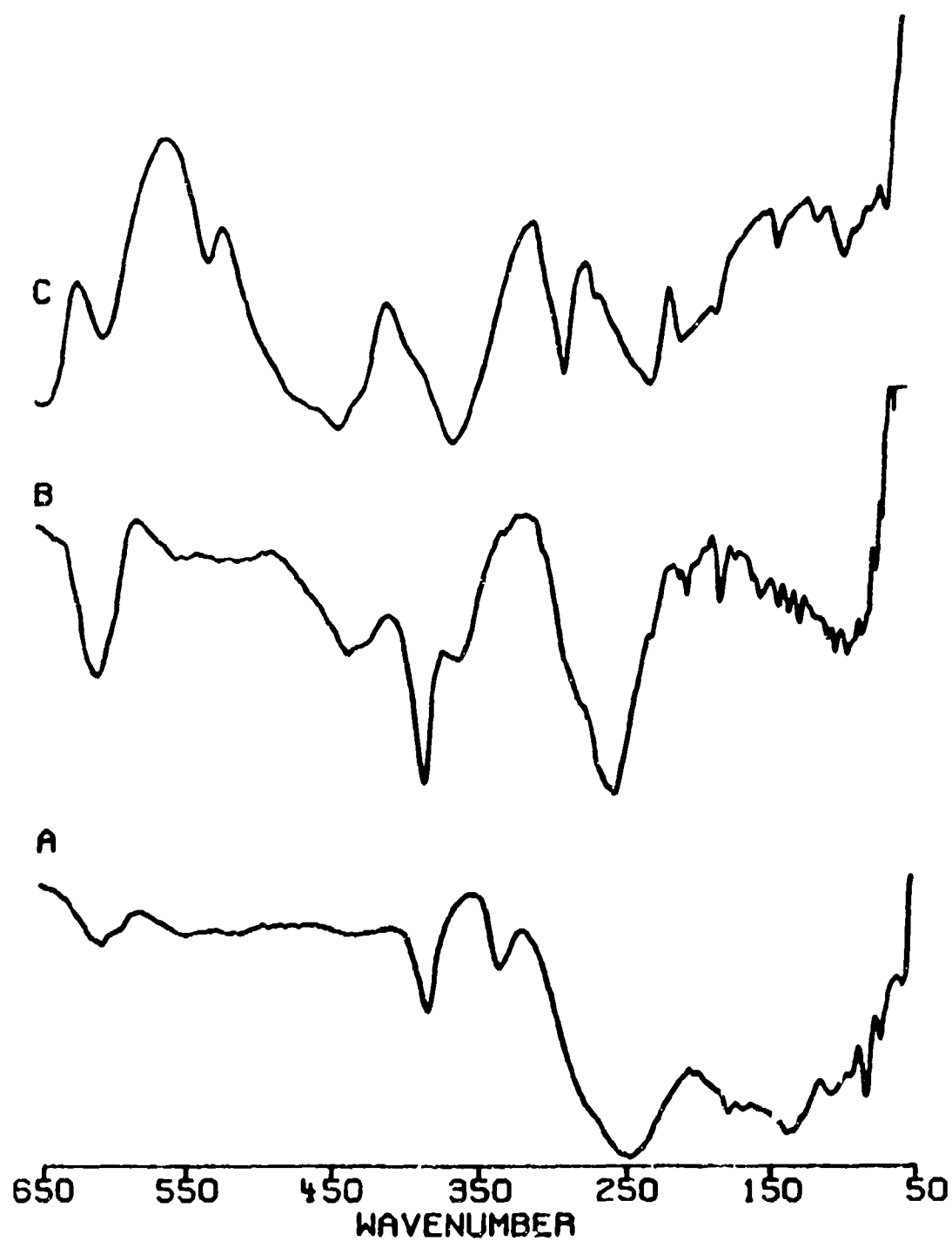


Figure 47. Far IR of  $\text{Sb}_2\text{S}_5$  (A) 400°C in Air; (B) 525°C in Air; (C) 700°C in Air.



Figure 48. Mid IR of  $\text{Sb}_2\text{S}_5$  (A) 400°C in Air; (B) 525°C in Air; (C) 700°C in Air.



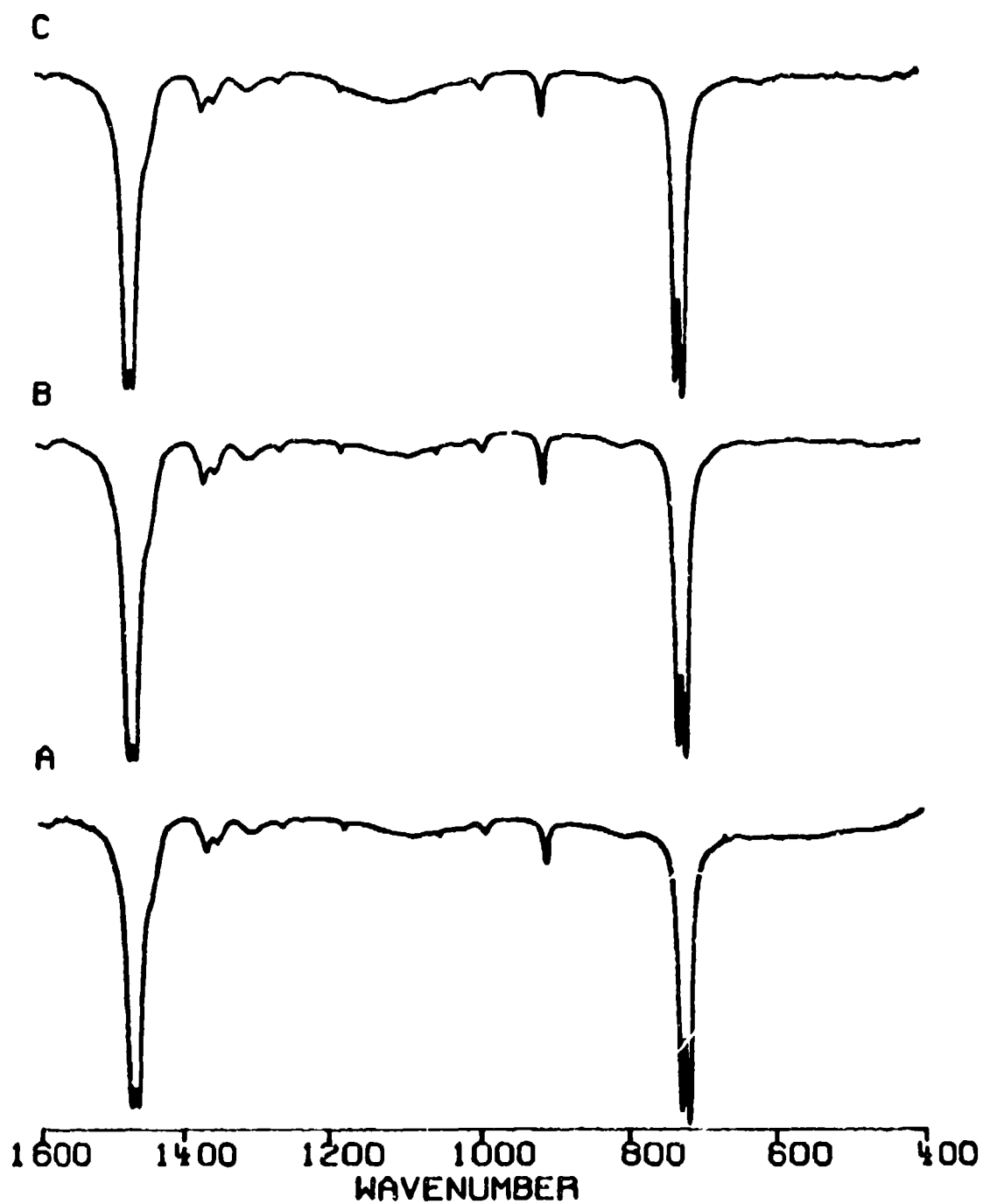


Figure 49. Mid IR of  $\text{Sb}_2\text{S}_5$  (A)  $\text{Sb}_2\text{S}_3$ ; (B)  $\text{Sb}_2\text{S}_5$ ; (C)  $\text{Sb}_2\text{S}_5$  at 275°C in  $\text{N}_2$ .

cooling the melt. When slowly cooled,  $\text{Sb}_2\text{S}_3$  solidifies in its crystalline form as evidenced by the lack of a glass transition and heat of crystallization. (See Figure 51.)

The thermal stability of extracted antimony pentasulfide is somewhat different from the unextracted material. In TGA experiments, (Figure 52) both under nitrogen and air, only a 2 percent weight loss is observed between 227 and 243 °C as compared to 16 percent for the unextracted material. This 2 percent is most likely due to residual sulfur not removed by extraction. After the initial loss, in nitrogen, the extracted material demonstrates the same thermal stability as  $\text{Sb}_2\text{S}_3$ , ultimately reacting with the platinum pan at temperatures above 600 °C.

In air, extracted  $\text{Sb}_2\text{S}_5$  undergoes a series of weight losses between 290 and 580 °C. These losses are similar in pattern to unextracted  $\text{Sb}_2\text{S}_5$  (Figure 53), but different in magnitude. A loss of 8.9 percent occurs at 291 °C in the extracted sample - 4 percent less and 25 °C earlier than unextracted  $\text{Sb}_2\text{S}_5$ . The total weight loss for the extracted sample is 16 percent, compared with 29 percent for unextracted  $\text{Sb}_2\text{S}_5$  - a difference approximately equal to the amount of sulfur removed by extraction.

DSC experiments on extracted  $\text{Sb}_2\text{S}_5$  parallel those of the unextracted  $\text{Sb}_2\text{S}_5$  with the exception of the melting and volatilization of the excess sulfur. (See Figure 54.) On closer

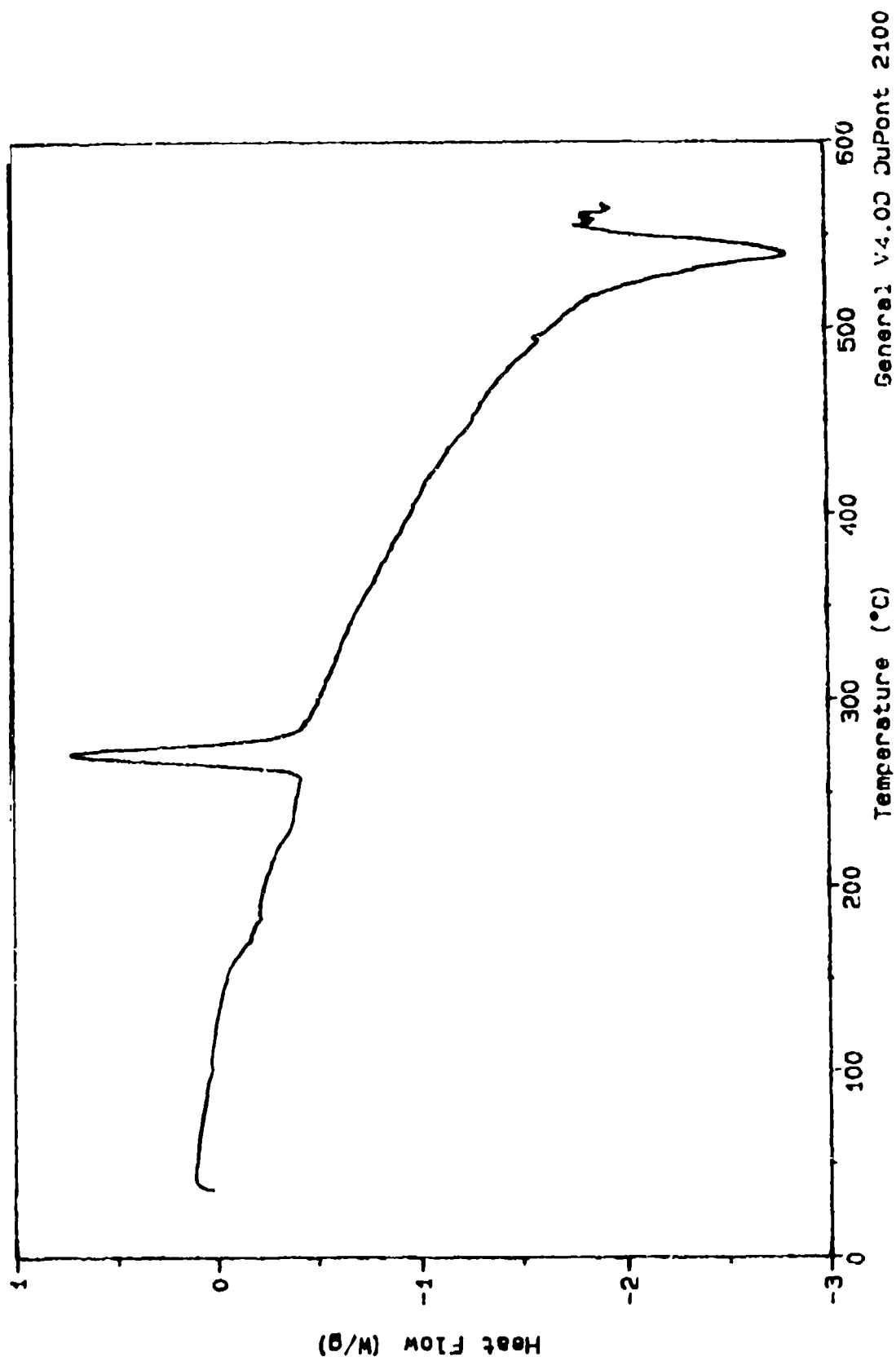


Figure 50. DSC of Generated Amorphous  $\text{Sb}_2\text{S}_3$  ( $\text{Sb}_2\text{S}_5$  rapidly cooled from melt in  $\text{N}_2$ ).

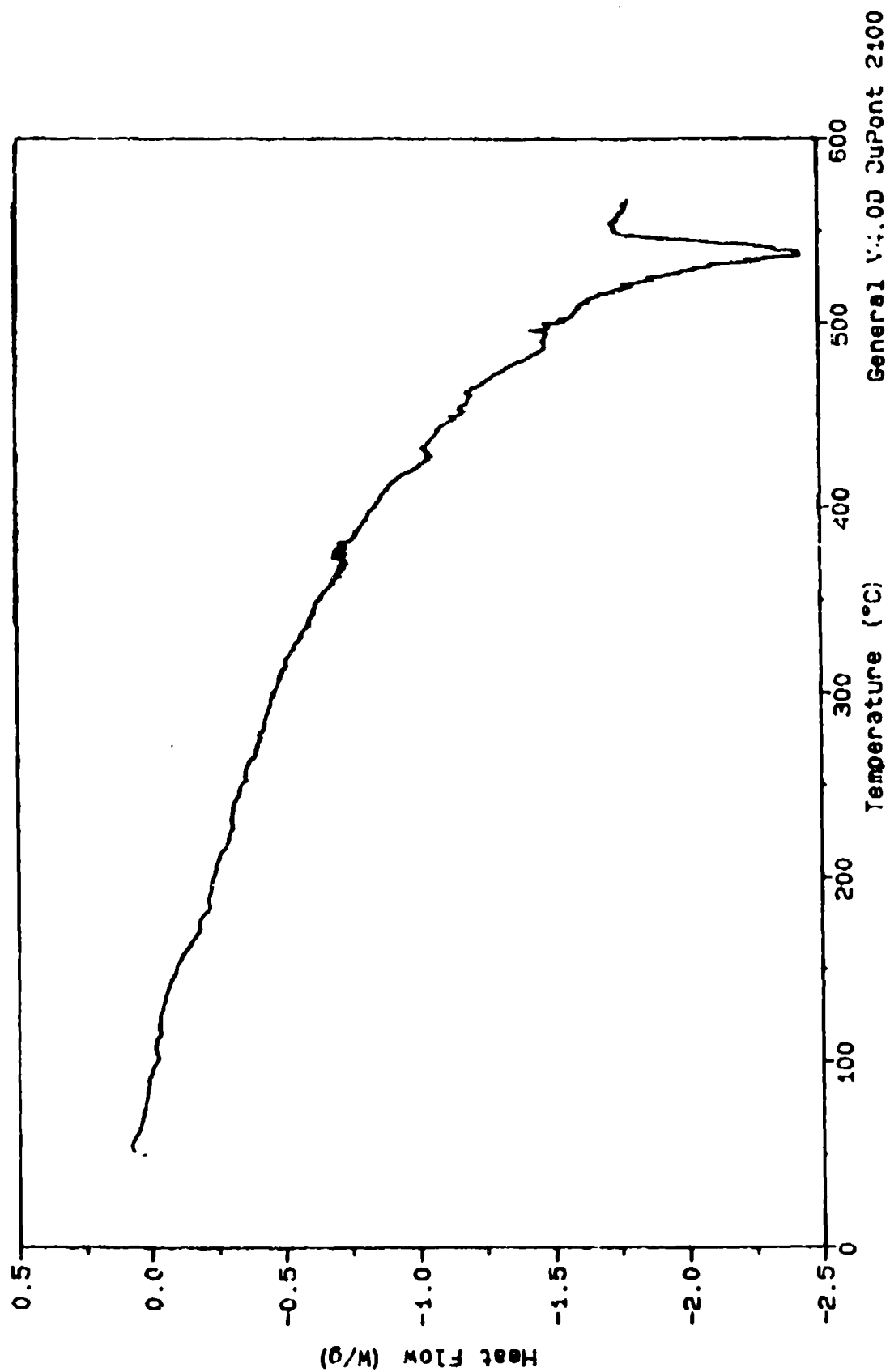


Figure 51. DSC of Generated Crystalline  $\text{Sb}_2\text{S}_3$  ( $\text{Sb}_2\text{S}_5$  slow cooled from melt in  $\text{N}_2$ ).

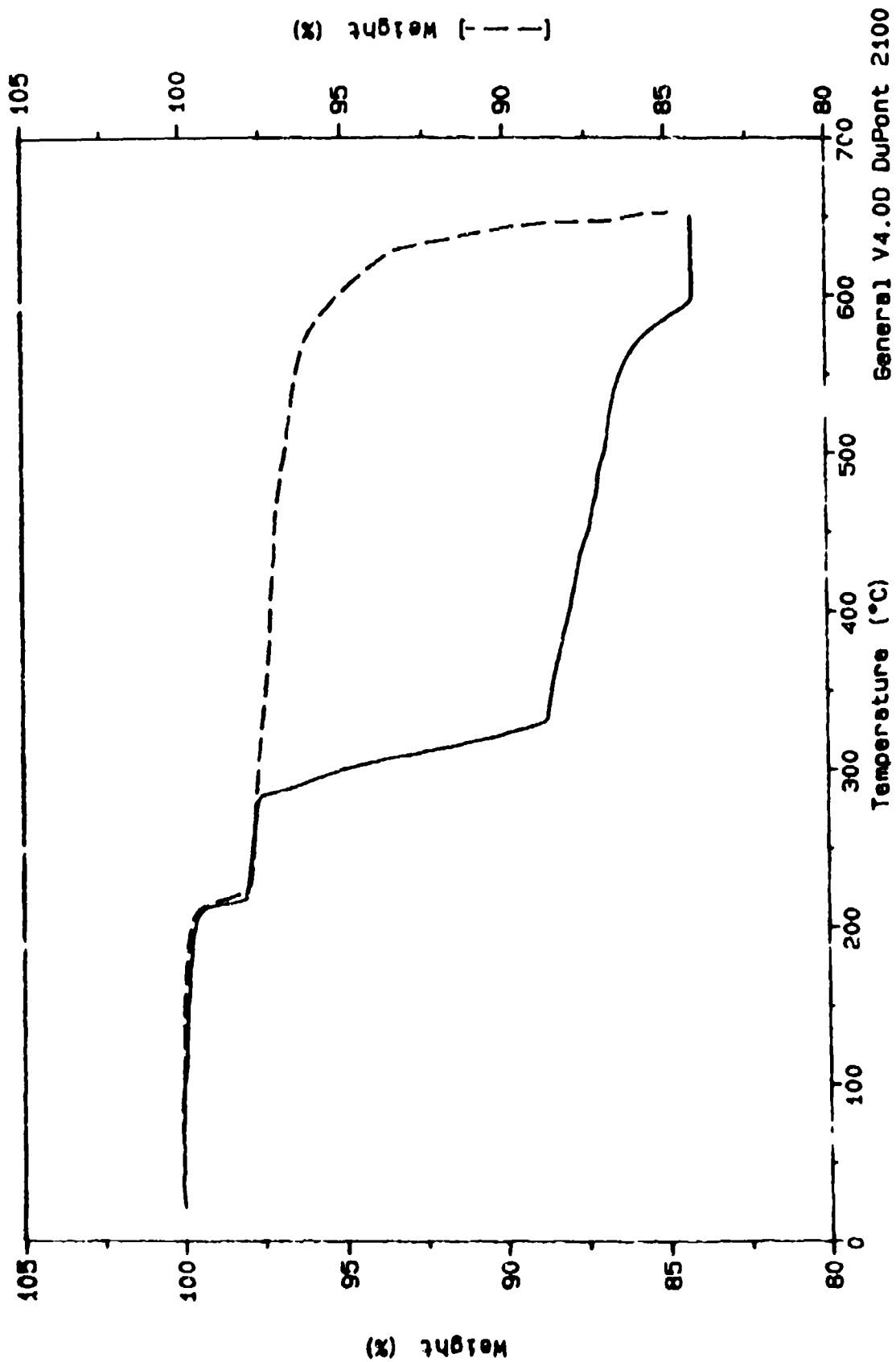


Figure 52. TGA of Extracted  $Sb_2S_5$  (—) in Air; (----) in  $N_2$ .

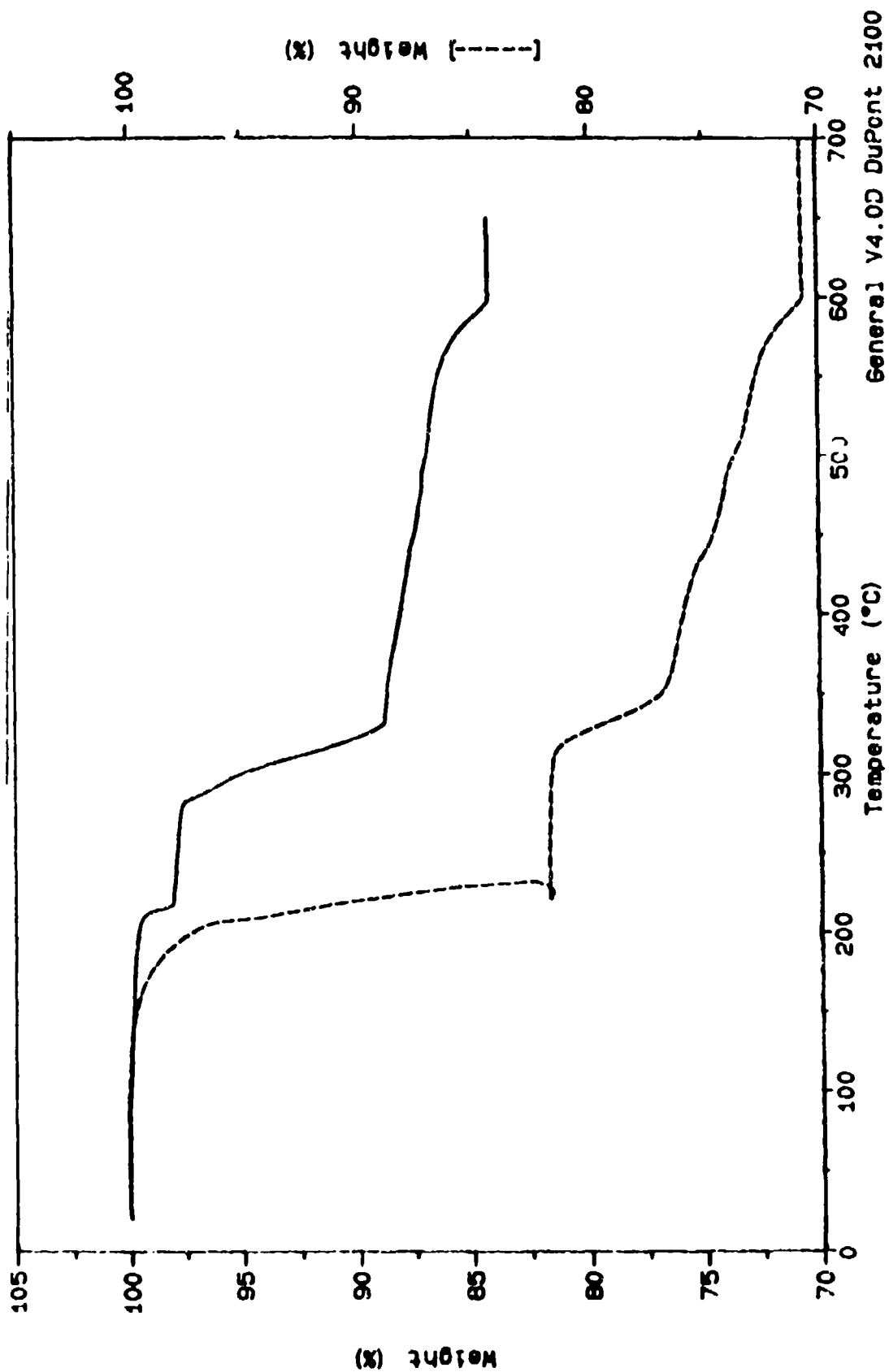


Figure 53. TGA of (----) Extracted vs (—) Unextracted  $Sb_2S_5$ .

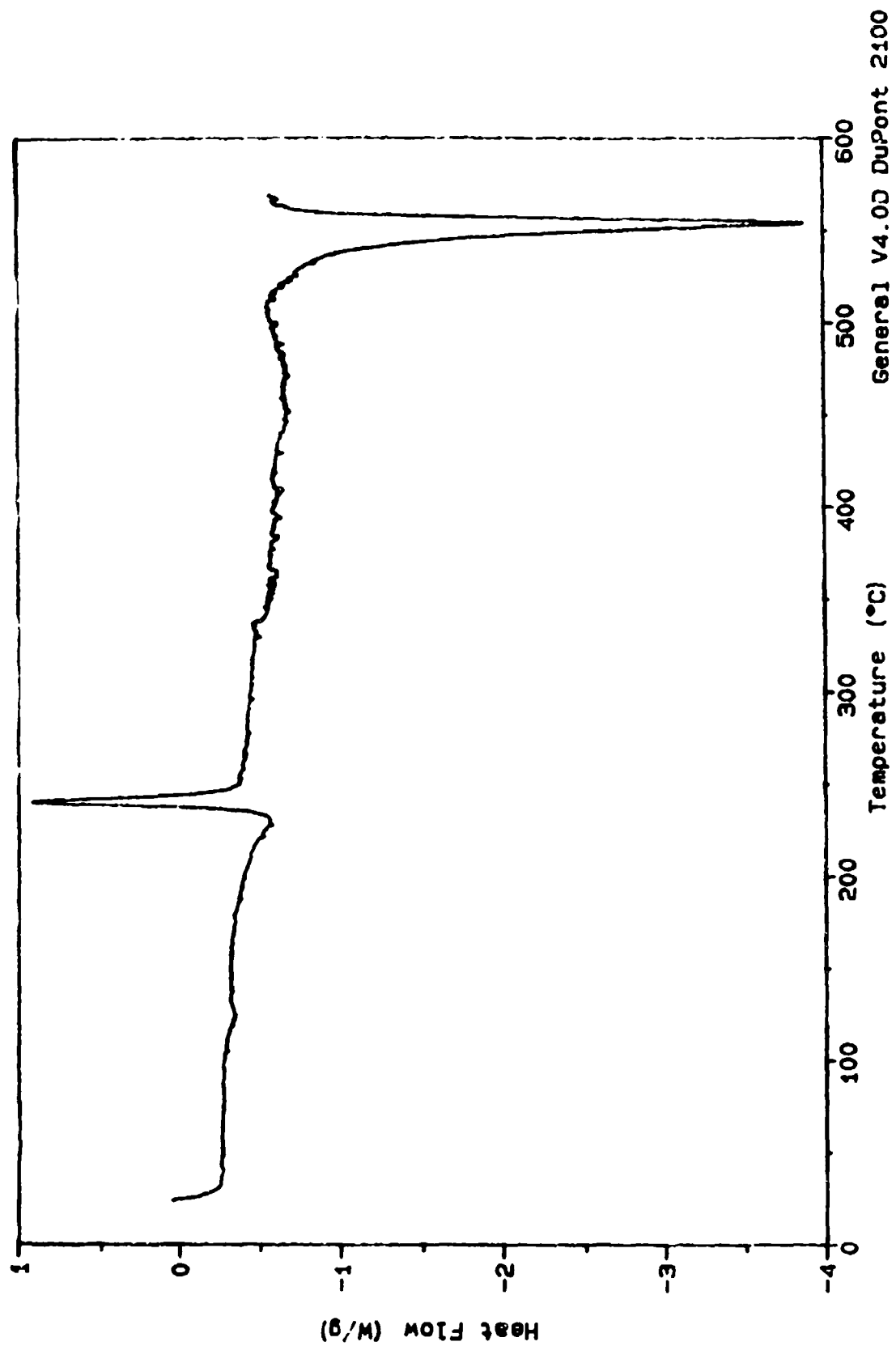


Figure 54. DSC of Generated Amorphous  $\text{Sb}_2\text{S}_3$  (Extracted  $\text{Sb}_2\text{S}_5$  rapidly cooled from melt).

examination, one sees that the exotherm is asymmetric and contains a contribution from an underlying endotherm. The maximum at 239 °C is 7 °C higher than that observed for unextracted  $\text{Sb}_2\text{S}_5$ . This does not however, take into account the contribution from the endotherm, the real maxima may well be the same as that of the unextracted sample. The melting point of the generated  $\text{Sb}_2\text{S}_3$  is unaffected by the extraction process.

Results of DSC performed on extracted  $\text{Sb}_2\text{S}_5$  under oxidative conditions, are shown in Figure 55 along with previously reported results for the unextracted material. The initial exotherm occurs at a slightly higher temperature (241 °C), also the magnitude of the exotherm is larger - 23 J/g vs 12 J/g. The higher temperature may be the result of the extracted sulfur. The corresponding exotherm in  $\text{Sb}_2\text{S}_4$  shifted to lower temperatures when elemental sulfur was added.

The extracted  $\text{Sb}_2\text{S}_5$  does not display the two well defined exotherms at 292 and 403 °C, only one broadband containing several shoulders is observed. Again, this may be a result of a smaller amount of sulfur present in the extracted sample reducing the size of the exotherm at 286 °C, previously identified as the oxidation of sulfur, to a point where it appears as a shoulder on the larger exotherm.

Infrared analysis of samples of extracted  $\text{Sb}_2\text{S}_5$  heated under oxidative conditions mirror results obtained for all the sulfides



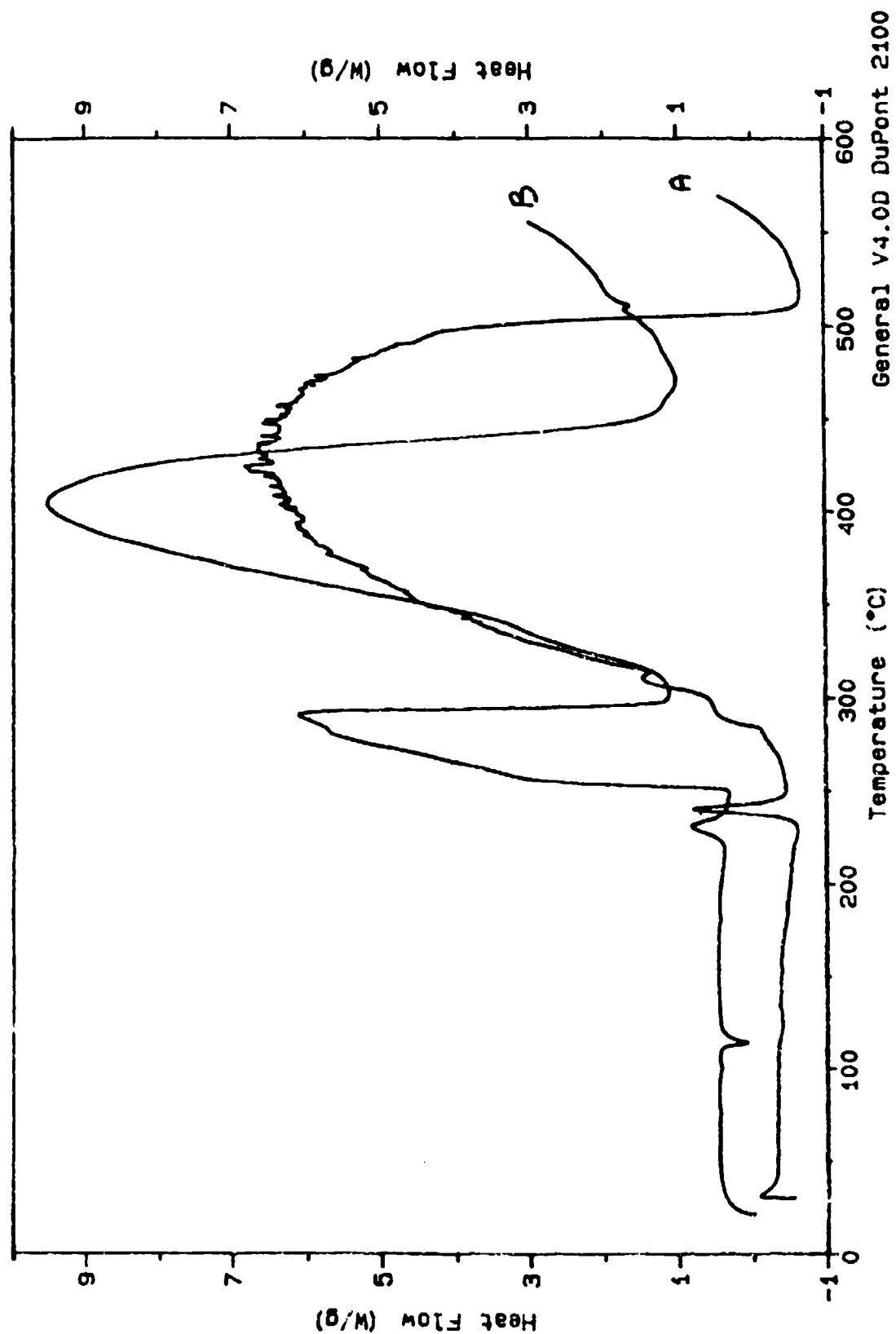


Figure 55. DSC of (A) Extracted vs (B) Unextracted  $\text{Sb}_2\text{S}_5$  in Air.

previously examined. Shown in Figure 56, heating at 400 °C, produces bands at 384, 264, and 180 cm<sup>-1</sup> indicating formation of cubic Sb<sub>2</sub>O<sub>3</sub>; while at 600 °C, bands at 440, 365, 287, and 227 cm<sup>-1</sup> identify the presence of Sb<sub>2</sub>O<sub>4</sub>. Again, mid IR (Figure 57) reveals the presence of the characteristic 1100 cm<sup>-1</sup> band for the samples heated in air and its absence (Figure 58) in virgin and nitrogen heated samples. Finally, as with Sb<sub>2</sub>S<sub>4</sub> and unextracted Sb<sub>2</sub>S<sub>5</sub>, heating in a inert environment produces Sb<sub>2</sub>S<sub>3</sub>. (See Figure 59.)

Solidification from a melt patterns the unextracted Sb<sub>2</sub>S<sub>5</sub>. On rapid cooling, DSC (Figure 60) shows the typical glass transition (225 °C) and crystallization exotherm (272 °C) indicating that amorphous Sb<sub>2</sub>S<sub>3</sub> formed from the melt. Allowing the melt to cool slowly results in formation of crystalline Sb<sub>2</sub>S<sub>3</sub> as evidenced by the lack of a glass transition and crystallization exotherm. (See Figure 61.)

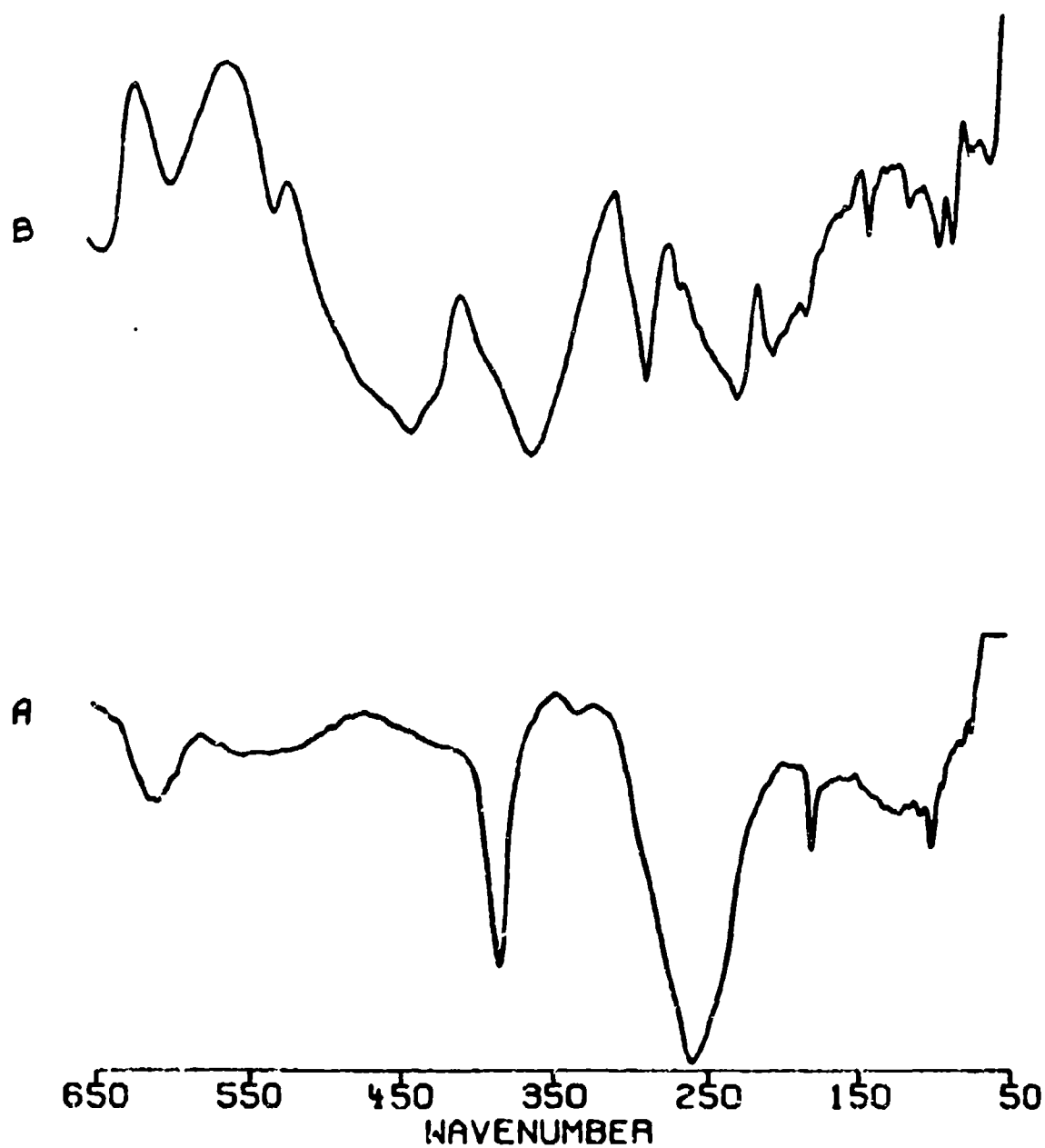


Figure 56. Far IR of Extracted Antimony Pentasulfide (A) 400°C in Air;  
(B) 60°C in Air.

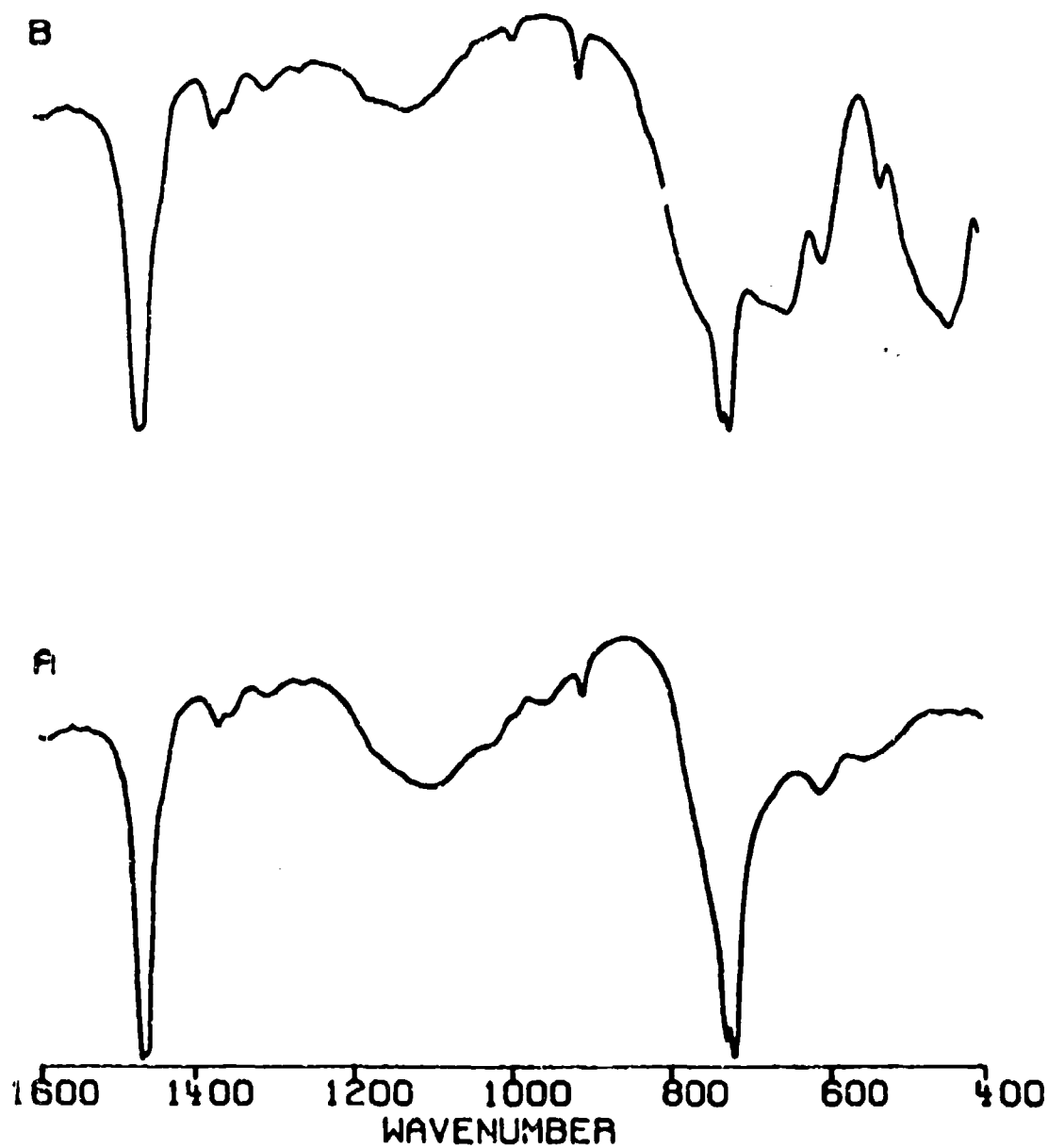


Figure 57. Mid IR of Extracted  $\text{Sb}_2\text{S}_5$  (A) 400°C in Air; (B) 650°C in Air.

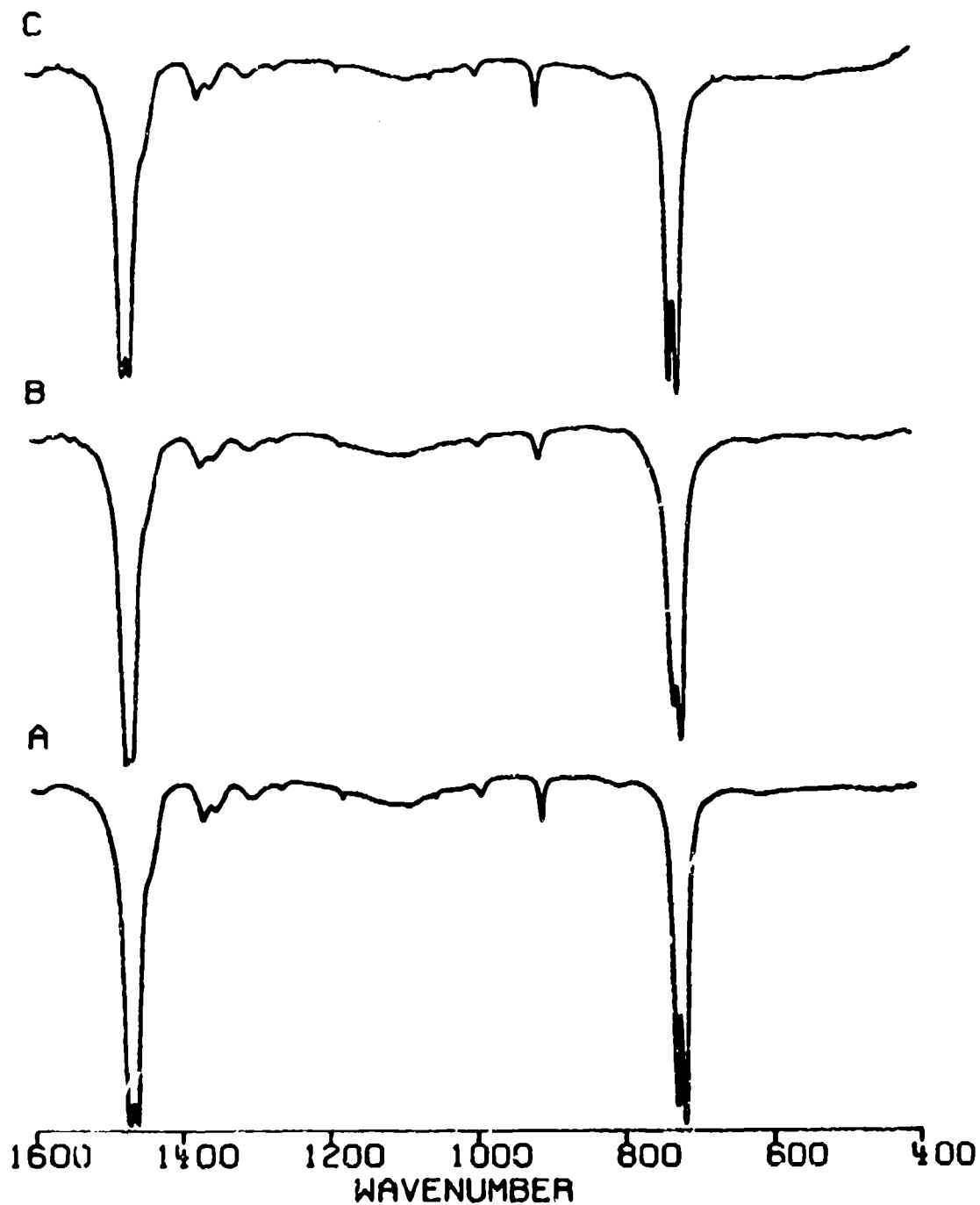


Figure 58. Mid IR of Extracted  $\text{Sb}_2\text{S}_5$  (A) Virgin; (B) 350°C in  $\text{N}_2$ ; (C)  $\text{Sb}_2\text{S}_3$ .

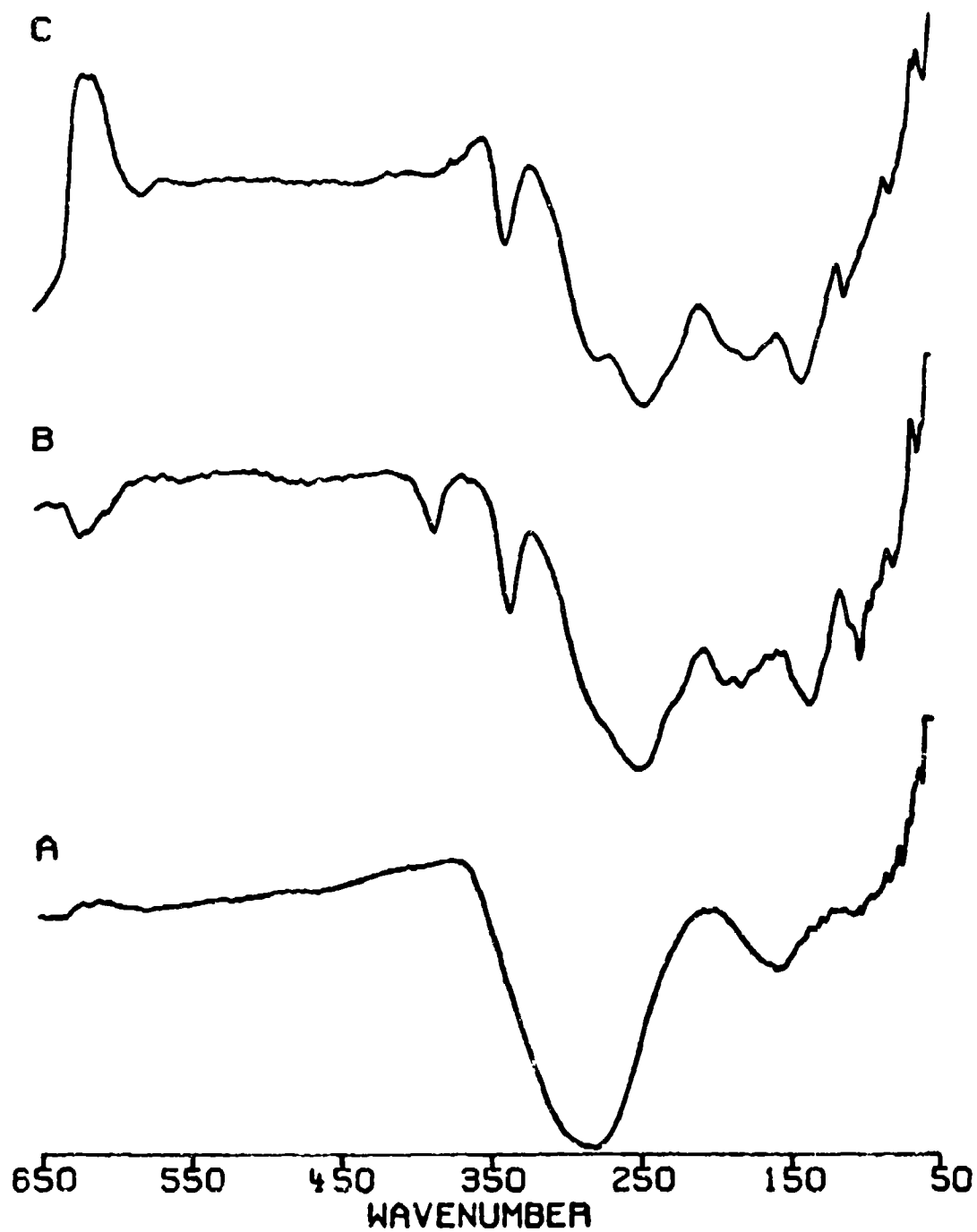


Figure 59. Far IR of Extracted  $\text{Sb}_2\text{S}_5$  (A) Virgin; (B) 350°C in  $\text{N}_2$ ;  
(C)  $\text{Sb}_2\text{S}_3$ .

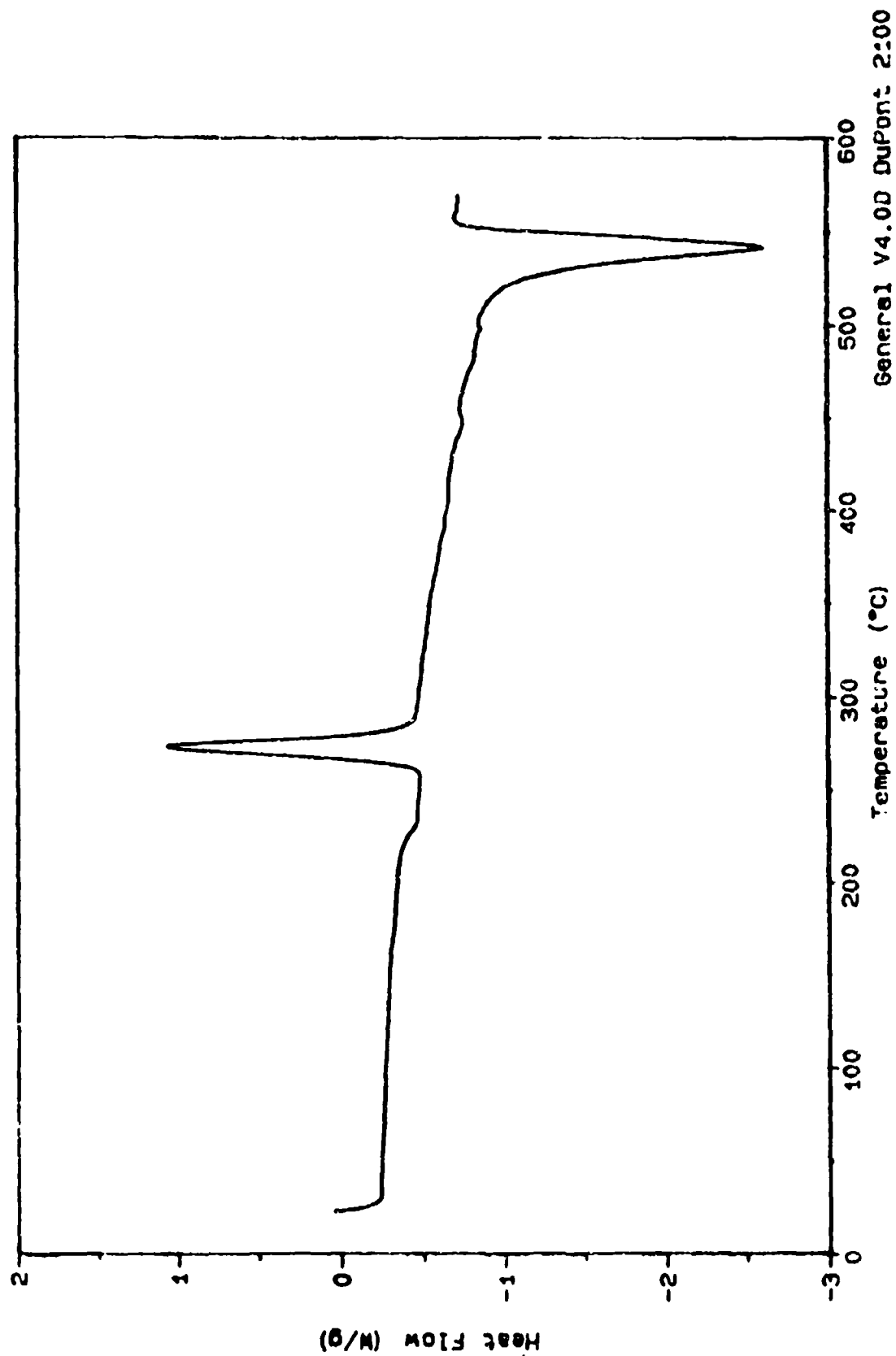


Figure 60. DSC of Generated Amorphous  $\text{Sb}_2\text{S}_3$  (Extracted  $\text{Sb}_2\text{S}_5$  rapidly cooled from melt in  $\text{N}_2$ ).

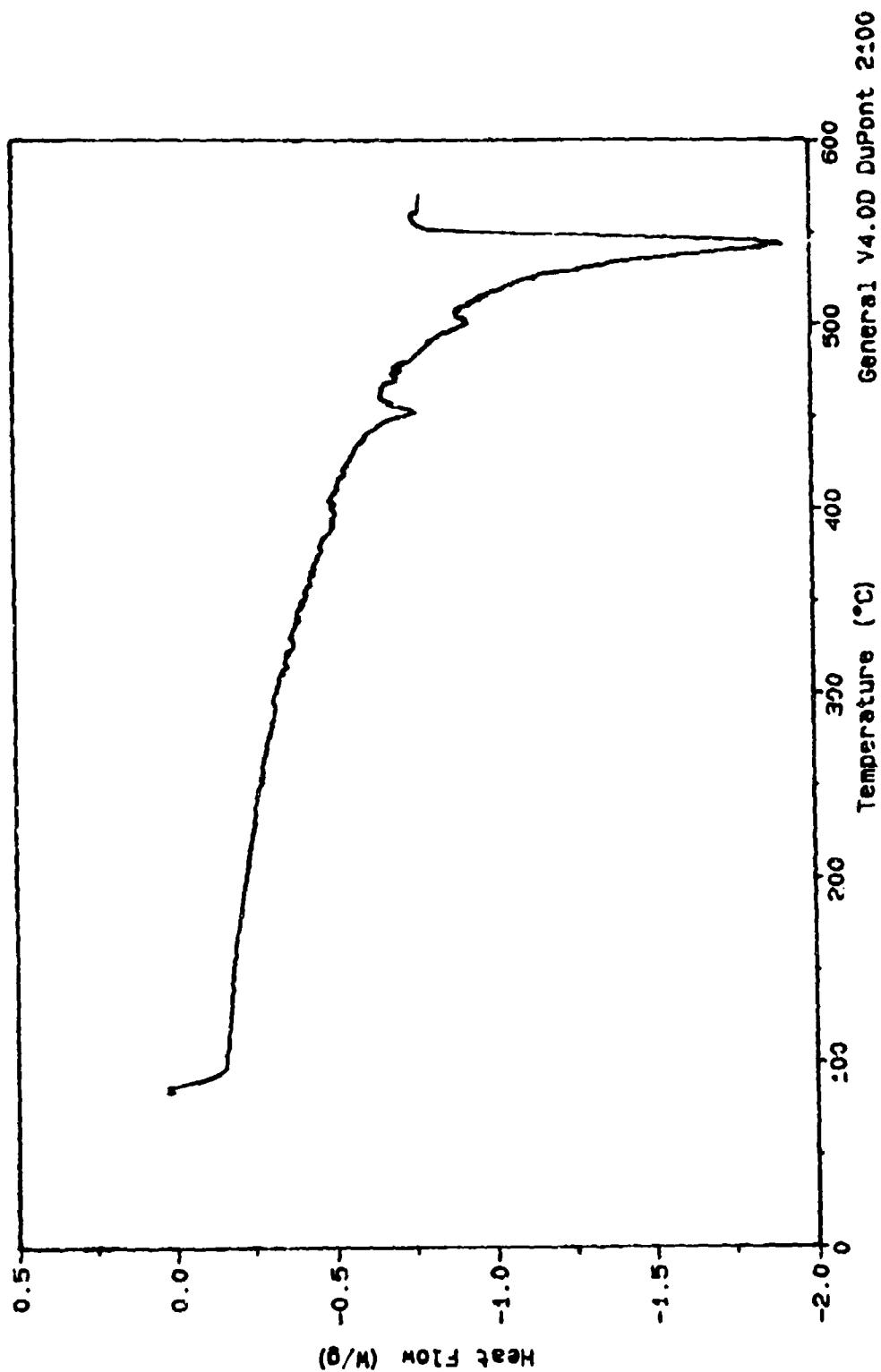


Figure 61. DSC of Generated Crystalline  $\text{Sb}_2\text{S}_3$  (Extracted  $\text{Sb}_2\text{S}_5$  slow cooled from melt in  $\text{N}_2$ ).



#### SECTION IV CONCLUSION

1. Antimony trisulfide: Under nitrogen, antimony trisulfide is thermally stable to 575 °C.  $\text{Sb}_2\text{S}_3$  oxidizes at 300 °C. The oxidation produces a sulfate containing species along with cubic  $\text{Sb}_2\text{O}_3$ . At 604 °C, cubic  $\text{Sb}_2\text{O}_3$  oxidizes to form  $\text{Sb}_2\text{O}_4$ . The amorphous form of  $\text{Sb}_2\text{S}_3$  can be created in situ in the DSC, by rapidly cooling a sample from a melt. The amorphous  $\text{Sb}_2\text{S}_3$  undergoes a glass transition at 232 °C and a crystallization at 318 °C. Addition of elemental sulfur to  $\text{Sb}_2\text{S}_3$  raises the observed melting point from 510 °C to 520 °C.

2. Antimony tetrasulfide:  $\text{Sb}_2\text{S}_4$  releases sulfur between 195 and 230 °C to form  $\text{Sb}_2\text{S}_3$ . The corresponding transition to  $\text{Sb}_2\text{S}_3$  is seen in the DSC at 210 °C. The  $\text{Sb}_2\text{S}_3$  generated in situ melts at 548 °C. It undergoes the same oxidative behavior as virgin  $\text{Sb}_2\text{S}_3$ ; forming an intermediate sulfate and the cubic trioxide at temperatures below 600 °C, and the tetraoxide above 600 °C. Amorphous  $\text{Sb}_2\text{S}_3$  generated from a rapid cool undergoes a glass transition at 227 °C and a crystallization at 279 and 293 °C. The addition of elemental sulfur lowers the temperature of the transition to  $\text{Sb}_2\text{S}_3$  to 186 °C in the DSC.

3. Antimony pentasulfide:  $\text{Sb}_2\text{S}_5$  contains approximately 15 percent excess sulfur - as determined by  $\text{CS}_2$  extraction. The

excess sulfur is present within the antimony sulfide in two forms as demonstrated by the biphasic weight loss in the TGA between 193 and 239 °C. The associated change in the DSC occurs at 231 °C. The  $\text{Sb}_2\text{S}_3$  generated in situ, melts at 553 °C. It's oxidation follows the same pattern as the tri and tetrasulfides. Amorphous  $\text{Sb}_2\text{S}_3$  generated by a rapid cool of a melt, undergoes a glass transition at 228 °C and a crystallization at 271 °C. Extracted  $\text{Sb}_2\text{S}_5$  has a sulfur to antimony ratio of 3:2, and undergoes a 2 percent weight loss between 227 and 243 °C. The corresponding change in the DSC occurs at 239 °C; however, this exotherm overlaps an endotherm which in effect raises the measured maximum. Removal of the excess sulfur by extraction does not effect the melting of generated  $\text{Sb}_2\text{S}_3$ . Amorphous  $\text{Sb}_2\text{S}_3$  created by a rapid cooling of a melt, has a glass transition at 225 °C and a crystallization at 272 °C.

## REFERENCES

1. M.M. Sekkina, Z.M. Hanafi, and M.A. Moharm, "Studies on Ultraviolet and Dielectric Properties of Antimony Trisulfide," Indian J. Phys., A, 54, (5,6), 462-471, 1980.
2. J. George and M.K. Radhakrishnan, "Space-Charge Limited Conduction in Antimony Trisulfide Films," J. Phys., D, 14, (5), 899-905, 1981.
3. K.A. Mady, S.M. Hammad, and W.Z. Soliman, "On the Structural and Transformation of the Orange Form of Antimony Trisulfide ( $\text{Sb}_2\text{S}_3$ ) Layers," J. Mater. Sci., 22, (11), 4153-4157, 1987.
4. Z.M. Hanafi and F.M. Ismail, "Colour Problem of Antimony Trisulfide," Z. Phys. Chem. (Leipzig), 244, (3,4), 219-225, 1970.
5. G.G. Long, J.G. Stevens, L.H. Bowen, and S.L. Ruby, "The Oxidation Number of Antimony in Antimony Pentasulfide," Inorg. Nucl. Chem. Letters, 5, 21-25, 1969.
6. J.P. King and Y. Asmerom, "Investigation of Extreme Pressure and Antiwear Properties of Antimony ThioAntimonate," ASLE Transactions, 24, 4, 497-504, 1981.
7. L.K. Ives, M.B. Peterson, J.B. Harris, P.A. Boyer, and A.W. Ruff, "Investigation of the Lubrication Mechanisms of the Complex Metal Sulfide,  $\text{SbSbS}_4$ ," NBSIR, 82-2545 (ONR), 1982.
8. W.J. Bartz, R. Holinski, and J. Xu, "Wear Life and Frictional Behavior of Bonded Solid Lubricants," Lubrication Engineering, 42, 12, 762-769, 1985.
9. P.W. Centers and F.D. Price, "Tribological Performance of  $\text{MoS}_2$  Compacts Containing Sulfur,  $\text{SbS}_3$ , or  $\text{SbS}_4$ ," Wear, 129, 205-213, 1989.
10. S.E. Golunski, T.G. Nevall, and M.I. Pope, "Thermal Stability and Phase Transitions of the Oxides of Antimony," Thermochemica Acta, 51, 153-168, 1981.
11. P.W. Centers, "Sublimation-Controlled Oxidation of Antimony Trioxide," J. Solid State Chem., 72, 303-308, 1988.
12. F.A. Miller and C.H. Wilkins, "Infrared Spectra and Characteristic Frequencies of Inorganic Ions," Anal. Chem., 24, 1253-1294, 1952.

# REFERENCES (CONTINUED)

13. P. Bohac and P. Kaufman, "Zone Refining of Antimony Trisulfide," Mater. Res. Bull., 10, (7), 613-622, 1975.
14. W. Pierce, E. Haenish, and D. Sawyer, Quantitative Analysis, 4th Ed., 1958, John Wiley and Sons, New York, NY, 283-284.